Thermomechanical Exergy Recovery From Liquid Hydrogen Cryofuel

by

K. Michael Flaherty

B.A.Sc., University of Toronto, 1989

A Thesis Submitted in Partial Fulfilment of the
Requirements for the Degree of

MASTER OF APPLIED SCIENCE

in the Department of Mechanical Engineering

We accept this thesis as conforming to the required standard

[redacted]

Dr. David S. Scott, Supervisor (Department of Mechanical Engineering)

[redacted]

Dr. John. A. Barclay, Department Member (Department of Mechanical Engineering)

[redacted]

Dr. Maarten Van Emden, Outside Member (Department of Electrical & Computer Engineering)

[redacted]

Dr. Keith Prater, External Examiner (Ballard Power Systems Inc.)

University of Victoria

Abstract

Hydrogen (H_2) is a potential zero emission fuel for transportation vehicles. A barrier to its implementation is the issue of on-board storage, due to low densities at ambient conditions. Cryogenic liquefaction increases the volumetric energy density of H_2 but requires considerable energy input during the liquefaction process. Refrigeration work, required to liquefy the fuel, results in the fuel containing thermomechanical exergy. Vehicle powertrains typically utilize the chemical exergy contained in a fuel, but waste the thermomechanical exergy. With liquid hydrogen (LH_2), the thermomechanical exergy amounts to more than 10% of the chemical exergy.

This thesis investigates a hierarchy of options for recovering the thermomechanical exergy on board a LH_2 powered vehicle. Operating conditions are determined from the Ballard Phase II fuel cell powered bus. This work explores using the cold of LH_2 as a heat sink for a cryogenic heat engine. Such a heat engine could generate work to augment the main vehicle powerplant. Alternatively, the cold LH_2 can reduce the parasitic air compression load of the fuel cell powerplant and improve fuel cell operation. This work provides a thermodynamic comparison of several thermomechanical exergy recovery options. The systems are modelled and the net performance improvements quantified.

[redacted]

Dr. David S. Scott, Supervisor (Department of Mechanical Engineering)

[redacted]

Dr. John. A. Barclay, Department Member (Department of Mechanical Engineering)

[redacted]

Dr. Maarten Van Emden, Outside Member (Department of Electrical & Computer Engineering)

[redacted]

Dr. Keith Prater, External Examiner (Ballard Power Systems Inc.)

Table of Contents

Abstract ii

Table of Contents iii

List of Figures vi

List of Tables viii

Nomenclature ix

Acknowledgements xi

CHAPTER 1 INTRODUCTION 1
- 1.1 Motivation 1
- 1.2 Objective 3
- 1.3 Exergy 4
  - 1.3.1 Thermomechanical Exergy 6
  - 1.3.2 Chemical Exergy 10
- 1.4 Cryogenic Fuels 11
- 1.5 Project Background & Methodology 15

CHAPTER 2 PREVIOUS WORK 17
- 2.1 Relevant Prior Work 17
- 2.2 Cryogenic Process Cooling 17
- 2.3 Cryogenic Power Generation 19

CHAPTER 3 FUEL CELL VEHICLES 22
- 3.1 Hydrogen (H2) Fuel 22
- 3.2 Fuel Cell Powertrains 23

3.3 The Ballard Bus Program 27
3.4 Bus Design Conditions 29

CHAPTER 4 HEAT ENGINE CYCLES 30
4.1 Relevant Heat Engine Principles 30
4.2 Cryogenic Heat Engine Principles 31
4.2.1 Cryogenic Heat Engine Inefficiencies 32
4.3 Thermomechanical Exergy Recovery From Cryofuels 35
4.4 Ideal Cryogenic Exergy Recovery System (CERS) Cycle 37
4.4.1 Cooling Water Heat Recovery 40
4.5 Rankine Enhanced Cryogenic Exergy Recovery System (ECERS) and Modifications 42
4.6 Stirling ECERS 46
4.6.2 Stirling Heat Engine Model 50
4.7 Direct Expansion (DE) ECERS 54
4.7.1 Direct Expansion Heat Engine Model 55

CHAPTER 5 UNIQUE FEATURES OF ECERS FOR FUEL CELL VEHICLES . . 58
5.1 Compression Work Requirement 58
5.2 Cryogenic Air Compression 59
5.3 Cryogenic Air Separation 60
5.4 Low Temperature Heat Removal 62

CHAPTER 6 AIR ENHANCEMENT MODELS 64
6.1 Thermodynamic Modelling 64
6.2 System Model 65
6.2.1 AspenPlus Code Overview 65
6.2.2 Bus Schematic Model 66
6.3 Thermodynamic Data 68
6.3.1 Ortho-Para Hydrogen Conversion 68
6.3.2 AspenPlus Thermodynamic Data 70
6.4 Fuel Cell Model 71
6.5 Baseline Bus Model 72

6.6 Air Precooling 74
6.6.1 Direct Expansion/Air Precooling 77
6.7 Air Enrichment 79
6.7.1 Enriched Air Production for Storage 80
6.7.2 Peak Load Matching 81
6.7.3 Two Pass Heat Exchange 84
6.7.4 Steady-State Enriched Air Operation 86
6.8 Cryogenic Exergy Recovery to Increase Cooling 88
6.9 Cooling Load Reduction 88
6.10 Model Comparisons 90

CHAPTER 7 CONCLUSIONS & RECOMMENDATIONS 92
7.1 Conclusions 92
7.2 Recommendations for Future Work 94

REFERENCES 95

Appendix A

Fuel Cell Voltage Model 103

Appendix B

Fuel Cell Types and Applications 109

Appendix C

AspenPlus Model of Steady-State Air Enrichment 110

Appendix D

USABC Dynamic Stress Test 127

List of Figures

1.1: Combined system 5

1.2: Dimensionless exergetic temperature (t) vs. temperature 9

1.3: The Energy Service Palette 12

1.4: Chemical/thermomechanical exergy content of fuels 14

1.5: Hydrogen/methane thermomechanical and chemical exergy 15

3.1: Schematic PEM fuel cell 24

3.2: Typical fuel cell polarization characteristics 26

3.3: Basic fuel cell system 27

4.1: Reversible 2 Temperature engine 30

4.2: Carnot heat engine cycle 31

4.3: Work per unit cooling vs. thermal efficiency 34

4.4: H_2 temperature-entropy plane 36

4.5: Latent/sensible exergy ratios 37

4.6: Ideal Crogenic Exergy Recovery System (CERS) cycle 38

4.7: Enhanced Cryogenic Exergy Recovery System (ECERS) temperature-entropy plane 41

4.8: Superheated Rankine cycle and temperature-entropy plane 42

4.9: Mixed Working Fluid (MWF) Rankine cycle 44

4.10: Stirling heat engine cycle 47

4.11: Single stage Stirling machine power output vs. efficiency 51

4.12: Three stage Stirling schematic 52

4.13: Two stage Stirling engine output vs. Stirling efficiency 53

4.14: Supercritical Direct Expansion (DE) cycle 54

4.15: DE gross output vs. cycle pressure, isentropic efficiency 56
4.16: DE pump input power vs. output pressure 57
5.1: Binary phase diagram of O_2/N_2 mixture 61
6.1: AspenPlus code process modelling sequence 65
6.2: Basic bus system 67
6.3: Equilibrium para-H_2 concentration as a function of temperature 68
6.4: H_2 enthalpy vs. temperature data 71
6.5: Compressor, expander power vs. isentropic efficiency 73
6.6: Air precooling system 74
6.7: Compressor input power vs. efficiency 76
6.8: Compressor input power vs. heat exchanger ΔT 76
6.9: Compressor & fuel cell power vs. operating pressure 77
6.10: DE/air precooling system 78
6.12: Air enrichment schematic 81
6.13: Fuel cell output vs. current density, O_2 concentration 83
6.14: Non-recirculating air condensation 85
6.15: Mixed flow air enrichment system 86
6.16: Fuel cell output/cooling load 89
A.1: Voltage model results vs. actual data 107
D.1: USABC Dynamic Stress Test 127

List of Tables

1.1: Volumetric energy densities of H_2, NG and gasoline fuels 2

1.2: Comparison of fuels and carbon content 13

6.1: System descriptions 90

6.2: Steady-state output comparison 91

B.1: Fuel cell types and applications 109

Nomenclature

c_p	specific heat at constant pressure
E	thermodynamic potential
g	specific Gibb's free energy
H	enthalpy
h	specific enthalpy
$h_{r->p}$	heat of reaction
I	current density
i	current
m	mass
$\dot{m}$	mass flow rate
P	pressure
Q	heat
$\dot{Q}$	heat rate
Q_h	input (high temperature) heat
Q_c	output (low temperature) heat
R_{Ξ}	thermomechanical/chemical exergy ratio
$R_{electronic}$	electrical resistance
S	entropy
s	specific entropy
T	temperature
T_o	environmental temperature
T_h	hot end temperature
T_c	cold end temperature
U	internal energy
V	volume
v	voltage
W	work
W_{cs}	work out of combined system
$\dot{W}$	work rate

$\dot{W}_{fc}$	fuel cell output power
$\dot{W}_{c}$	compressor input power
$\dot{W}_{e}$	expander output power
y_e	environmental mole fraction
ΔT	temperature differential
η	thermal efficiency (1st law)
η_C	Carnot efficiency
η_S	Stirling efficiency
η_{act}	activation overvoltage
η_{ohmic}	ohmic overvoltage
Π	entropy production
σ	specific entropy production
τ	dimensionless exergetic temperature
Ξ	exergy
ξ	specific exergy
Ξ_{tm}	thermomechanical exergy
Ξ_{ch}	chemical exergy

Acknowledgements

I wish to thank my supervisor, Dr. David Scott, for convincing me to undertake this project and his guidance and support during the past two years. I wish also to thank the entire staff of IESVic and Cryofuel Systems, for the encouragement, wisdom and friendship. The contributors are too extensive to list but special thanks to Dolores Bogusz, Susan Walton and those who painfully read my early work. Special thanks also to Dr. John Barclay for the hardware access which was invaluable to this thesis.

I would like to acknowledge the Natural Science and Engineering Research Council of Canada and Ballard Power Systems Incorporated for their support through an Industrial Post-Graduate Fellowship.

Finally, I wish to thank my family and friends for their support in this endeavour. Special thanks to my sister-in-law Helen for her assistance in getting me started.

CHAPTER 1 INTRODUCTION

1.1 Motivation

The Institute for Integrated Energy Systems (IESVic) at the University of Victoria is engaged in the development of energy systems that simultaneously [1]:

- Offer a foundation for economic growth and industrial diversification,
- Cause minimal environmental intrusion and reduce climate destabilizing emissions,
- Provide flexibility and resilience in response to technical, geopolitical and environmental change.

An opportunity identified at IESVic is the adoption of low and zero carbon fuels, such as Natural Gas (NG) and Hydrogen (H_2), in the transportation sector. Currently, petroleum based fuels such as gasoline and diesel dominate the transportation sector. The combustion of petroleum based fuels is a main source of greenhouse gas emissions, contributing to the prospect of climate instability. If NG and H_2 are to significantly displace petroleum based fuels, they must penetrate the transportation sector [2].

The greatest barrier to the implementation of H_2 and NG as transportation fuels is the issue of on-board storage. Unlike conventional, liquid, petroleum based fuels, H_2 and NG are gases at standard temperature and pressure (STP). To increase their volumetric energy densities, H_2 and NG can be stored as high pressure gases or as cryogenic liquids. A cryofuel is a fuel liquefied at low temperature to increase its volumetric energy density. Table 1.1 shows the density and volumetric energy density (based on Lower Heating Value) of H_2 and NG fuels.

Table 1.1: Volumetric energy densities of H_2, NG and gasoline fuels

Fuel	Density (kg/m^3)	Volumetric Energy Density (MJ/l)
Compressed Natural Gas (CNG) @ 20 MPa	157	7.9
Liquid Natural Gas (LNG)	422	21.1
Compressed H_2 @ 20 MPa	15	1.7
Liquid H_2 (LH_2)	71	8.4
Gasoline	703	33.4

Liquefaction at low temperature (112 K for NG and 21 K for H_2 at atmospheric pressure) creates a higher energy density fuel suitable for transportation applications. Liquefied fuels would likely be the storage mode of choice were it not for the high cost of liquefaction, particularly in the case of liquid H_2 (LH_2). LH_2 requires a large work input to liquefy, which results in the fuel being out of thermomechanical equilibrium with the environment. Thermomechanical exergy represents the extent that the fuel is out of temperature and pressure equilibrium with the environment. Typically, the greater the work input required to liquefy the fuel, the greater the thermomechanical exergy.

Powertrains are usually chemical energy conversion devices. Conventional fuels, such as gasoline, contain only chemical exergy. Gasoline is chemically out of equilibrium with the environment, but stored at environmental temperature and pressure. As powertrains are engineered to use low and zero carbon fuels, the opportunity exists to recover the otherwise wasted thermomechanical exergy associated with the mode of storage.

LH_2 is not the only fuel containing thermomechanical exergy. Compressed H_2, liquified NG (LNG), compressed NG (CNG) and liquified petroleum gas (LPG) all contain thermomechanical exergy. Each must have work input as refrigeration or compression. LPG is stored as a liquid at elevated pressure (approximately 0.5 Mpa) and ambient temperature. The work input to produce LPG from propane is considerably less than that to liquefy H_2, which requires cooling to 21 K at atmospheric pressure. LH_2 has the highest thermomechanical to chemical exergy ratio of any of the aforementioned fuels.

The opportunity to exploit the thermomechanical exergy of LH_2 in transportation applications is the motivation of this thesis. The utilization of the thermomechanical exergy of LH_2 has the potential to improve vehicle powertrain efficiency and power output.

1.2 Objective

This thesis investigates the opportunities to recover thermomechanical exergy from LH_2 vehicle fuel. A goal of this thesis is to provide a pathway for future design and development work that will improve overall powertrain efficiency and facilitate the use of LH_2 as a vehicle fuel. The objective of this thesis is to identify the most promising thermomechanical exergy recovery options in a vehicular application. Several configurations for exergy recovery are compared and their improvement on powertrain performance is quantified.

The principles of this study are applicable to other lower carbon fuels, such as CNG, LNG and compressed H_2, but LH_2 has the greatest thermomechanical exergy content and thus offers the greatest rewards through exergy recovery. The concepts explored within this thesis are applicable to a wide range of transportation applications. Analysis on a case specific basis determines the design and viability of thermomechanical exergy recovery for particular vehicle/fuel combinations.

This study uses the design specifications of the Ballard Phase II bus. This is a fuel cell powered, urban transit bus manufactured by Ballard Power Systems of Burnaby, British Columbia. This vehicle currently operates on compressed H_2.

Several options exist to exploit the "cold" contained within LH_2. The configurations explored in this thesis are evaluated on a thermodynamic basis to identify possible powertrain improvements through exergy recovery. Although not a focus of this thesis, economics will ultimately determine the viability of any exergy recovery system. Exergy recovery has the opportunity to displace fuel cell capacity and reduce capital cost.

Incorporating an exergy recovery system into a powertrain will have the following effects on the overall vehicle powertrain:

- Increased efficiency.
- Increased power output.
- Potentially increased capital cost.

The focus of this work is on the first two points, but the third will be equally important in determining the suitability of an exergy recovery device. Capital cost of an exergy recovery device will have to compete with the capital cost of the fuel cell powerplant on a unit output basis to determine its viability. The most promising systems are identified and the net output improvements quantified. This work is meant to a basis for future design work to incorporate a cryogenic exergy recovery device into a vehicle powertrain.

1.3 Exergy

A cryofuel offers unique opportunities by being out of thermomechanical equilibrium with the environment. Exergy, a measure of "disequilibrium" with the environment, is a true indicator of the work that can be produced through equilibrating the fuel with the environment. This thesis uses exergy as a measurement of a fuel's utility to identify opportunities. Exergy of a stream of matter is defined as:

> "the maximum amount of work obtainable when the stream is brought from its initial state to the dead state by processes during which the stream may interact only with the environment" [3]

A simple system, shown in Figure 1.1, at a pressure P, and temperature T surrounded by an environment at P_o, T_o can illustrate the principle of exergy.

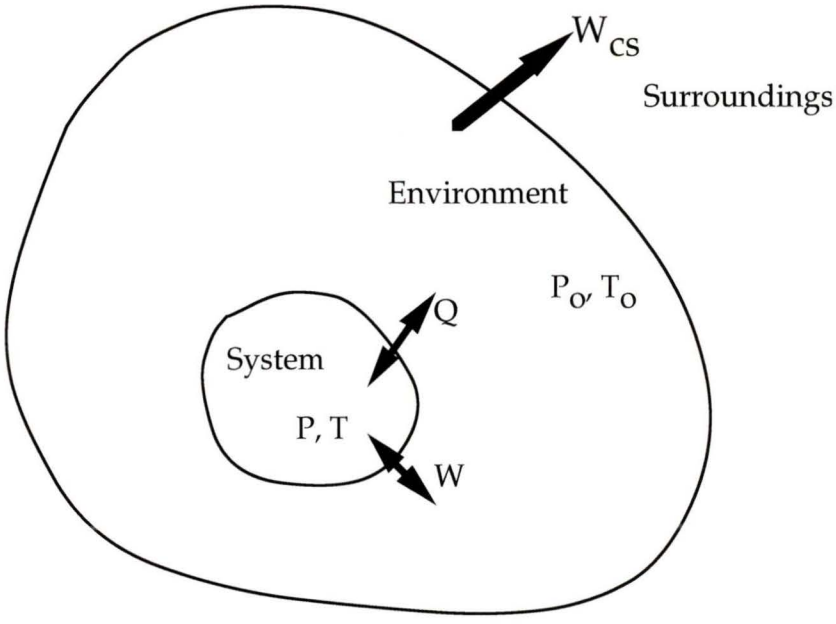

Figure 1.1: Combined system used to describe exergy

In this analysis, the system boundaries are a choice of convenience defined by the analyst for the particular problem at hand [4]. The environment is defined as the region surrounding the system and that with which it interacts. The environment is considered sufficiently large that its properties are unaffected by any interaction between it and the system. The surroundings represent the background conditions sufficiently removed from the system so that no interaction takes place between the system and the surroundings. There may be work and heat interactions between the system and its environment and through these interactions work may be produced by the combined system (system + environment). The work of the combined system is W_{cs}.

The exergy of the system is defined as the maximum amount of work which can be extracted from the combined system, as the system is brought to equilibrium with the environment. Internal heat, work and chemical reactions may be involved. Thus exergy is a property of not only the state of the system but also that of the environment.

Exergy differs from energy because it is a consumable property (energy is conserved). Exergy analysis of systems can give valuable insight into processes as it is a true measure

of the work that can be extracted by an ideal process. Energy analysis, or 1st law analysis, can cause confusion as the results give no insight into what degree a process approaches the ideal. Energy is a poor measure of the work required for low temperature refrigeration. A very low temperature body may have a minimal energy content but this does not imply that little energy is required to reach this state. Exergy reflects differences between the system and the environment, whether the system has a greater or lesser energy content than the environment.

Exergy can be divided into two components, thermomechanical exergy (also called physical exergy) and chemical exergy [3]. The analysis can be split between physical processes and chemical processes equilibrating the system with the environment.

1.3.1 Thermomechanical Exergy

Consider the system in Figure 1.1. If the pressure changes through a process from P to P_o and the temperature from T to T_o, the system is brought to an equilibrium state called the restricted dead state. In this state, the system is in thermomechanical equilibrium with the environment, but there have been no chemical or mass interactions with the environment.

The thermomechanical exergy, Ξ_{tm}, is defined as the maximum work obtainable by bringing the system into thermal and mechanical equilibrium with the environment. The thermomechanical exergy is determined by the states of the system and the environment, and in no way reflects any particular equilibrating process. The expression for thermomechanical exergy, an extensive property, is;

$$\Xi_{tm} = [(U+KE+PE+...)-U_o] + P_o(V-V_o) - T_o(S-S_o) \qquad (1.1)$$

U, V, S are the internal energy, volume and entropy of the system, respectively. U_o, V_o, S_o, and T_o are the internal energy, volume, entropy and temperature of the same substance at the environmental conditions. The total energy of the system represents all forms of energy including kinetic energy (KE), potential energy (PE), electromagnetic and nuclear

[5]. In this thesis, KE, PE and electromagnetic energy are neglected. However, in the case of LH_2, the energy difference in its two nuclear states, ortho and para, becomes significant and must be considered [6].

If we extend this expression to the work produced for the combined system through the equilibrating process, we obtain the relationship:

$$W_{cs} = (E-U_o) + P_o(V-V_o) - T_o(S-S_o) - T_o \Pi \tag{1.2}$$

where Π is the entropy produced in the system. The final term is the exergy destruction, or irreversibility, of the process. Thus, the real work obtainable from a system is the difference between exergy, a state property, and the irreversibility of a particular process.

The thermomechanical exergy change between two states, denoted as 1 and 2, is equal to the sum of the exergy "fluxes" crossing the system boundary. In an open system, this is:

$$\Xi_2 - \Xi_1 = \Xi_Q + \Xi_W + \Xi_F - T_o \Pi \tag{1.3}$$

where Ξ_Q, Ξ_W, and Ξ_F are exergy flows associated with heat, work, and mass flows across the system boundary, respectively.

The exergy transfer with work, Ξ_W, is

$$\Xi_W = \{W_{cs} - P_o(V_2 - V_1)\} \tag{1.4}$$

where W_{cs} is the work out of the system and the $P_o(V_2 - V_1)$ is the work done on the environment through any volume change. Any work out of the system is pure exergy. The fuel cell electrical output, as well as any mechanical work produced in an exergy recovery system, are 100% exergy streams.

The exergy transfer with heat, Ξ_Q, is given as

$$\Xi_Q = \oint \left(1 - \frac{T_o}{T}\right) dQ \tag{1.5}$$

which, for a finite number of heat transfers, can also be expressed as:

$$\Xi_Q = \sum_j \left(1 - \frac{T_o}{T_j}\right) Q_j, \tag{1.6}$$

so, for a given quantity of heat, at a fixed temperature T

$$\Xi_Q = \left(1 - \frac{T_o}{T}\right) Q \tag{1.7}$$

When dealing with cryogenic applications the dimensionless exergetic temperature, τ, defined as $(1 - T_o/T)$ [3], is an important parameter. With $T > T_o$, τ is always < 1 and exergy and heat flow in the same direction, and the magnitude of Ξ_Q is always less than Q. Intuitively, if we add heat to a hot body, we will increase the exergy of that body. However, if $T < T_o$, as Q flows into the system, the system's exergy decreases as it is brought closer to temperature equilibrium with the environment. If $T < 1/2\ T_o$, the magnitude of exergy accompanying a heat flow exceeds the quantity of energy itself. Figure 1.2 plots τ as a function of temperature, illustrating the significant exergy, and thus work capacity, that accompanies a fixed amount of heat in cryogenic applications. At very low temperatures a high amount of exergy accompanies a fixed amount of heat. Thus the work required to produce, or the work available from, a given amount of heat increases disproportionally as the temperature decreases.

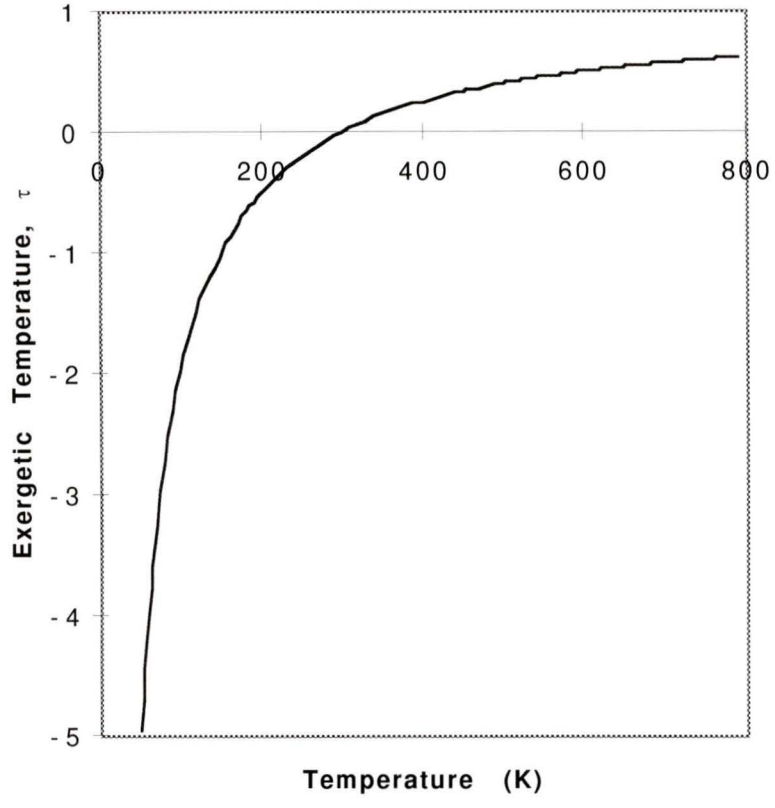

Figure 1.2: Dimensionless exergetic temperature (τ) vs. temperature

The exergy transfer accompanying a unit mass flow across the system boundaries is

$$\Xi_F = H - T_oS - (H_o - T_oS_o) + KE + PE \tag{1.8}$$

Defining the exergy functions $B = H - T_oS$ and $B_o = H_o - T_oS_o$, equation (1.8) simplifies to:

$$\Xi_F = B - B_o + KE + PE \tag{1.9}$$

The exergy function has also been referred to as the steady flow availability function, a [4].

The exergy balance for an open system, with mass transfer across the boundaries, is defined as follows [7]:

$$\Xi_2 - \Xi_1 = \int_1^2 (1 - \frac{T_o}{T})dQ - \{W - P_o(V_2 - V_1)\} + B_i - B_e - T_o\Pi \qquad (1.10)$$

B_i and B_e are the entering and exiting exergy functions of the streams of matter crossing the system boundary as previously defined.

1.3.2 Chemical Exergy

Chemical exergy may be defined as:

> *"Chemical exergy is equal to the maximum amount of work obtainable when the substance under consideration is brought from the environmental state to the dead state by processes involving heat transfer and exchange of substances only with the environment."* [3]

The chemical exergy of a material is the maximum work obtained by bringing the individual components into chemical equilibrium with the environment. If the components present are not present in the reference environment, they must be reacted to produce reference components. Therefore, to calculate the work available in a non-reference component, we react it to produce reference components, and then equilibrate the concentration of the reference components to the environmental levels.

Studying H_2 as a fuel for a fuel cell, the overall cell reaction is

$$H_2 + \frac{1}{2}O_2 \rightarrow H_2O$$

The specific chemical exergy of the H_2 fuel, $\xi_{ch,H2}$, is a function of the specific Gibb's functions, $g(T_o,P_o)$, of the reactants and products at the reference environment conditions,

the reaction stoichiometry and the concentration of the reference materials in the reference environment, y_e.

$$\xi_{ch,\,H_2} = \left[g_{H_2} + \frac{1}{2} g_{O_2} - g_{H_2O} \right](T_o, P_o) + RT_o \ln \left[\frac{y_{e,\,O_2}^{1/2}}{y_{e,\,H_2O}} \right] \tag{1.11}$$

Equation (1.11) can be discussed in two parts; the reaction to reference materials (in this case H_2O) and the compression/decompression to the environmental partial pressures of the individual components. The Gibb's functions (evaluated at T_0 and P_0), multiplied by the stoichiometric coefficients, account for the reaction to reference components. The second term accounts for the expansion/compression of the reference components to the environmental concentrations.

Conventional powertrains harness chemical exergy. Gasoline, for example, at STP is combusted to produce products with lower chemical exergy. Some portion of this chemical exergy is converted into useful work to move the vehicle.

1.4 Cryogenic Fuels

Although we typically think of the energy system from a source perspective, it is services that really drive the system. Fuels function as an "energy currency", enabling a given service upon demand [8]. A fuel's utility lies in it transporting energy from a distant source to the point of use. The service at the point of use can be powering an automobile, cooking a roast, or drying newsprint.

The need to differentiate between energy sources and energy currencies is a relatively new concept [9]. Traditional energy currencies have masked the distinction between sources and currencies because they have often had a commonality of material. Coal, wood and gasoline as currencies all share material with their respective sources and involve varying degrees of processing to convert from raw material to useable fuels.

As we enter the 21st century, emerging alternate energy sources will require the decoupling of the source-currency material bonds. Sources and currencies may share no common material, as they have with petroleum based fuels. Solar or wind energy, as an example, require an independent currency to provide services. Electricity is a convenient energy currency for many services, such as illumination or communication, but is difficult to store or transmit long distances. In this target study of a transportation vehicle, electricity is not a convenient energy currency, as it is difficult to use in high demand, mobile applications. H_2 provides a pathway for electricity, or at least energy sources tailored to electricity generation, to reach the transportation sector.

Figure 1.3 presents the "energy service palette". Traditional fossil energy sources provided chemical and electrical energy services. In the future, as new energy sources are developed, electrolytic H_2 will become a necessary energy currency to deliver transportation services.

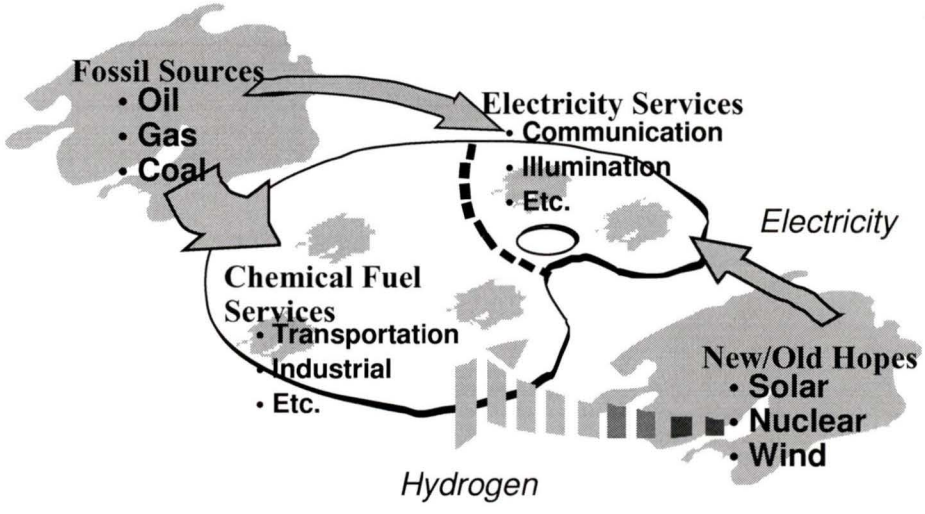

Figure 1.3: The Energy Service Palette [10]

The environmentally benign nature of NG and H_2 stems from the high H_2 to carbon ratios. Carbon directly results in the production of greenhouse gases, a contributor to the prospect of climatic instability. These fuels are naturally less dense than carbon rich conventional fuels because of the absence of the heavy carbon molecules. The normal boiling points and ideal work of liquefaction at 300 K, 0.1 MPa reference conditions of traditional, low- and zero-carbon fuels are shown in Table 1.2.

Table 1.2: Comparison of fuels and carbon content [11] [12] [13]

Fuel	Chemical Formula	Normal Boiling Point (K)	Critical Temperature (K)	Ideal Work of Liquefaction (kJ/kg)
Octane	C_8H_{18}	399	569	0
Propane	C_3H_8	231	370	140
Methane	CH_4	112	191	1091
Hydrogen	H_2	20	33	12019

The critical temperature of the fuel determines the nature of the required liquefaction work. Substances with critical temperatures well below ambient, such as CH_4 and H_2, require refrigeration to liquefy.

The production of H_2, whether electrolytic or through Steam Methane Reforming of NG, requires processing which increases its chemical exergy. Low carbon fuels in high pressure gaseous or low temperature liquid form have also undergone processing that increases their thermomechanical exergy.

The chemical and thermomechanical exergy can be calculated for all fuels. A useful parameter is the ratio of thermomechanical to chemical exergy, R_Ξ. R_Ξ can range from zero for gasoline or diesel, to infinity for steam, a common "fuel" used in industrial environments. The first transportation systems designed to use next generation fuels have not yet turned attention to recovering the thermomechanical exergy which is quite substantial within certain fuels. Figure 1.4 shows the chemical and thermomechanical exergy content of some common energy currencies.

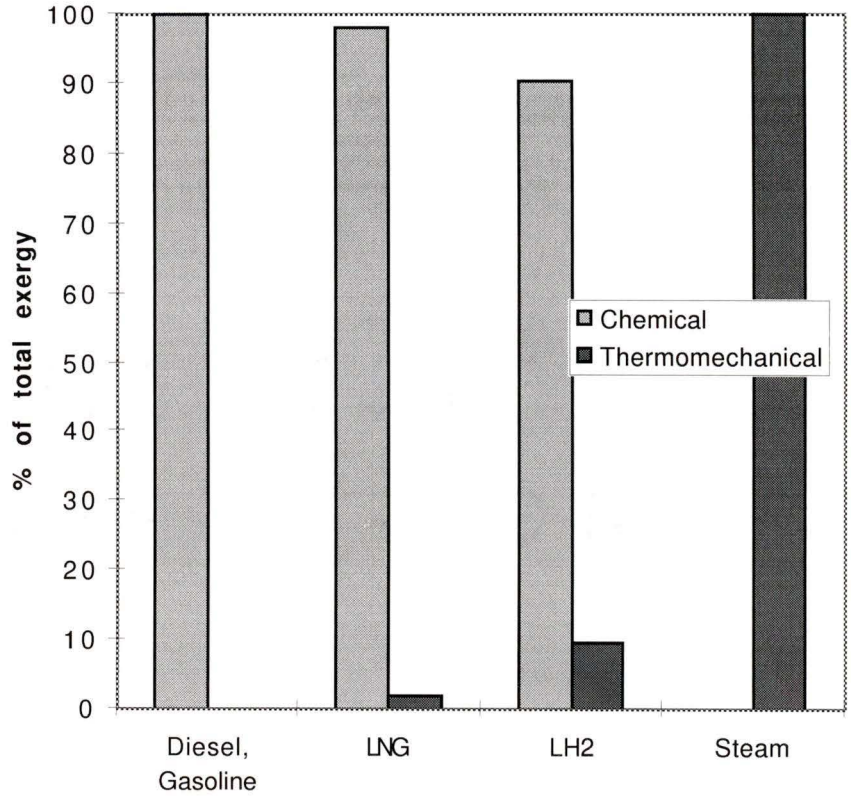

Figure 1.4: Chemical/thermomechanical exergy content of fuels

Energy conversion devices are typically engineered to recover only one form of exergy, whether they are steam turbines, gas barbecues or automobile engines. R_{Ξ} becomes significant for low carbon fuels stored at high pressure or low temperature. R_{Ξ} of LNG is approximately 2% and that of LH_2 is 10% (see Figure 1.5). LNG exergy recovery has been pursued in high volume utility applications (summarized in Chapter 2) but LH_2 exergy recovery shows greater promise in transportation applications. Innovative powertrains can utilize the thermomechanical exergy. This serves to further increase the energy utility of the on board fuel as well as recuperate some of the energy expenditures incurred in initially liquefying the fuel.

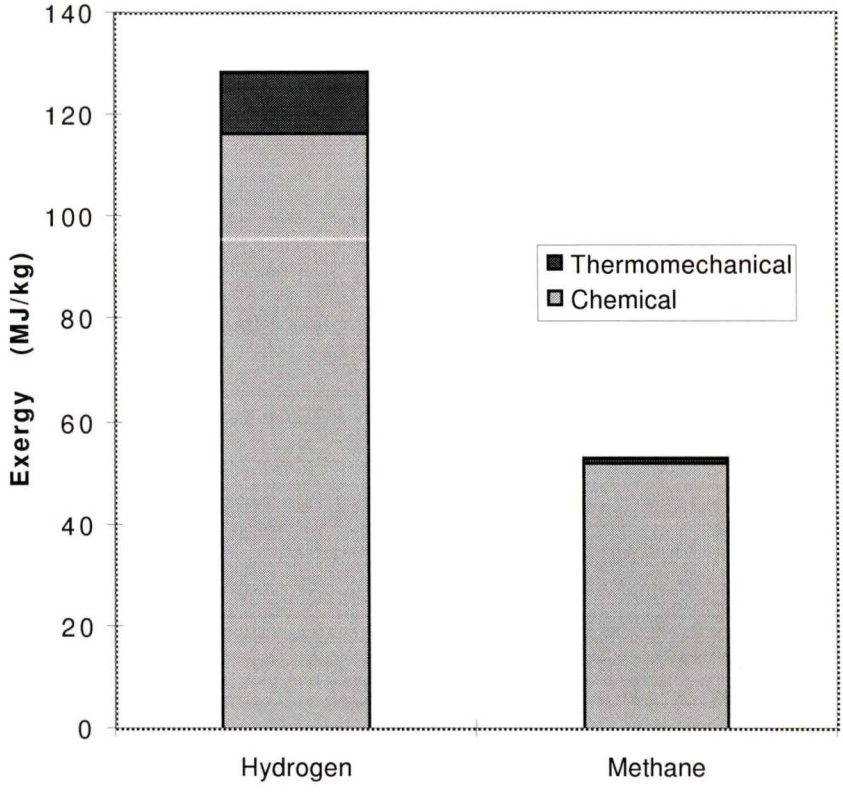

Figure 1.5: Hydrogen/methane thermomechanical and chemical exergy content

1.5 Project Background & Methodology

A Cryogenic Exergy Recovery System (CERS) was first envisioned as a work producing device that could operate between the vapourization temperature of a warming cryofuel and ambient [34]. Thermodynamically, this is a low temperature heat engine, or cryoengine. A cryoengine on a fuel cell bus could operate an air compressor or drive an electrical generator.

The concept of CERS was expanded to an Enhanced Cryogenic Exergy System (ECERS) by further examining the interaction of the heat engine and the main vehicle powerplant.

ECERS is defined as any thermomechanical exergy recovery system that synergistically interacts with specific operating conditions in a particular application to improve overall performance and efficiency. Powertrains typically have a high temperature waste heat stream available for heat input to a low temperature heat engine cycle. Higher temperature heat addition increases heat engine efficiency and output.

In a fuel cell vehicle, the cold LH_2 could improve powertrain operation by precooling the air stream prior to compression, thereby reducing the parasitic compression load. Furthermore, cooling could be used to produce an oxygen (O_2) rich stream to enhance the performance limiting cathode reaction in a fuel cell.

ECERS configurations for the Ballard Phase II bus are described and modelled in this thesis. The configurations are categorized into heat engines and air system enhancements.

The next two chapters provide background information on cryogenic exergy recovery and the particular fuel cell application studied in this thesis. Chapter 4 explains heat engine ECERS and contains thermodynamic analyses of the most promising cycles. Chapter 5 describes possible air system enhancements and their modelling. Since air system enhancements have a direct impact on fuel cell performance, these models include a fuel cell performance model to predict the response to various air system changes. Chapter 6 details the air system enhancement models completed using AspenPlus, a commercial process simulation code. Results are concluded in Chapter 7 with recommendations for future work.

CHAPTER 2 PREVIOUS WORK

2.1 Relevant Prior Work

Little work has been done on thermomechanical exergy recovery in transportation systems in the past. As indicated in Chapter 1, traditional vehicle fuels have contained only chemical exergy. This Chapter reviews previous work in cryogenic exergy recovery. Most of this work has focused on LNG regasification as it involves large quantities of exergy and has been in existence for more than three decades.

2.2 Cryogenic Process Cooling

LNG has been imported into France and England since 1965 [14]. Japan began importing LNG in 1969 and as of 1985 total imports were 27 million tons per year [15]. Liquefaction reduces the storage volume compared to gas (at atmospheric pressure) transport by a factor of 600 to 1 [16]. However a considerable amount of energy, typically 17% of the combustion value of the fuel, is required to liquefy natural gas at its normal boiling point of 112 K.

The quantities of NG handled at large receiving terminals, most notably in Japan, coupled with the significant cold energy content of the LNG has led to the development of technologies to utilize the LNG cold. At such terminals LNG is received by tanker and stored in liquid form. Initially, LNG was regasified through heat exchange with sea water but the opportunity exists to use the cold for a variety of purposes. Cryogenic Exergy Recovery has been in existence since the 1970's [17] with the initial influx of large quantities of LNG into Japan and France.

Applications for LNG cold utilization have been suggested for carbon dioxide (CO_2) liquefaction and solidification, food freezing and storage, sea water desalination, petrochemical processing and cryo-refrigeration [17] [16]. The world's first industrial venture to recapture LNG thermomechanical exergy was Tokyo Liquefied Oxygen Co., started on December 23, 1969 specifically to commercialize the utilization of LNG cold in air separation. The original Negishi works air separation plant, completed in 1971, was designed to utilize 8 t/hr of Tokyo Gas' 15 to 45 t/hr LNG load [16] [18]. Since this time, several other plants have been built. Power consumption savings of 30 - 40% compared to conventional air separation plants have been reported and typically displace the necessary electrical input power to the facility [17] [19] [20].

Other applications include deep freeze warehousing of foodstuffs, beginning in 1974, and cryogenic crushing operations which have operated since 1977 [17]. LNG has also been proposed, over short distances, as a cryogenic cooling medium for superconducting power transmission cables [21].

The main challenges experienced in the various efforts to exploit LNG cryogenic exergy pertain to coupling two separate facilities with asynchronous characteristics [16]. The NG utility ultimately controls the flow of LNG available based on gas and power demand. NG demand, however, does not coincide with fluctuations in cooling requirement at the adjoining facilities. LNG cryogenic exergy recovery facilities have been constrained to operate on a LNG flow rate of 20 - 30% of the average LNG flow available [21][18]. In addition, proposals for LNG cold use are physically constrained by the location of the regasification facility. A limit of 2 to 3 km has been given as the maximum for a cryogenic pipeline capable of handling LNG to a user facility, based on installation costs and heat losses [16].

Witwer [22] evaluated several industrial options for the most efficient use of LNG cold. These included district air conditioning, power plant condenser cooling, and liquid nitrogen (LN_2) backhaul systems; LN_2 produced while regasifying LNG is returned by tanker to be used in the LNG liquefaction process. Generally, the cold must be utilized at a low temperature to make it economically feasible. One of the proposals made was the development of an integrated coldplex including multiple uses such as air separation, ethylene production and ammonia production. The predicted energy savings in the

processes amount to one third of the energy input to liquefy the NG prior to shipment. The energy savings in the gas processing plants are realized by displacing cooling loads that would otherwise be required and through precooling gas streams prior to compression to reduce the compression work requirement. In addition to reducing the compression work requirement in gas processing industries, Mitsubishi and others have investigated using LNG to improve gas turbine cycle efficiencies through inlet air precooling [23] [24]. Such gas cycles can be incorporated with larger Rankine power cycles which typically are the large consumers of regasified NG.

Research concerning cryogenic exergy recovery in transportation applications using LNG has been relatively limited, due to the relatively small quantities of exergy available. Nevertheless, meeting an on-board cooling load with a regasifying cryofuel stream can be economically preferred to supplying equipment and energy. Acker [25] has proposed using the cooling available from a LNG marine powerplant to freeze shrimp on board.

H_2 active cooling of airframe surfaces is part of the National Aero-Space Plane (NASP) design. This proposed hypersonic aircraft is powered by slush H_2, a solid-liquid H_2 mixture. The heat stress generated by high speed flight requires active cooling of leading edge surfaces, which is accomplished by the vehicle fuel [26].

2.3 Cryogenic Power Generation

Numerous proposals have been made using LNG revapourization as the heat sink for cryogenic electrical power generation. The Tokyo Electric Power Co. began operation of the first cryogenic power plant using sea water as a heat source in 1979, producing 442 kW at a LNG flow of 10 ton/hr [17] using a composite Direct Expansion (DE), Rankine cycle. The basic DE cycle consists of pressurizing the LNG, warming it to ambient conditions through constant pressure heat exchange, and then expansion to low pressure in a turbine, producing work. To date, more than 15 such plants have been built, with electrical generating capacity in excess of 9 MW at a LNG flow of 150 tons/hr [27].

Power generating facilities have been built utilizing direct NG expansion, secondary working fluid power cycles, gas power cycles and various combinations [24] [28]. Exergy efficiencies of up to 37% have been quoted for both composite DE/regenerative Rankine and mixed refrigerant Rankine cycles [27]. Ruhemann [29] has claimed the design of a 2 step cascade type mixed working fluid system with an exergy efficiency of 45%.

Hybrid Brayton LNG cycles have been propsed with energy efficiencies of 44% for open and 27% for closed systems [27]. A hybrid plant has been proposed using H_2 combustion as a heat source and gasifying LH_2 as a heat sink in a Brayton power cycle [30]. This system has a predicted exergy efficiency of 35%.

Stirling cycle, large scale cryogenic power plants have been proposed for LNG or LH_2 operation, receiving waste heat if available or heat from the environment and discharging heat to the cryogenic fuel. A four cylinder experimental model has been built and tested using helium (He) at a mean pressure of 3.6 MPa as the working fluid. Work output of 47 W has been obtained, corresponding to an efficiency of 14.7% of Carnot [31].

In terms of transportation applications, a Rankine cycle heat engine has been designed and tested to augment the LH_2 powered Internal Combustion (IC) engine developed at Musashi Institute of Technology. The engine was designed to operate using either atmospheric heating or, preferably, the exhaust gas of the main engine. An experimental expander has been built using CH_4 as a working fluid and LN_2 as a heat sink. The experimental set up has produced power at a rate of 0.89 kW, consuming 12.9×10^{-3} kg/s of LN_2 at a thermal efficiency of 26%. For comparison, the ideal Carnot efficiency is 63.5% over the same 115 K to 315 K operating range [32].

Research is being conducted at the University of Washington on a purely LN_2 powered engine as a zero emission powerplant [33]. The principle of operation is an open DE type Rankine cycle. It is doubtful that such a powerplant relying solely on the LN_2 thermomechanical exergy would be practical from an energy and power density perspective. However, the principles involved are directly applicable to a powerplant that would harvest first the thermomechanical exergy of a fuel and then the chemical exergy in the main fuel cell or combustion engine.

Research began in 1992 at the University of Victoria to evaluate options for LH_2 cryogenic exergy recovery on the Ballard Phase I Bus [34] [35]. The work focused on the preliminary design of a cryogenic heat engine to generate electricity. The electricity could then be used wherever required on the bus platform, displacing fuel cell output. The work outlined the thermomechanical exergy available and identified the most promising heat engine candidates. The conclusion of the preliminary analysis was that Stirling heat engines showed the most promise for cryogenic latent exergy recovery. The work of this thesis follows on that by Drs. D. Scott and D. Li, and A. Fyke and P. Crane over the 1992 -1994 timeframe.

CHAPTER 3 FUEL CELL VEHICLES

3.1 Hydrogen (H_2) Fuel

H_2 is one of the cleanest fuels available for transportation applications. H_2 has the benefit of zero local pollutants at the point of consumption. If produced from water using a clean energy source, it is truly an emission-free fuel [36]. H_2 production from Steam Methane Reforming (SMR) of NG or fossil based electricity does involve emissions of potential greenhouse gases, but generally less than that of conventional fuels. H_2 may be used as fuel for either fuel cell or IC engine powertrains, although fuel cells are the focus of this work. Fuel cells are more efficient power conversion devices than modern IC engines.

There are many ways to store H_2 fuel on vehicles. In addition to LH_2, fuel cell vehicles can operate with compressed H_2, methanol, or H_2 stored in metal hydrides. LH_2 has the advantage of a liquid fuel with high energy density, without the need for any complex on-board "chemical plant" [37]. LH_2 storage on board a vehicle achieves a H_2 mass fraction of 6 to 15% of the total fuel storage system. Comparable values are 1.5% for metal hydrides and 4% for compressed H_2 [38]. Daney et al have identified that LH_2 vehicles require the least amount of fuel and the smallest drivetrain for H_2 vehicles operating over a fixed range. LH_2 provides the high energy density and convenience required to penetrate the transportation market. Although cost currently works against LH_2 as a vehicle fuel, the technology is still in its infancy. A standard technology life-cycle learning curve will result in reduced costs, and allow the benefits of H_2 to be realized [39].

3.2 Fuel Cell Powertrains

Several types of fuel cells exist and are under development for a variety of applications. A brief summary of fuel cell types, operating temperatures and potential applications are given in Appendix B. Low temperature fuel cells show the most promise in transportation applications. Alkaline (AFC), Phosphoric Acid (PAFC), and Polymer Electrolyte Membrane (PEMFC) fuel cells, classified by electrolyte type, have been the subject of the most research and development in transportation applications [39].

The European Elenco Eureka bus project has produced an 80 passenger AFC articulated bus, powered by an 80 kW alkaline stack with a hybrid Ni-Cd buffer battery. The U.S. DOE has been investigating PAFC systems for bus powertrains [39].

Perhaps the most successful development to date in vehicle FC powertrains is in the PEMFC field. General Electric demonstrated the first application of such a fuel cell with a 1 kW unit used in Gemini space flights [39].

Ballard Power Systems of North Vancouver, B.C., have successfully demonstrated 20 seat, 32 foot and 60 passenger, 40 foot PEMFC powered buses.

The electrode reactions of the PEMFC and the PAFC are identical:

(anode) $H_2 \rightarrow 2H^+ + 2e^-$

(cathode) $\frac{1}{2} O_2 + 2H^+ + 2e^- \rightarrow H_2O$

The key element to the PEMFC system is the extremely thin membrane electrolyte permitting high ionic conductivity but low electronic conductivity. Figure 3.1 illustrates the principle of PEMFC operation. H_2 dissociates into 2 protons at the anode which are carried through the polymer electrolyte to the cathode where they associate with the O_2 to form product H_2O. The 2 electrons travel through an external circuit from cathode to

anode, powering an external load. The dissociation/association processes are accelerated by the presence of a catalyst at the electrode/membrane interface.

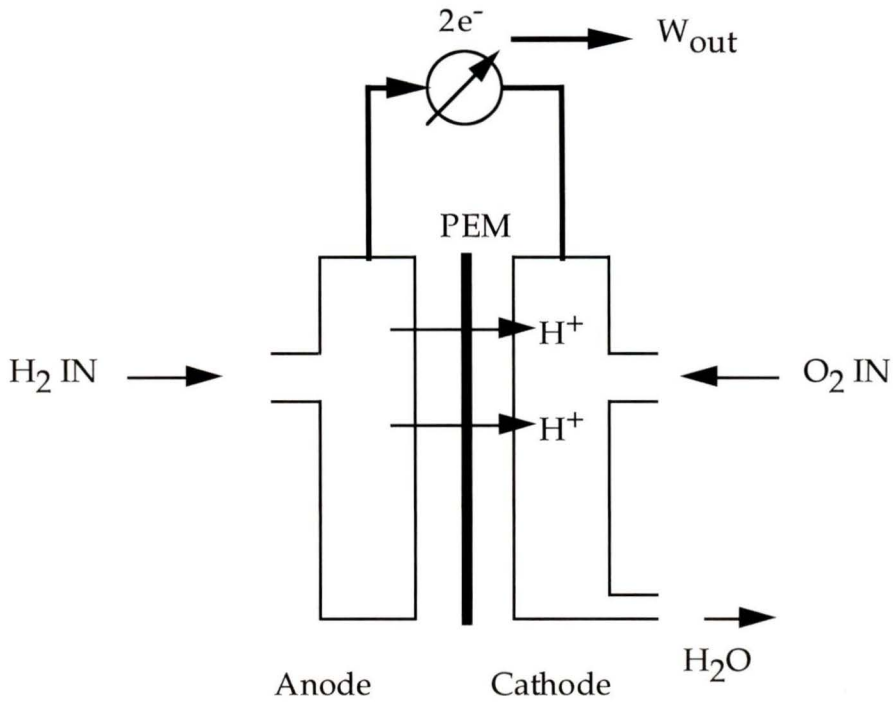

Figure 3.1: Schematic PEM fuel cell

Advantages of the PEMFC over AFC designs in transportation applications are:
- high current density; reduced weight and size,
- potentially lower cost,
- tolerance of CO_2; operation on air as an oxidant and reformates of H_2 as fuel,
- immobilized electrolyte.

Disadvantages at present are:
- sensitivity to even low concentrations of CO,
- high cost and loading of platinum catalyst,
- high membrane costs,
- membrane hydration required: humidification of fuel gases required,
- pressurization of oxidant stream and parasitic losses incurred to increase O_2 partial pressure at the cathode.

The voltage output of a PEMFC is given by the relation:

$$v = E + \eta_{act} + \eta_{ohmic} \quad (2.1)$$

E is the thermodynamic potential of the reaction $H_2 + 1/2\ O_2 \rightarrow H_2O$. Activation overvoltage (η_{act}) is the overvoltage applied at the electrodes to overcome slow reaction kinetics. The cathode reaction is slow when compared to the anode reaction, and is compounded by an O_2 partial pressure of 0.21 x air pressure [62]. The activation voltage drop can be primarily attributed to the slower cathode reaction. PEMFC system designs typically incorporate air compression to increase the O_2 partial pressure and overcome slow cathode reaction kinetics. Air compression, however, requires additional equipment and represents a parasitic load on the fuel cell system. A significant focus of this thesis is on the reduction of this parasitic load.

Ohmic overvoltage (η_{ohmic}) is due to resistance to proton transfer in the solid polymer membrane and follows an Ohm's law equation of the form:

$$\eta_{ohmic} = - i \times R_{electronic} \quad (2.2)$$

$R_{electronic}$ represents the electrical resistance of the fuel cell and i is the current flowing through the cell. Typical polarization characteristics of a PEMFC show a near linear decline in voltage as current increases. The open circuit voltage is less than the thermodynamic potential (1.23 V) due to cathode activation polarization. Gaseous diffusion becomes significant at higher current densities and the voltage-current relationship becomes non-linear. Low power output and poor fuel efficiency preclude operation past the linear regime. A characteristic polarization curve is presented in Figure 3.2.

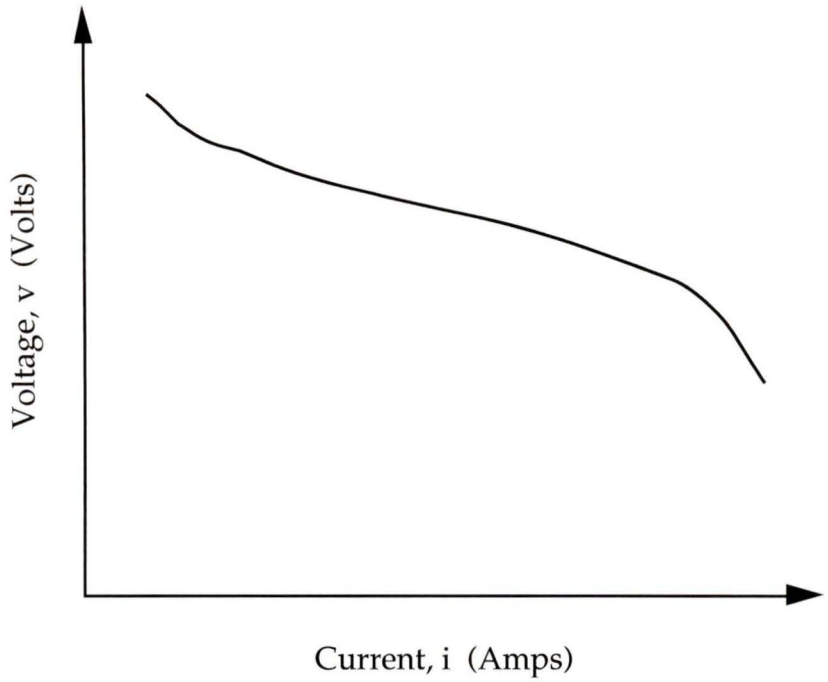

Figure 3.2: Typical fuel cell polarization characteristics

In PEMFC designs, pressurizing the oxidant stream to increase the O_2 partial pressure overcomes the low exchange current density of the cathode. This pressurization results in a net parasitic load reducing the gross fuel cell power delivered to the drivetrain. This parasitic load, on the order of 15% of the gross power produced, provides a unique opportunity for an ECERS as will be explained in further chapters.

Figure 3.3 illustrates the basic fuel cell powertrain. "Additional" major features in the basic vehicle powertrain are fuel reformers (allowing use of methanol, ammonia, NG, etc.) and hybrid power systems using various battery technologies. In addition, various regenerative braking arrangements can be applied, working in conjunction with the electrical power output of the vehicle.

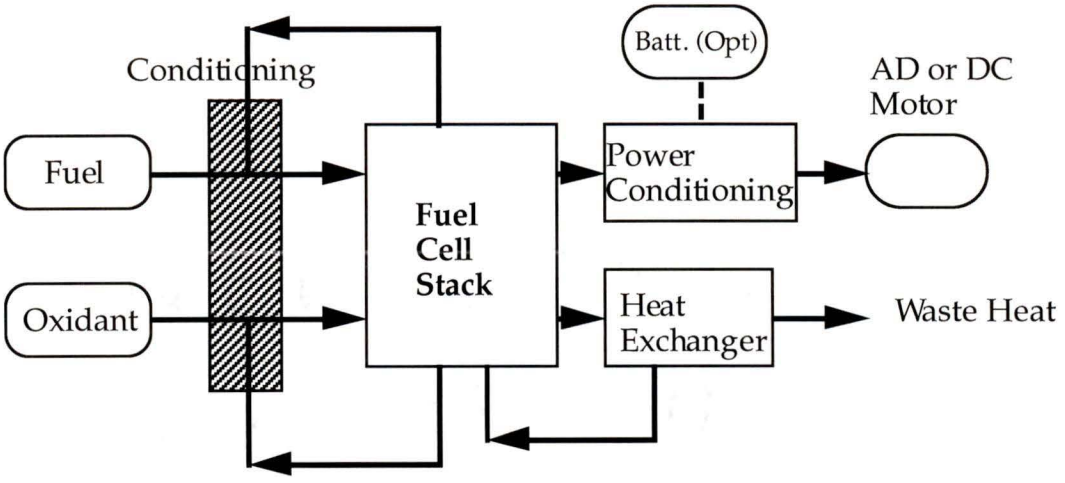

Figure 3.3: Basic fuel cell system

A pure H_2 powered vehicle has a powertrain that produces electrical output to drive an electrical traction motor as in a conventional trolley bus. The only "waste" product produced in the powertrain is high purity water as a result of the $H_2 + 1/2\ O_2 \rightarrow H_2O$ combination reaction. Such a powerplant operates with zero local pollutants, comparable to electric trolley and battery vehicles. The fuel cell powered vehicle, however, has considerably greater range and thus a much greater realm of applicability. Although battery and trolley vehicles can compete in certain niche markets, fuel cell vehicles are the only ZEV option for many transportation applications. Highway freight transport, which contributes significantly to local air quality deterioration in dense urban areas, is a market segment well suited to a H_2 ZEV [37].

3.3 The Ballard Bus Program

A target application was needed to serve as a model in the thermodynamic analysis of this thesis. The vehicle studied is the Ballard Phase II urban transit bus developed and manufactured by Ballard Power Systems of Burnaby, B.C. This is the second generation vehicle produced by Ballard.

The Phase I bus is a National Coach Corporation Model RE-32 bus. This is a 32 foot (9754mm) fuel cell powered vehicle with seating for 20 passengers [40]. The powerplant driving the vehicle is a fuel cell engine consisting of twenty-four Mark V 5kW PEMFC stacks. The stacks are arranged in 3 parallel strings of 8 stacks connected in series, with a gross power output of 120 kW. An electrically driven automotive supercharger combined with a turbocharger supplies air to the fuel cell stacks. An electric pump circulates stack cooling water through a forced air, fan cooled radiator. Fuel is stored in the form of compressed hydrogen at 20 MPa in underfloor fiberglass wound aluminum containers. The range of the Phase I bus is 160 Km (100 mi).

The second generation Ballard bus underwent its first road tests in the summer of 1995. The Phase II bus is based on the full sized New Flyer 40DL low floor chassis. It is a 40 foot, 60 passenger model powered by two, 750 cell fuel cell strings connected in parallel. The fuel cell stack has a nominal gross power output of 250 kW. As in the first generation bus, the incoming air is pressurized in two stages by an automotive supercharger and turbocharger. The bus operates at a air flow stoichiometry of 1.5 to 2.0 to ensure no depletion of O_2 at the all important cathode reaction. The balanced fuel cell reaction for an air stoichiometry of 2 is:

$$H_2 + (O_2 + 3.76N_2) \rightarrow H_2O + \tfrac{1}{2}O_2 + 3.76N_2$$

The air supply system accounts for a nominal 16 - 17% of gross fuel cell power, used to drive the variable speed AC motor connected to the supercharger. Total parasitic losses through the powertrain are approximately 45 kW at full load, with a net power output of 205 KW.

Fuel storage on the Phase II bus is compressed H_2, stored in roof top cylinders. This vehicle represents the maximum storage of compressed H_2 without interfering with passenger capacity [41], and the upper realm of compressed H_2 vehicle range (400 km) with current technology.

The targeted application of this thesis is the Phase II bus powertrain and configuration, utilizing LH_2 storage.

3.4 Bus Design Conditions

The various ECERS configurations are based on the following bus design conditions:

- 1.076 A/cm^2 (1000 ASF) current density at the design point (the following information corresponds to this operating point)
- 250 kW gross power output
- 45 kW nominal parasitic air compression load
- Air/H_2 stoichiometric ratio of 2
- H_2 flow rate of 4.71 g/s (2.33 mole/s)
- LH_2 storage and H_2 consumption at 0.3 MPa pressure
- LH_2 thermomechanical exergy = 57.5 kW
- Cooling water supplied at 350 K to the fuel cell stack, exiting at 360 K

CHAPTER 4 HEAT ENGINE CYCLES

4.1 Relevant Heat Engine Principles

A review of heat engine principles illustrates the opportunity for exergy recovery from low temperature sources in addition to conventional, high temperature sources. The laws of thermodynamics impose physical limitations on heat engine cycles. Any heat engine working in a cycle must extract heat from a source at T_h and discharge heat to a sink at T_c. Conceptually, the simplest of any engine is the Reversible 2 Temperature (R2T) engine [4].

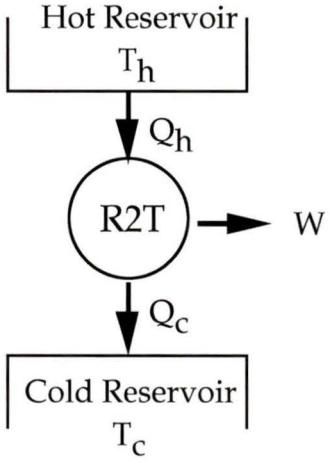

Figure 4.1: Reversible 2 Temperature engine

The Carnot version of the R2T engine has 2 isentropic and 2 isothermal processes. An energy balance yields $W = Q_h - Q_c$ and the expression for 1st law efficiency

$$\eta = \frac{W}{Q_h} = \frac{Q_h - Q_c}{Q_h} = 1 - \frac{Q_c}{Q_h} \tag{4.1}$$

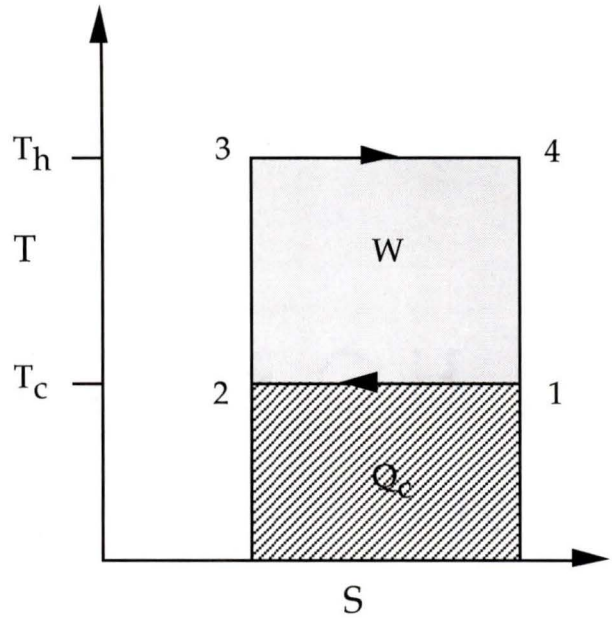

Figure 4.2: Carnot heat engine cycle

The two isothermal heat transfers can be expressed as:

$$Q_h = T_h \Delta S \tag{4.2}$$

$$Q_c = T_c \Delta S \tag{4.3}$$

Since ΔS is equal in both expressions, we can express efficiency:

$$\eta = 1 - \frac{T_c}{T_h} \tag{4.4}$$

4.2 Cryogenic Heat Engine Principles

Cryogenic exergy recovery differs from conventional power cycles in that the heat source is the environment (or a warmer waste heat stream) and the heat sink is a limited supply of cryogen. Traditional high temperature heat engines and power systems are designed with a limited heat source and an infinite, atmospheric heat sink.

If we consider once again the Carnot heat engine of the previous section

$$\begin{aligned} Q_h &= T_h \Delta S \\ Q_c &= T_c \Delta S \\ \text{and } W &= Q_h - Q_c \\ &= (T_h - T_c)\,\Delta S \end{aligned} \tag{4.5}$$

Looking at work produced as a function of the finite heat sink:

$$\frac{W}{Q_c} = \frac{(T_h - T_c)\Delta S}{T_c \Delta S} \tag{4.6}$$

we can see that if $T_c < 1/2\ T_h$, then $W > Q_c$. The produced work can exceed the amount of heat transferred into the heat sink, at T_c. In fact, in the case of cryogenic temperatures, T_c can be much less than T_h and W many times greater than Q_c.

The work W that can be extracted from an "ideal" cryogenic engine is equal to the exergy associated with the heat flow, Q_c, to the available heat sink. The product of the dimensionless exergetic temperature τ ($=1-T_o/T$) and Q_c represents the magnitude of ideal work which can be obtained by transferring heat at a temperature of T_c.

In real heat engines entropy is produced because heat must transfer occurs across finite temperature differences, and there are mechanical losses. Nevertheless, ideal processes are useful in understanding the principles of exergy recovery and a measure against which actual processes can be benchmarked.

4.2.1 Cryogenic Heat Engine Inefficiencies

In the previous section the relationship between the maximum work produced and the heat transferred to the cold sink was developed. The magnitude of work that can be produced

by a cryogenic heat engine can far exceed the magnitude of heat transferred to the heat sink. If however, the cryogenic heat engine has internal irreversibilities, as a result of mechanical friction, pressure drop, etc., we can expect less than ideal performance.

Considering a heat engine, if the real device produces entropy of an amount σ, an additional amount of heat must be rejected to the cold sink. This heat energy is equal to $T_c\sigma$. The laws of thermodynamics state that for a fixed input of heat (the limited quantity in such an engine), the work produced by the "real" engine will be the ideal work less the amount of additional heat rejected with the entropy produced, $T_c\sigma$. A high temperature heat engine, rejecting heat at the temperature of the environment, must reject an additional heat, $T_o\sigma$. At T_o there is typically an infinite heat sink available, limited only by the design of the cooling system.

An energy, or first law, balance on a heat engine cycle indicates that any irreversibilities result in lost work and additional heat rejected. In the specific case of a cryogenic heat engine, any inefficiencies resulting in an entropy production of σ must still be rejected to the heat sink as $T_c\sigma$. However, in this specific application, the amount of heat that can be received is finite. Thus the production of entropy and its subsequent rejection not only reduce the amount of work produced, but also decrease the magnitude of the available heat sink. Considering a heat engine with a thermal efficiency η, the work that can be extracted from such a cycle is

$$W = \eta Q_h \tag{4.7}$$

Upon rearranging and using the energy balance equation $Q_h = W + Q_c$, the work produced, expressed as a function of the heat rejected, becomes

$$W = \frac{\eta}{1-\eta} Q_c \tag{4.8}$$

Thus the work produced is not a linearly decreasing function of the heat rejected, as is intuitively expected from high temperature operating experience. The non-dimensional relationship between W/Q_c and η is plotted in Figure 4.3. In this relation, η is the cycle

thermal efficiency, the product of Carnot efficiency, η_c, and a "real" coefficient. This curve is valid for any temperature and combination of Carnot and real efficiencies.

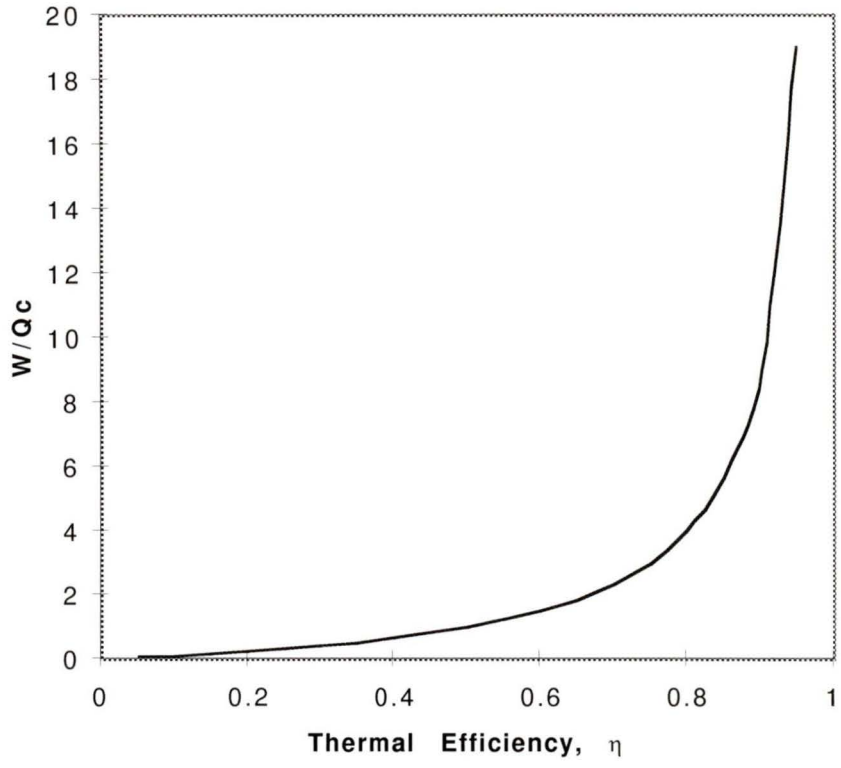

Figure 4.3: Work per unit cooling vs. thermal efficiency

The work output ratio to a fixed cooling capacity, W/Q_c, is a large value for an ideal heat engine operating between ambient and LH_2 temperatures. With $T_h = 300$ K and $T_c = 20$ K, the Carnot efficiency is

$$\eta_C = 1 - \frac{T_c}{T_h} = 1 - \frac{20}{300} = 0.93$$

The work produced per unit cooling is

$$\frac{W}{Q_c} = \frac{0.93}{1 - 0.93} = 13.3$$

If, however, the heat engine operates at a nominal efficiency of 50% of Carnot, or $\eta=0.5\eta_C$, the work produced per unit Q_c is only

$$\frac{W}{Q_c}=\frac{0.5(0.93)}{1-0.5(0.93)}=0.87$$

Thus a heat engine thermal efficiency of 50% of Carnot results in a loss of work by a factor of 15.3.

A simple example can help to illustrate the effect of a limited heat sink. If an ideal heat engine operates between 300 and 20 K, the Carnot efficiency is 93%. Thus if 100 J of heat energy is added, then 93 J is available as work and 7 J is rejected to the heat sink. If the type of real heat engine used has an efficiency of 50% of Carnot, and the same input heat provided, 0.5(93) = 46.5 J of work would be produced. However, 53.5 J of heat is rejected to the heat sink, a factor of over seven times the amount in the original calculation. Less heat must be introduced to the cycle and hence less work done to not exceed the magnitude of the finite heat sink.

If any cryogenic heat engine is to show promise while operating over a large temperature span, it must be an efficient converter of input energy to useful work output. The impact of seemingly acceptable moderate thermal efficiencies has a severe effect on the total work output when rejecting heat to a finite heat sink.

4.3 Thermomechanical Exergy Recovery From Cryofuels

The constant pressure warming curve of H_2 at 0.1 MPa is shown on a T-s plane in Figure 4.4 from saturated liquid to ambient conditions.

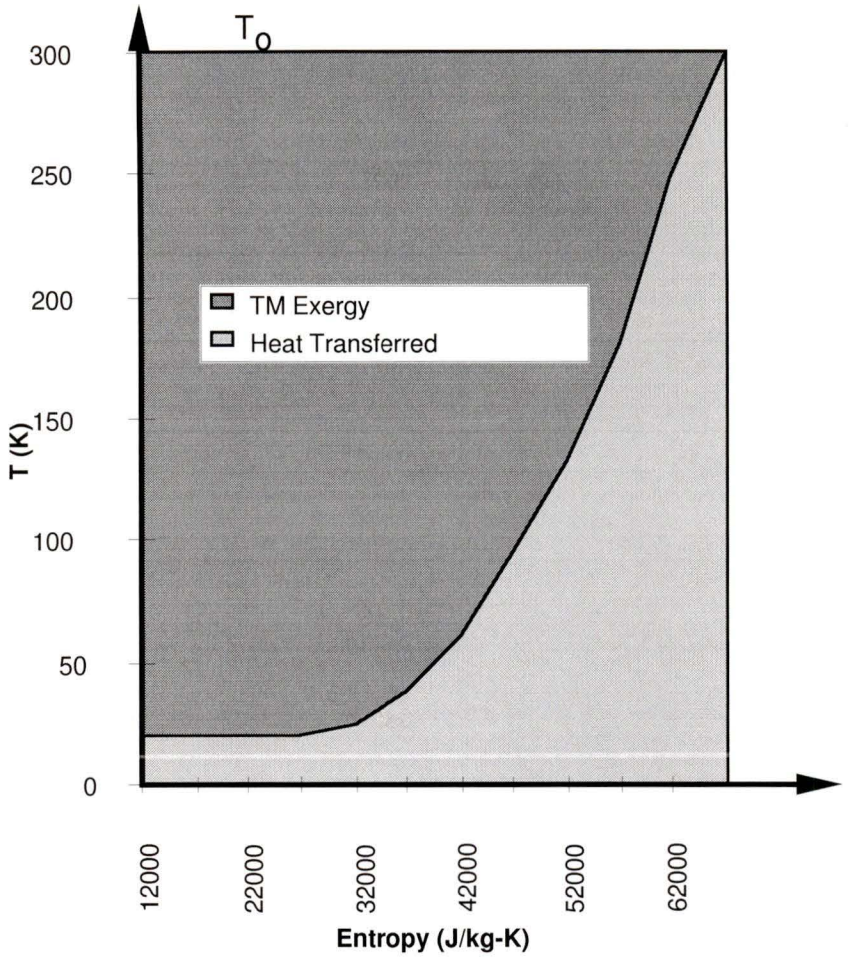

Figure 4.4: H_2 temperature-entropy plane (T_o=300 K)

The area under the constant pressure curve represents the heat transferred to the cryofuel to warm it from its liquefied state to ambient conditions. The area above the constant pressure curve represents the exergy (work) which can be recovered by bringing the cryofuel into thermomechanical equilibrium with the environment, given a fixed inlet and outlet pressure.

In the case of LH_2, approximately half of the thermomechanical exergy is "latent exergy", the exergy associated with the phase change. The remainder is in the form of sensible heat, rejected to the H_2 as it warms from saturated vapour at ~20 K to 300 K. To successfully recover all the thermomechanical exergy available, any device must utilize both the latent and sensible heat portions of the warming cryofuel. Several devices could be used in a

stepped configuration, but capital costs of any multiple unit system could become prohibitive. Figure 4.5 illustrates the latent and sensible thermomechanical exergy values of LH_2 and LNG.

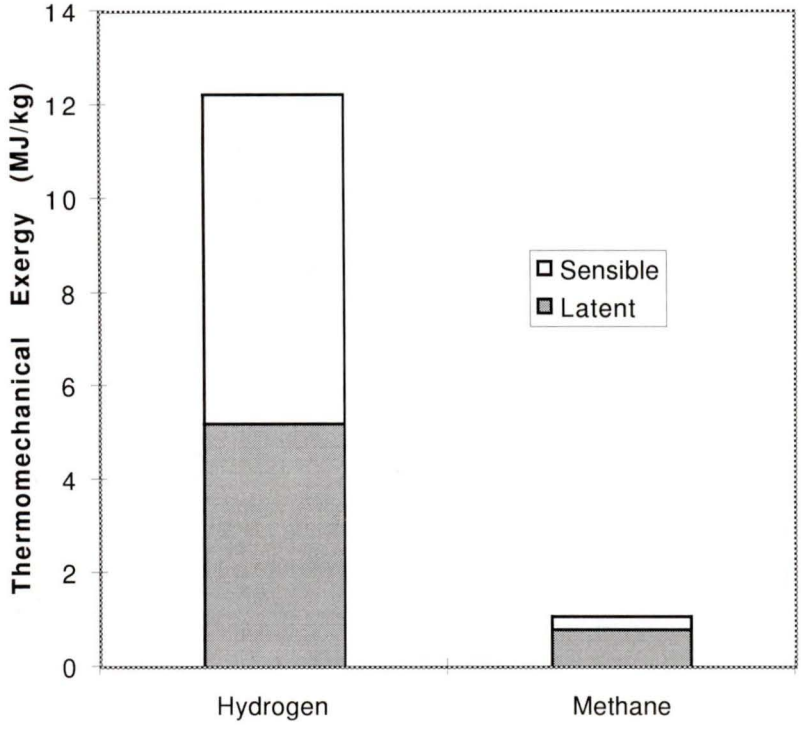

Figure 4.5: Latent/sensible exergy ratios

LNG (assuming 100% methane) thermomechanical exergy is 75% latent and 25% sensible LH_2 thermomechanical exergy is 45% latent and 55% sensible. An efficient device recovering thermomechanical exergy from LH_2 must recover both latent and sensible exergy.

4.4 Ideal Cryogenic Exergy Recovery System (CERS) Cycle

The thermodynamically ideal CERS can be conceptualized and used as a basis to compare alternatives for exergy recovery. Thermodynamically, the reversible CERS cycle is

analogous to the ideal liquefaction cycle. The ideal cycle and its representation on the T-S plane are shown in Figure 4.6.

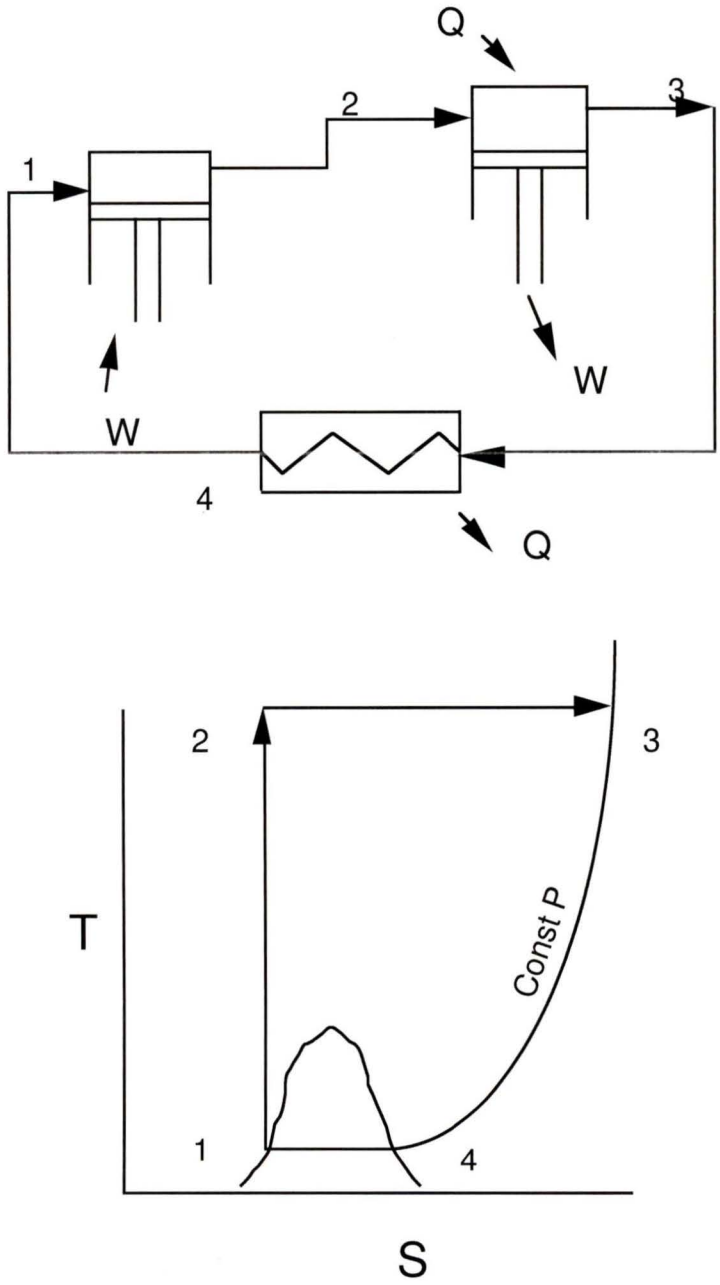

Figure 4.6: Ideal Crogenic Exergy Recovery System (CERS) cycle

The schematic of Figure 4.6 is a heat engine cycle operating in a closed loop. The cryogenic liquid undergoes isentropic pressurization from (1-2), and then isothermally expanded from (2-3). Process (3-4-1) is isobaric cooling and condensation. States (1) and

(3) lie on a constant pressure line. In this cycle all heat is accepted at the environment temperature, T_o, through isothermal expansion. In a closed system, heat is rejected with an infinitesimal temperature difference to the cryogen in its sensible range (3 - 4) and through the phase change (4 - 1).

An open system is also possible. Incoming liquid would be pressurized (1-2) and then isothermally expanded (2-3). The additional heat exchanger requirement would be eliminated. An energy balance on the open system yields

$$\begin{aligned} Q - W &= \sum_{o} mh_o - \sum_{i} mh_i \\ &= m(h_3 - h_1) \end{aligned} \tag{4.9}$$

The isothermal heat transfer is $Q = mT_3(s_3 - s_2)$

$$= mT_3(s_3 - s_1) \tag{4.10}$$

so $W = -m(h_3 - h_1) + mT_3(s_3 - s_1)$

$$= m\,[(h_1 - h_3) - T_3(s_1 - s_3)] \tag{4.11}$$

Since the subscript 1 denotes the cryofuel inlet state and 3 the environment, this expression for the work available is equal to the thermomechanical exergy content of the cryogen at state 1,

$$\xi_{tm} = m\,[(h - h_o) - T_o(s - s_o)] \tag{4.12}$$

We now have a cycle which, in theory, is 100% exergy efficient, and analogous to an ideal liquefaction cycle [11]. Practically the ideal cycle is limited by the difficulties of achieving true isothermal expansion, and the enormous pressures of state 2 following the isentropic pressurization of the saturated liquid. Isentropic pressurization of 0.1 MPa saturated LH_2 to 100 MPa (chosen as an upper limit of practical pressure) yields an outlet temperature of only ~ 41 K, far from the 300 K required for the ideal cycle.

4.4.1 Cooling Water Heat Recovery

In virtually all vehicle powertrains (fuel cell or IC engine) there exists a waste heat stream, available at a temperature above that of the environment. This elevated temperature source increases the amount of work which can be provided by a CERS heat engine. In addition, this heat stream constitutes heat which must be rejected to the environment to maintain steady-state operation of the vehicle powertrain and is usually available in a high heat capacity liquid with excellent heat transfer characteristics. Utilizing this "waste" heat stream as input energy to a heat engine cycle reduces the amount of heat which must be rejected to the environment. The external heat transfer loop and the associated equipment can then be made smaller and less expensive.

The higher the heat source temperature available, the greater the work a cryogenic exergy recovery heat engine can produce, as shown by:

$$W = \left[1 - \frac{T_c}{T_h} \right] Q_h \tag{4.13}$$

A heat engine operating between the waste heat temperature and the cryogen temperature is an Enhanced Cryogenic Exergy Recovery System (ECERS). Figure 4.7 shows the additional work that can be produced using a heat source at a temperature higher than ambient. This diagram assumes a waste heat source of much larger heat capacity than the cryogenic heat sink. This is an accurate assumption in most applications. In reality T_h will decrease slightly as heat is removed from the high temperature cooling water source (approximately 2.5 K across the diagram).

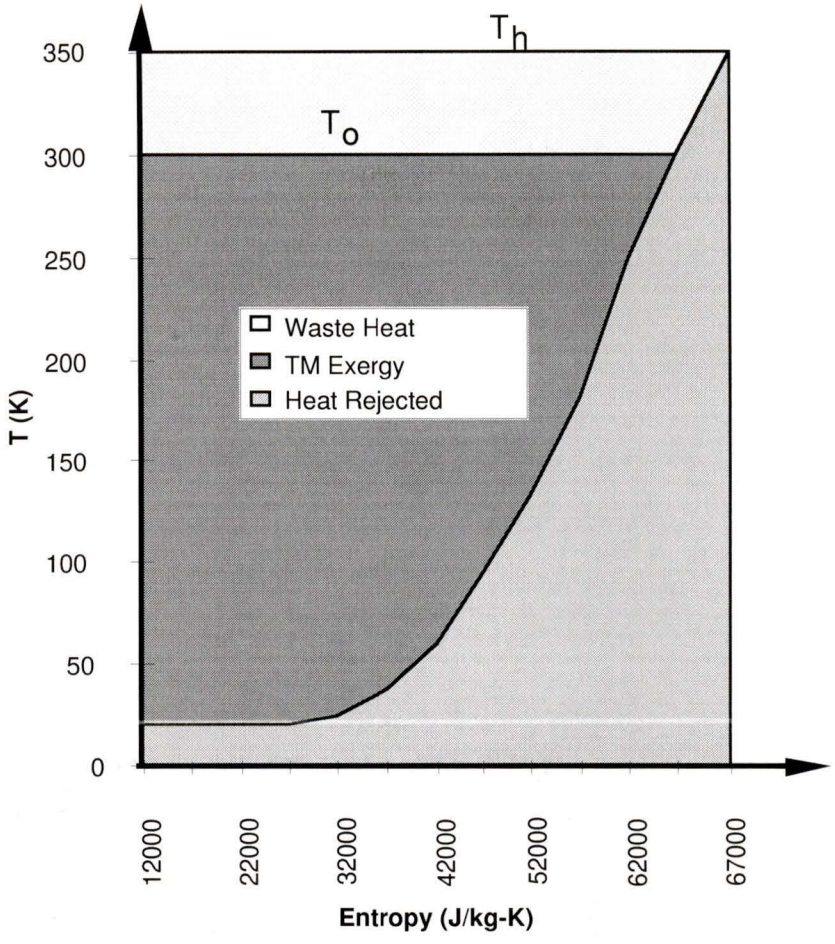

Figure 4.7: Enhanced Cryogenic Exergy Recovery System (ECERS) temperature-entropy plane

The maximum work that an ideal ECERS can produce is represented graphically on the T-s plane by the composite area of the cryofuel thermomechanical exergy and the additional waste heat input to the cycle at a temperature above ambient. The additional heat available is the area bracketed between T_h and T_o.

The 350 K heat source adds 15 kW of exergy to the 57.4 kW of cryogenic exergy, an increase of 22%. By utilizing the available waste heat as input to an ECERS cycle the output can be significantly improved. In addition, a liquid heat transfer fluid with high heat capacity and thermal conductivity provides the input heat to the cycle. The difficulties of transferring heat to the engine from ambient air with poor heat transfer capabilities are overcome. Heat transfer requires a smaller temperature differential and produces less entropy.

4.5 Rankine Enhanced Cryogenic Exergy Recovery System (ECERS) and Modifications

The Rankine heat engine cycle has two isentropic and two isobaric processes. The working fluid undergoes a phase change in both the heat addition and heat rejection processes. However, supercritical Rankine cycles do exist in which there is no clear phase transformation during the heat addition process. A superheated Rankine power cycle can operate over the 20-300 K cryogenic operating range as the critical temperatures of any cryogens are much lower than ambient temperature. The basic Rankine cycle with superheat is outlined in Figure 4.8.

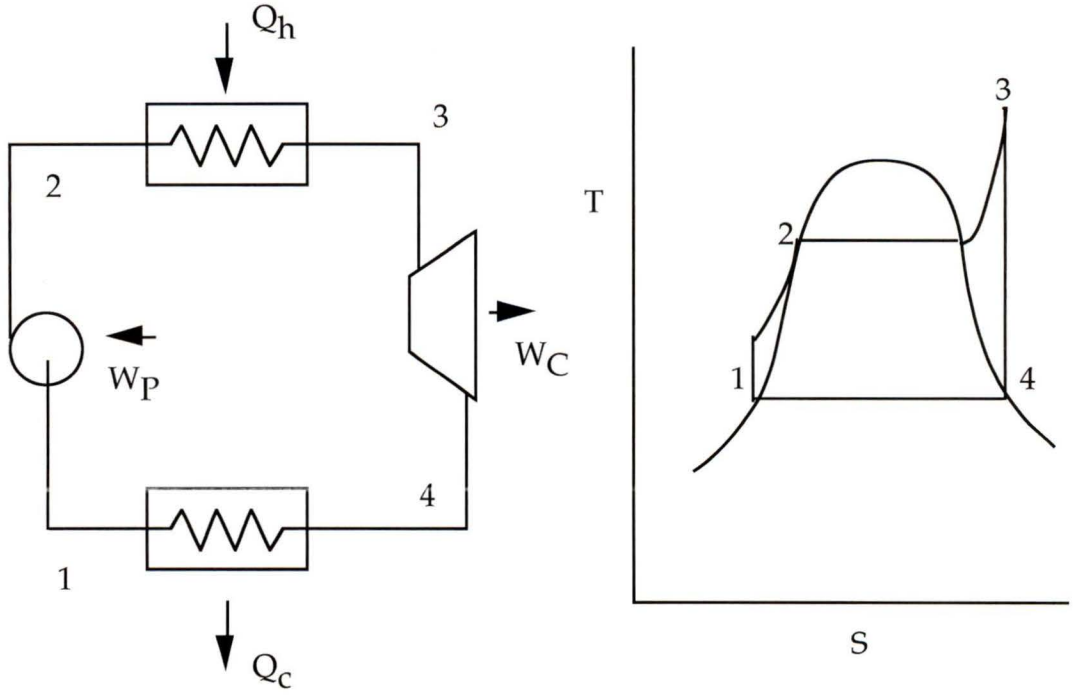

Figure 4.8: Superheated Rankine cycle and temperature-entropy plane

The existence of a saturated liquid at state 1 allows pressurization with a pump (unlike the compressor of a Brayton cycle) with a significant reduction in work input required. The pumping process, (1-2), is followed by isobaric heat addition, during which the fluid undergoes a phase change (2 - 3). Isentropic expansion (3 - 4) and condensation at

constant pressure (4 - 1) complete the cycle. Furuhama [32] has proposed a Rankine cycle cryogenic heat engine, utilizing the environment as a heat source and warming LH_2 as a heat sink. Experimental tests using methane as a working fluid and N_2 as a heat sink, produced 0.89 kW at a thermal efficiency of 26%. The machine operated between fixed low and high temperatures of 115 and 315 K. The Carnot efficiency between these temperatures is 63.5%.

The inefficiencies of the Rankine cycle are a result of the inability of matching the warming and cooling curves of the working fluid to the respective cooling and warming curves of the available heat source and sink. From Figure 4.8, it is evident that a constant temperature heat source (the environment) results in heat transfer over a large ΔT throughout the cycle, because the maximum temperature of the superheated fluid cannot exceed the heat supply temperature. Exergy loss due to heat transfer across a finite temperature difference for a given Q is given by the relation [42]:

$$\Delta \Xi = Q \cdot T_o \cdot \frac{\Delta T}{T^2} \tag{4.14}$$

where ΔT is the heat transfer temperature difference at temperature T. Rankine cycles are well suited to applications where the heat input is generated by combustion. The products of combustion can be cooled to extract the maximum available energy while providing feedwater heating [43]. In a cryogenic exergy recovery application, the Rankine cycle suffers a severe penalty due to the constant, high mean temperature of environmental heat available.

Reheat improves the efficiency of Rankine power systems by increasing the mean temperature of heat addition. As the number of turbine stages increases, the process approximates isothermal expansion but capital costs, particularly in the case of small equipment suited to a transportation application, become prohibitive. Regeneration, during which a portion of the expanding fluid is extracted to preheat working fluid prior to external heat transfer, also increases cycle efficiency. In typical power systems, the different heat capacities of the condensing vapour and warming liquid compromise the efficiency improvement. In large steam power generating stations regeneration is widely used [44] to increase system efficiency where large savings warrant the additional capital expenditure.

Mixed working fluid (MWF) cycles have been developed to overcome some of the limitations of the Rankine cycle in cryogenic power generation applications [45] [46]. Used in several LNG regasification plants, mixed working fluids with different boiling points allow continuous condensation and evaporation over a wide range of temperatures. Regeneration can operate efficiently with heat transfer over a small temperature differential [27]. Exergy efficiencies as high as 37% have been quoted in LNG power generating installations. Exergy efficiencies in excess of 40% have been quoted for liquefaction cycles [42].

Heat transfer to the cryofuel is done at varying temperatures as the cryofuel warms up, reducing exergy destruction due to heat transfer across a large temperature difference. In addition, the varying condensation and evaporation temperatures allow regeneration, reducing irreversibility due to heat transfer from the environment to the evaporating fluid. A schematic of a MWF Rankine power cycle with a cryogenic heat sink is given in Figure 4.9.

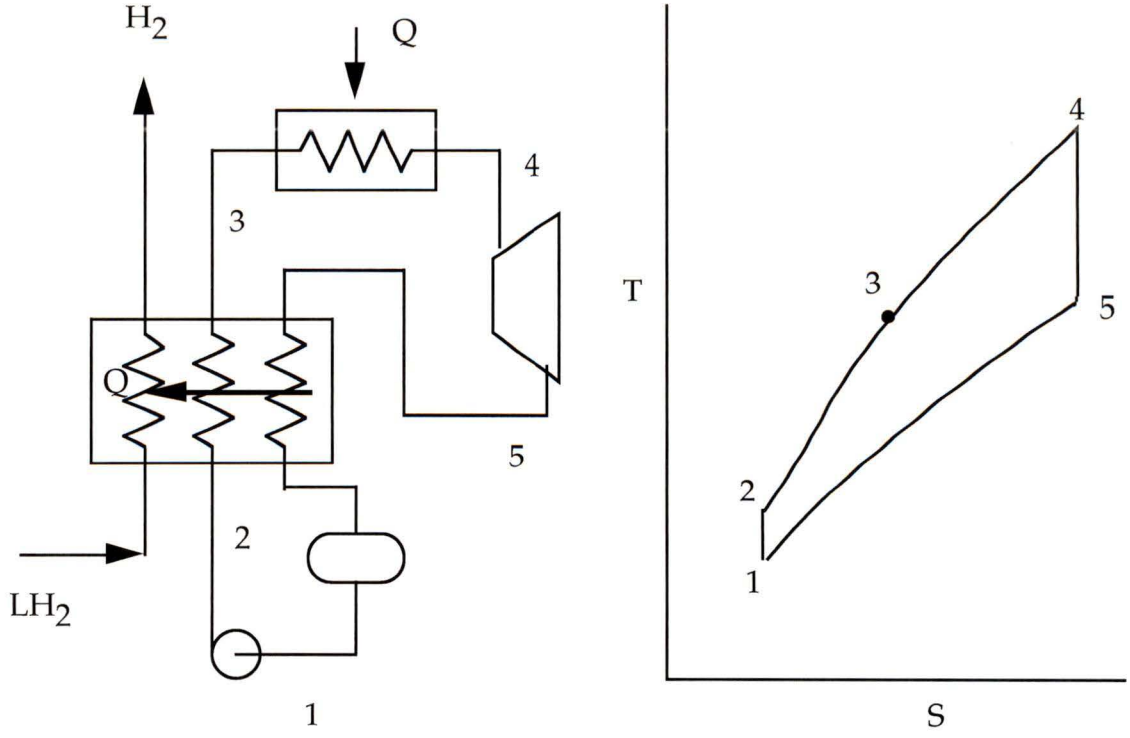

Figure 4.9: Mixed Working Fluid (MWF) Rankine cycle

A key element to the process is the 3-pass heat exchanger that condenses the low pressure working fluid while transferring heat to the evaporating working fluid and cryofuel streams. The 3-pass heat exchanger transfers heat from the condensing (5-1) stream to the warming cryofuel and vapourizing (2-3) working fluid. The final heat transfer from the environment (3-4) takes the working fluid to its maximum temperature and enthalpy prior to expansion. An energy rate balance on the heat exchanger yields the following relation:

$$(\dot{m}\Delta h)_{wf,lp} = (\dot{m}\Delta h)_{wf,hp} + (\dot{m}\Delta h)_{cryofuel} \tag{4.15}$$

where $\dot{m}_{wf,lp}$ and $\dot{m}_{wf,hp}$ are the mass flow rates of the low and high pressure working fluid and are equal. If we assume constant specific heats, the temperature change of the cold streams related to that of the hot stream reduces to:

$$\frac{\Delta T_{cs}}{\Delta T_{hs}} = \frac{(\dot{m}c_p)_{wf,lp}}{(\dot{m}c_p)_{wf,hp} + (\dot{m}c_p)_{cryofuel}} \tag{4.16}$$

The greater the ratio of working fluid to cryofuel flow, the closer the cold side heat exchanger exit temperature will be to that of the environment. Less exergy will be destroyed due to temperature differential across the hot heat exchanger and the system will become more efficient, but the size and cost of such a system will increase correspondingly. In LNG regasification applications, the increase in power output with increasing working fluid to cryogen flow has been well documented [46].

The MWF configuration shows perhaps the greatest promise for a single cycle to recover exergy from a cryogenic liquid and has had widespread adoption in LNG regasification applications. To the author's knowledge, no work has been done to date on suitable working fluids for these devices at LH_2 temperatures.

Many papers have been written on mixed refrigerant, closed cycle throttle-type (or Joule-Thomson) cryocoolers [47] [48]. The lowest temperatures achieved by such systems are in the range of 80 K, still well above LH_2 temperature. To adopt mixed working fluid cycles to LH_2 operation, considerable research is required on suitable mixtures. The only

cryogens available are Neon (Ne), H_2 and He. Solubility issues will determine the mixture behaviour at low temperatures, as any solids formation must be avoided [49]. The study of working fluids for H_2 applications is considered out of the scope of this work. Increased LH_2 production will likely encourage research in low temperature refrigerant mixtures, with a wider range of applicability than exergy recovery.

A further difficulty foreseen with a mixed working fluid cycle arises from the cycle dependence on 3-pass recuperative heat exchange. Such a system will have long start-up times as thermal gradients are established, before operation will be stable, steady-state. In addition, operation at varying loads will affect the system stability. Kashimura [46] has reported on start-up and partial load operation of the Tokyo Gas Negishi Works LNG facility. Instability at flows of less than 35% of design is characteristic.

4.6 Stirling ECERS

4.6.1 Stirling Background

The ideal Stirling cycle has an efficiency equal to Carnot when operating between two fixed temperatures. The Stirling cycle consists of two isothermal processes (compression and expansion) and two constant volume processes.

There are various configurations of Stirling engines, but the key components are a piston, displacer and regenerator. The Stirling cycle is graphically shown in Figure 4.10 with its accompanying temperature-entropy and pressure-volume diagrams.

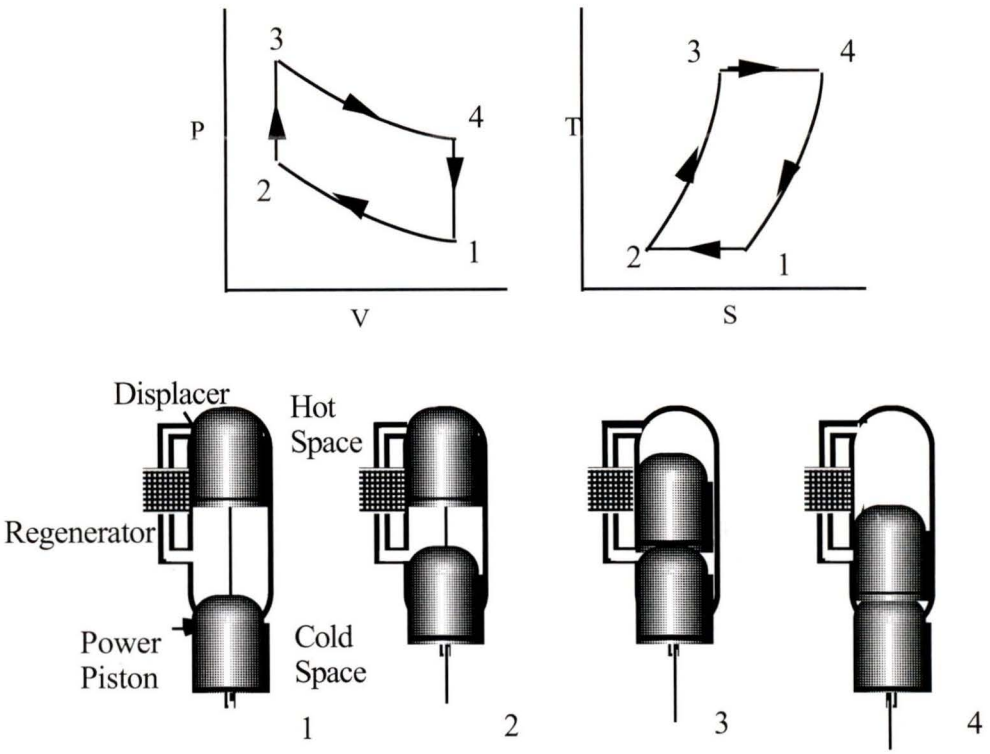

Figure 4.10: Stirling heat engine cycle [34]

The series of processes in a Stirling heat engine are as follows:

Process 1 - 2: Isothermal compression rejecting heat to the heat sink.

Process 2 - 3: Constant volume heating of the gas. The gas is forced through the regenerator by movement of the displacer, receiving heat stored in the regenerator.

Process 3 - 4: Isothermal expansion, during which heat is transferred from the heat source.

Process 4 - 1: Constant volume cooling of the gas, by heat transfer to the regenerator, back to the low temperature, T_c.

Robert Stirling invented the original Stirling engine in 1815 [50]. The advantages of the Stirling Hot Air engine were due to the use of a thermal regenerator, which permits heat to be transferred internally between the high and low pressure gases. The regenerator

transfers heat over a small temperature differential and not between fixed temperature heat sources and sinks and the warming or cooling working fluid.

Stirling engines were used for a variety of applications in the late 19th century but were virtually eliminated with the development of the cheaper IC engine. Much of the 20th century work on Stirling machines has been carried out by the Philips Company of Eindoven, Norway. A 1 kW engine was developed as a motive source for power generation to operate radio sets [50]. Refinements in electric radio efficiency and dry cell battery technology displaced the market for which these units were intended.

The Philips Stirling refrigerator has had greater success in cryogenic applications. The refrigerator has been used in the liquefaction of air at 5.5 l/hr, in gas separation systems and for cooling electrical components [11]. Due to the constant temperature cold end processes, Stirling liquefiers suffer a significant operating efficiency penalty when compared with refrigerators. By definition the Stirling process provides all of its cooling at the minimum temperature. Thus large irreversibilities occur when transferring heat from the cooling cryogen, initially at ambient temperature to the cold end of the Stirling liquefier, at the liquefaction temperature.

The same phenomenon prevails in any potential Stirling cryogenic heat engine system. An enthalpy mismatch occurs between the cryogen warming curve, to which heat is rejected at varying temperatures, and the constant temperature of the Stirling cold end. A cryogenic Stirling heat engine is, in theory, well suited to recovering "latent" exergy but not "sensible" exergy.

Quantifying the performance of Stirling machines is a complex task. The isothermal compression and expansion processes, and isovolumic heat transfer to and from the regenerator all involve considerable idealizations in the theoretical case. To simplify the losses of a real Stirling machine to their principal components, the efficiency can be expressed as [51]:

$$\eta = (\text{coeff. due to } \Delta T)(\text{coeff. due to Regen. losses})(\text{coeff. due to } \Delta P) \times \eta_{carnot} \qquad (4.17)$$

The first term represents the losses due to heat transfer over finite temperature differences and non-isothermal processes at the hot and cold ends of the machine. The second refers to regenerator losses because of a finite regenerator mass, non-infinite heat transfer coefficients, and longitudinal conductivity through the regenerator bed. The final term refers to pressure drop as the cycle working fluid moves through the different components. The above expression gives insight into the qualitative nature of the losses but does little to quantify them. These loss mechanisms are, by nature, intricate functions of a particular machine's design, geometry, and operating conditions.

Kohler [52] reports the four primary loss mechanisms of Stirling refrigeration machines: mechanical friction, pressure drop (gas friction), non-ideal heat transport, and insulation losses (heat leaks). Further, the regenerator losses are quantified: a 1% regenerator inefficiency induces a 21% loss in ideal cold production at LN_2 temperature (77 K), with the same loss accounting for 98% of cold production heat at LH_2 temperature. An extremely high regenerator efficiency is, therefore, required to achieve any cooling effect at 20 K.

Efficiencies for Stirling Machines are expressed in a variety of ways depending on the application. Second Law, and more specifically, exergy analysis is an effective tool to compare the performance of the different types of machines. A wide range of efficiencies is quoted in the literature and is dependent on the temperature range of operation. Actual efficiency values for real Stirling engines are of prime importance due to the profound effect which thermal efficiency has on the exergy efficiency of cryogenic heat engines (Section 4.2.1). The Philips cryogenic unit has a reported exergy efficiency of 30% when operating as a refrigerator at liquid air temperature (79 K) [11].

Martini [53] surveyed several Stirling engines and found efficiencies ranging from 28% to 69% of Carnot. Walker [54] suggests practical values of 30 to 50% of Carnot. Other values given for Stirling engines are 40 - 72% of Carnot [51].

The only data found for an experimental Stirling cryogenic heat engine was that for a four cylinder, wobble plate driven unit. The working fluid was He gas at a mean pressure of 3.6 MPa, in a total compression volume of 12 cm^3. Cold He gas was used as a heat sink

and warm water as a heat source. 47 W of mechanical work output was achieved at an efficiency of 14.7% of Carnot [55].

4.6.2 Stirling Heat Engine Model

This analysis uses characteristic performance values obtained from real operating machines to predict a Stirling engine's performance. The composite loss term given by the coefficients of equation (4.17) has been quoted as varying between 40 and 72% [51]. In this thesis, the characteristic efficiency of a "real" Stirling engine will be referred to as the percentage of ideal Stirling efficiency, η_s, so that:

$$\eta_S = \frac{W_{actual}}{W_{Carnot}} \tag{4.18}$$

Two approaches were pursued in modelling a Stirling heat engine system. The first constituted a single heat engine operating between a mean temperature determined by the ratio of the enthalpy change of the warming cryogen to its entropy change [51].

$$T_{mean} = \frac{\Delta h_{TL \to TH}}{\Delta s_{TL \to TH}} \tag{4.19}$$

where TL and TH are the lower and upper limits of the warming cryogen. For a single cycle operating with hydrogen warming from 20 K and 300 K as a heat sink, the mean temperature is 85 K. The heat sink available in warming the H_2 from 20 to 85 K is 5.43 kW, and the Carnot efficiency (with T_h = 350 K, the cooling water temperature) is:

$$\eta_C = 1 - \frac{85}{350} = 0.76$$

At this operating point a Stirling engine with Carnot efficiency would theoretically produce

$$\dot{W} = \frac{0.76}{1 - 0.76}(5.43\ \text{kW}) = 17.2\ \text{kW}$$

If, however, the efficiency is 50% of Carnot, the power produced is

$$\dot{W} = \frac{0.5(.76)}{1 - 0.5(0.76)}(5.43\ \text{kW}) = 3.3\ \text{kW}$$

The power produced is a very strong function of η_S. A plot of power output versus η_S of a single Stirling unit operating at an 85 K cold end temperature is shown in Figure 4.11.

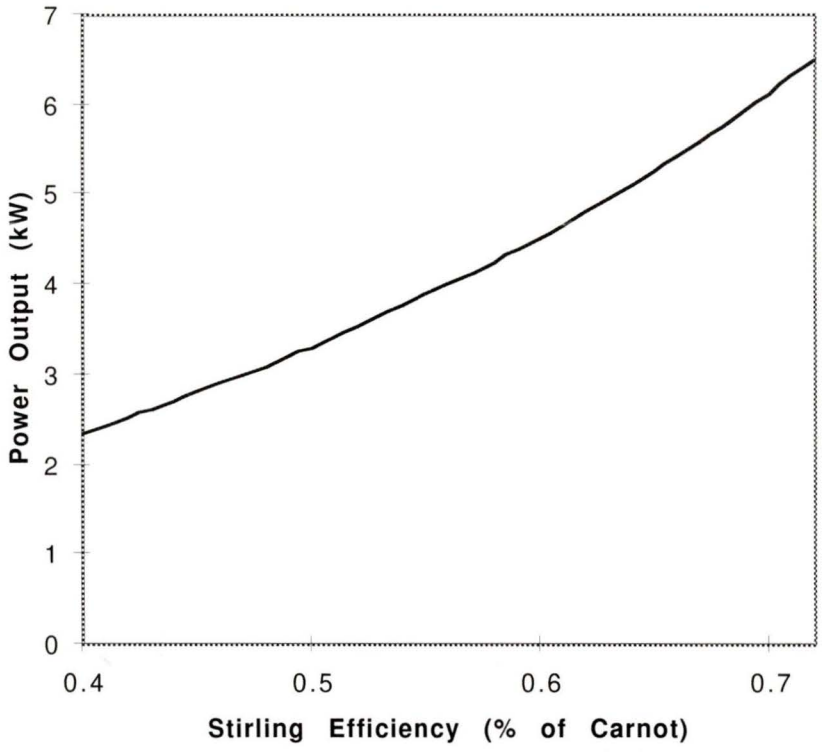

Figure 4.11: Single stage Stirling machine power output vs. efficiency

Utilizing multiple stage Stirling units to approximate the shape of the H_2 warming curve improves the overall cycle efficiency. Ideally the heat rejected matches the enthalpy curve of the warming H_2. A single unit can recover the exergy of the latent heat change and then

several units used to recover the sensible exergy. Figure 4.12 shows a schematic T-S plane of three Stirling machines, one used for latent and two for sensible exergy recovery.

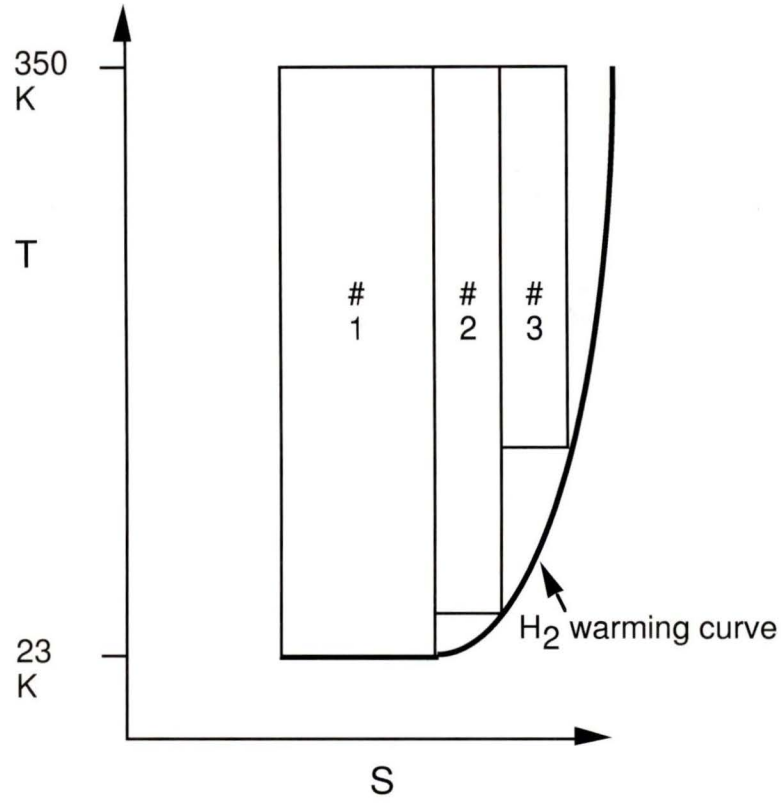

Figure 4.12: Three stage Stirling schematic

As the number of Stirling units increases to improve overall thermodynamic efficiency, the complexity and cost of the heat engine system rises dramatically. The upper limit on number of staged units has been set at two for practical purposes while developing a thermodynamic model. One stage will recover latent exergy and the other stage will recover sensible exergy. If the latent heat is the heat sink of the first unit, at 23 K, the cooling available is 2.2 kW, and the Carnot efficiency is .93. A Carnot engine could theoretically produce 28.8 kW, but if $\eta_s = 0.5$, the power output becomes 1.9 kW. The output of the second unit, operating at T_{cold} of 119 K and $\eta_s = 0.5$ is 2.7 kW. The cooling available at this temperature is 5.4 kW. Figure 4.13 illustrates the power output of the two Stirling machines as a function of η_s.

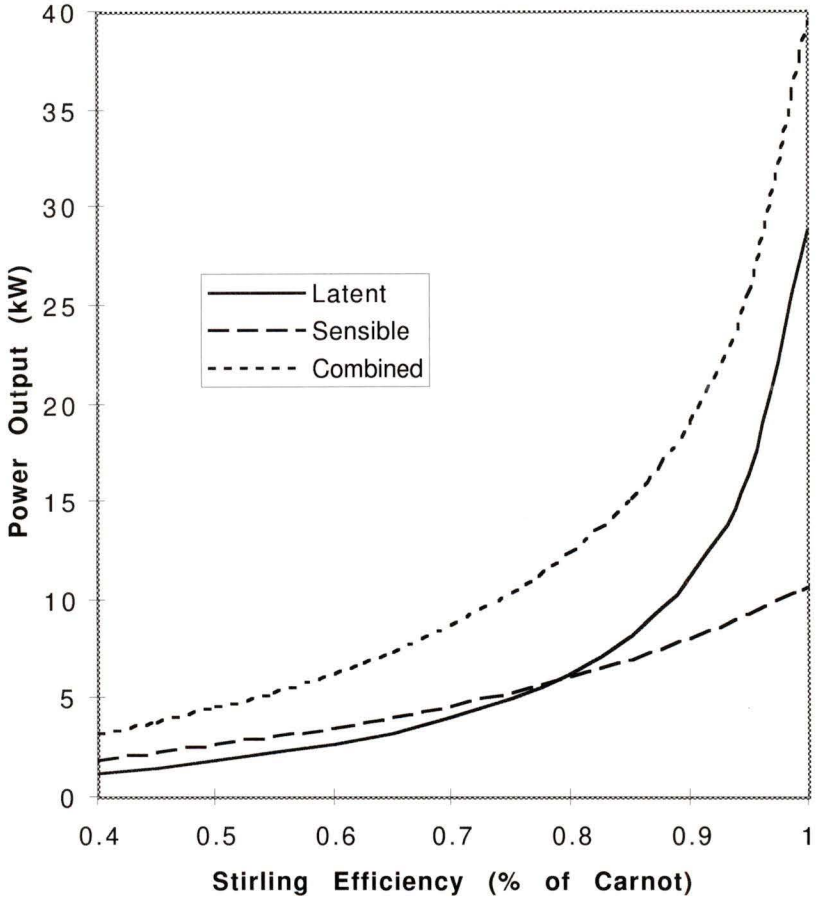

Figure 4.13: Two stage Stirling engine output vs. Stirling efficiency

The above figure is extended to a η_S of unity to emphasize the importance of high η_S at low temperatures. The latent unit operates at T_c=23 K and is much more sensitive to low η_S than the sensible unit, operating at T_c=119 K.

The results of the Stirling cycle do not suggest it is a practical means of taking advantage of LH_2 exergy. Efficiencies, as traditionally indicated, appear to be too low to be practical in vehicular cryogenic exergy recovery application. At the current time, Stirling machines are complex and costly devices. The benefits of using a Stirling device in the proposed application need to be weighed against the cost of developing and manufacturing a suitable machine.

4.7 Direct Expansion (DE) ECERS

Another simple heat engine system potentially applicable to ECERS is DE. DE is an open Rankine cycle. Saturated LH_2 is pressurized using a cryogenic pump, followed by isobaric warming and expanded to the final use pressure, producing work. Unlike most heat engine systems, there is no separate, enclosed working fluid. The H_2 cryofuel is the working fluid as it passes through the system. A schematic representation of the process equipment and its path on a T-S plane is shown in Figure 4.14.

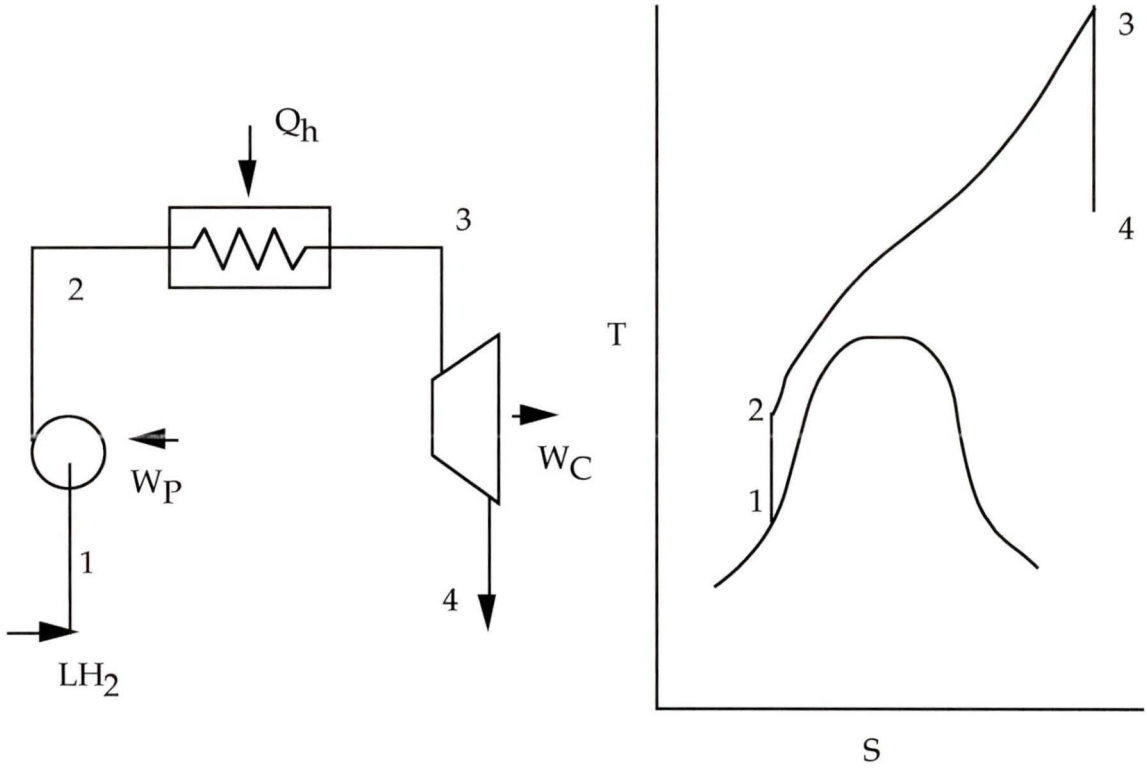

Figure 4.14: Supercritical Direct Expansion (DE) cycle

Two key operating parameters affecting the performance of DE cycles are the operating pressure, and the quantity of heat addition during isobaric warming. Such a cycle operating with LH_2 may or may not pass through the two phase region. If the intermediate (high) pressure of the process exceeds the critical pressure of H_2 (1.3 MPa), the cycle will be supercritical.

Heat addition during expansion will improve the performance of a DE cycle. This can be approached by two methods. The expander can be designed for isothermal expansion, a difficult task as this requires an extended heat transfer area, which will make such a machine larger, more expensive, and with lower power densities. Although no compact practical near-isothermal expander exists to the author's knowledge, isothermal expansion is one stage of the Stirling cycle. Stirling engine research could, in the future, potentially yield breakthroughs applicable to stand-alone expanders. Multiple expansion stages with reheat between is another alternative to enhance cycle performance and efficiency. This is a more simplistic approach to tailor the mean temperature of heat addition to the environment temperature at which heat is available. Less entropy is produced during heat transfer, resulting in a greater cycle efficiency and power output. Wilson [56] documents the advantages of multi-stage intercooled compression and reheat-expansion processes as they are applied to cryogenic Brayton cycle gas turbines. The principles and advantages of such processes, however, apply to a DE cryogenic cycle as well.

Karashima [27] gives an account of DE cycles and variants. Opportunities exist for the use of DE in combination cycles. A combination cycle uses heat supplied to a DE cycle as the heat sink for a separate process operating at a higher, but still below ambient, temperature process. Pressurized H_2 could be used as a heat sink for another power generating cycle or to provide cooling for some other application, as will be explored in Chapter 6. To date the more complicated systems have only been considered for large scale applications in LNG power generation.

4.7.1 Direct Expansion Heat Engine Model

DE cycle performance was predicted with a spreadsheet model. The LH_2 was pressurized to varying pressures, heated to 350 K at constant pressure, and then expanded in a turbine. Figure 4.15 illustrates the gross power output of a DE cycle, operating with a LH_2 cryogen at 0.3 MPa inlet and delivery pressure, as a function of intermediate cycle pressure and expander isentropic efficiency.

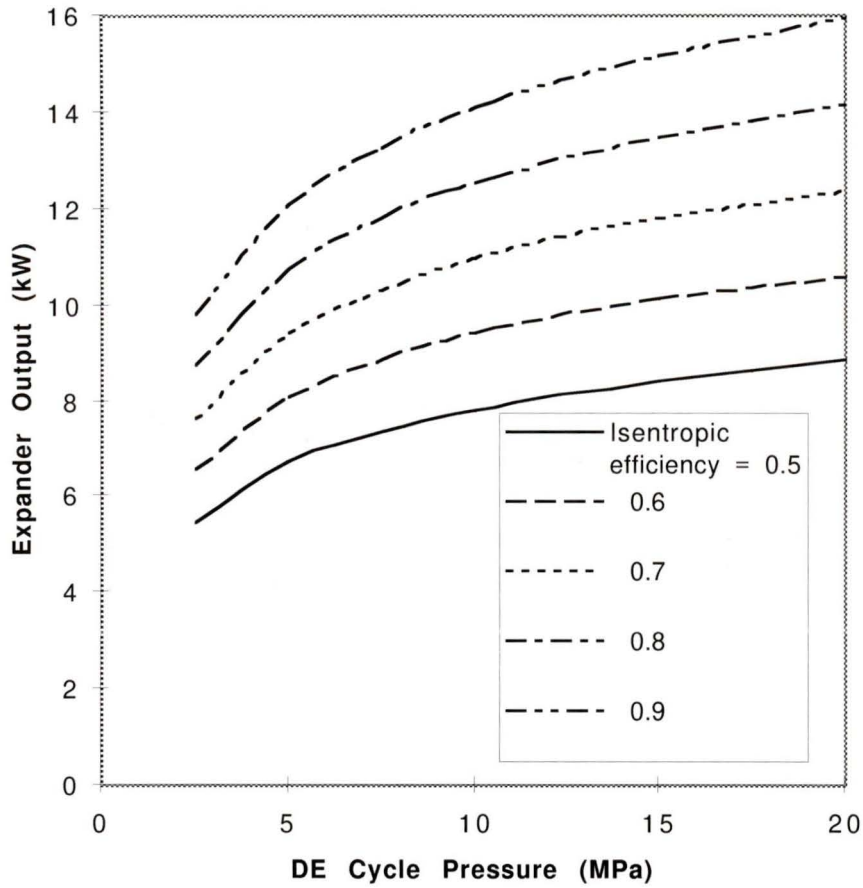

Figure 4.15: DE gross output vs. cycle pressure, isentropic efficiency

Pump work directly reduces the net output available to the system. In these calculations, the pump efficiency has a minor effect and is assumed to be 60%. The LH_2 pump input power is tabulated in Figure 4.16.

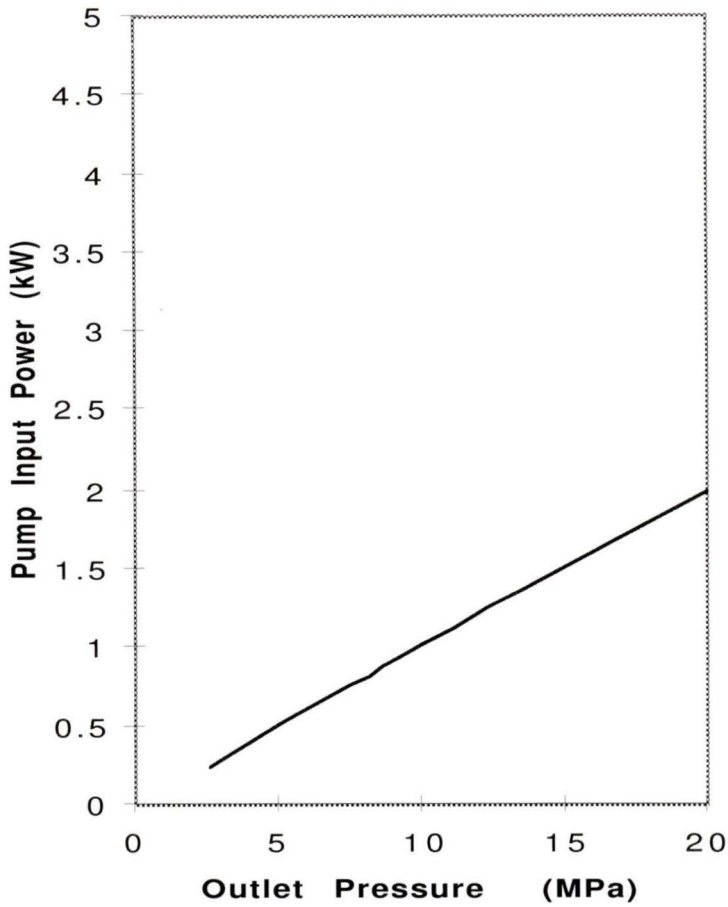

Figure 4.16: DE pump input power vs. output pressure (η=0.6)

Based on the above results, it appears a DE heat engine cycle producing a net output of 5 to 10 kW is possible. The standard DE cycle output is calculated at a 5.0 MPa pump pressure and 60% pump and expander efficiencies. The net output produced is 7.6 kW. This corresponds to 13.2% of the thermomechanical exergy of the LH_2. The main technical obstacle of such a cycle would be the availability of a suitable expansion turbine, operating at various loads.

CHAPTER 5 UNIQUE FEATURES OF ECERS FOR FUEL CELL VEHICLES

5.1 Compression Work Requirement

As illustrated in Chapter 3, the targeted Ballard Phase II bus uses a PEM fuel cell. Intrinsic to the PEM design is a power limiting cathode reaction. An O_2 activation overvoltage must be provided to drive the reaction.

Supplying the oxidant stream at elevated pressure to increase the effective O_2 partial pressure at the cathode enhances the cathode reaction rate. In addition, an air flow rate of 1.5 - 2 times stoichiometric is provided to overcome O_2 depletion as the stream flows through the cell [41]. As discussed previously, the air handling system represents a 16 -17% parasitic load at full output (45 kW @ 250 kW gross produced by the stack). The work that must be provided, on a unit mass basis is defined as:

$$W = -\int_{V_1}^{V_2} P \cdot dV \tag{5.1}$$

In the ideal, isothermal case, assuming air behaves as an ideal gas, this reduces to:

$$W = mRT \cdot \ln \frac{P_2}{P_1} \tag{5.2}$$

Although the molar requirement of O_2 for the fuel cell reaction is one half the H_2 molar requirement on a stoichiometric basis, the true mass of air that must be compressed is a large when compared to the H_2 flow. Considering a stoichiometric ratio of 2, and 21% O_2 by volume in ambient air, the mass flow ratio becomes:

$$\frac{\dot{m}_{air}}{\dot{m}_{H_2}} = \frac{1 \text{ mole } O_2}{2 \text{ mole } H_2} \cdot (\nu = 2) \cdot \frac{1 \text{ mole air}}{0.21 \text{ mole } O_2} \cdot \frac{\bar{M}_{AIR}}{\bar{M}_{H_2}} = 68.3 \frac{\text{kg air}}{\text{kg } H_2} \tag{5.3}$$

The mass flow ratio illustrates the importance of the air system and its parasitic load on powertrain performance and efficiency.

5.2 Cryogenic Air Compression

Looking at energy systems from the "other way around" can yield valuable insight into the system's behaviour and opportunities available to be exploited [57]. Although H_2 is generally considered the bus "fuel", the air system actually controls the powerplant output. The vehicle accelerator pedal increases the air stream flow and pressure to increase the fuel cell output. The air compression work is a barrier which, if overcome, provides significant opportunities for performance improvement. A significant focus of this thesis is the analysis of the air system and integration with an ECERS.

In the simplified representation of the air compression process of equation (5.2), work depends linearly upon the temperature of compression. Reducing the temperature of compression directly reduces the required work. Cooling the air stream prior to compression can yield significant energy savings. In reality the air mixture will increasingly deviate from ideal gas behaviour as the temperature approaches the O_2 critical temperature of 155 K and compression is far from isothermal.

Using the cryogenic H_2 to cool the incoming air stream reduces the work input required by the compression process. The most basic cryogenic exergy recovery system analyzed is a simple counterflow heat exchanger precooling the incoming air while warming the H_2 cryofuel. Although far from ideal exergy recovery, this basic system utilizes low cost, simple components.

In the analysis of the air system enhancements in this thesis, air is assumed to be a dry mixture of 21% O_2/79% N_2. This is not intended to undermine the importance of impurity removal, but it is felt that the technology is sufficiently developed, and outside the core of this thesis, to be omitted in this first pass thermodynamic analysis.

5.3 Cryogenic Air Separation

If sufficient cooling power is available, notwithstanding the approximately 60:1 mass flow ratios, a heat transfer system could actually condense (liquefy) air. The advantages of liquefied air are twofold. An incompressible (or near so) liquid whose work input for pressurization is, $W \approx V_1(P_2 - P_1)$, gives more than an order of magnitude improvement over the work required for ideal gas compression. This is the reverse effect that has led to the widespread adoption of Rankine power cycles; well designed Rankine systems require only 1 - 2% of the gas expansion (turbine) work as pump work. The second major advantage of cryogenic condensation is due to the properties of air as a binary mixture of O_2 and N_2. As a mixture is cooled, O_2 having a normal boiling point (NBP) of 90 K, condenses out at a higher temperature than N_2, with a NBP of 77 K. A binary phase diagram of an O_2/N_2 mixture is illustrated in Figure 5.1.

If one follows a constant temperature line across the diagram the intersections of this line with the dew and bubble point lines give the composition of both the liquid and vapour phases at that temperature. Due to the lower volatility of the O_2, the liquid formed is always richer in O_2 than N_2. The temperature at which the liquid stream is extracted determines the exact composition of the stream. At 80.5 K, the liquid stream composition is approximately 40% O_2.

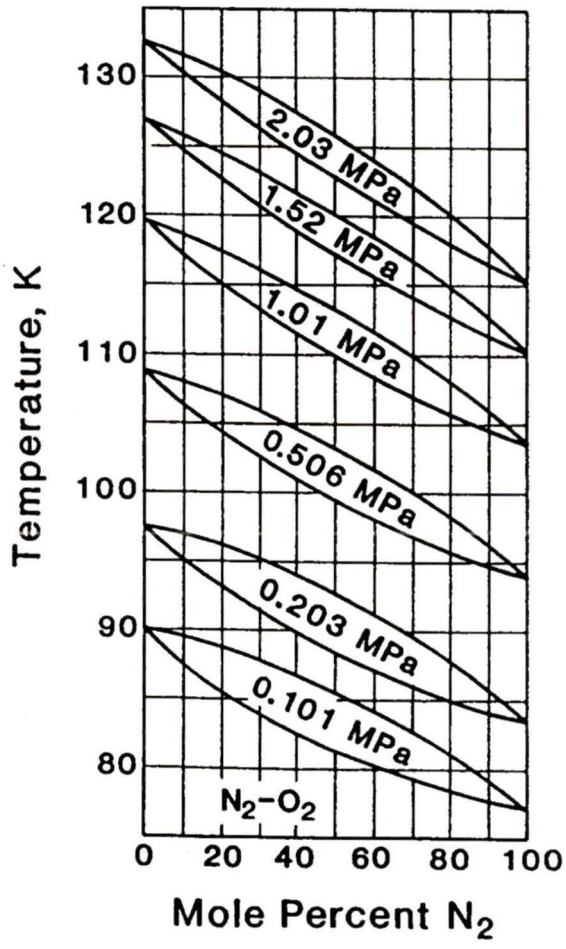

Figure 5.1: Binary phase diagram of O_2/N_2 mixture [58]

The simplest system that could be used is a single stage phase separator extracting the liquid and vapour at one temperature. The composition of 40% O_2 is selected as the target purity. This is based on recommendations from Ballard as the optimum due to difficulties in handling a high O_2 purity stream from safety and corrosiveness perspectives.

The thermodynamic analysis in this thesis used a single stage separation process. Single stage separation is the simplest separation process to incorporate into a vehicle powertrain. Opportunities may exist to increase the O_2 yield by refining the distillation process, but were not explored as part of this work.

5.4 Low Temperature Heat Removal

A unique opportunity presents itself when analyzing the warming and cooling curves of hydrogen and air. A system that incorporates both air enrichment and work extraction is possible by using a heat engine. In such a system the pre-cooling and condensation of the air stream supplies the heat to the hot end of the heat engine. This heat engine then produces work while rejecting heat to the low temperature H_2 heat sink. Latent heat is no longer transferred over a large (60 K) temperature span as in the single stage separation process of Section 5.3. Figure 5.2 illustrates a low temperature heat engine operating between the approximate phase transformation temperatures of air and H_2.

Any work (exergy) that can be extracted between the temperature of the high temperature air stream and low temperature H_2 stream results in additional cooling power available to the air stream. A unique, synergistic opportunity exists in which two variables we desire to optimize (maximum air cooling and maximum work output) actually complement each other.

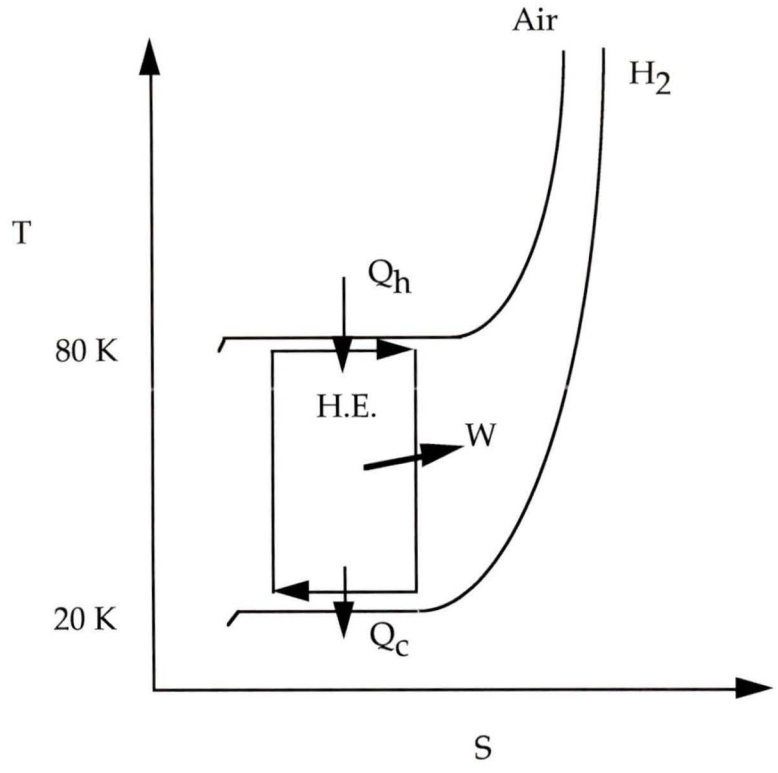

Figure 5.2: Heat engine increasing air cooling

In principle, a Stirling engine could operate between the vapourization temperature of the H_2 and the condensation temperature of O_2. This engine would produce useful work and increase the yield of enriched O_2 available to the fuel cell stack. If the H_2 is used directly to cool and condense air, there is a heat exchanger pinch point at the air condensation temperature. Extracting work below this temperature increases the cooling available, and increases the liquefied air stream yield.

There are several technical challenges to the design of such a system. The design of an all cryogenic heat engine suitable for transient operation poses significant difficulties. Indeed the principle of maximizing cooling effect by extracting work is the basis of much cryogenic refrigeration research, and is evident in the Heylandt and Kapitza liquefiers [11].

CHAPTER 6 AIR ENHANCEMENT MODELS

6.1 Thermodynamic Modelling

This chapter presents models of various ECERS air enhancement configurations and determines their suitability for the target bus application. The models were evaluated for constant, steady-state operation. No transient modelling was conducted.

The base configurations considered for modelling are shown in the list below. The models are listed in order of increasing technical complexity, with anticipated increasing performance benefits.

1) Air Precooling to reduce compression work input
2) Direct Expansion heat engine cycle coupled with air precooling
3) Air Enrichment to enhance cathode reaction performance
4) Air Enrichment coupled with a low temperature heat engine to produce work while simultaneously increasing enriched oxygen yield

The above air enhancement systems directly affect the operation of the fuel cell powertrain. Several options of system 3), Air Enrichment were evaluated. The most promising air enrichment configurations are included in Section 6.7. The systems designed around reducing the parasitic load of the oxidant conditioning stream have a direct impact on the fuel cell power output. Unlike the heat engine models of Chapter 4, the air enhancement configurations necessitated a system model incorporating the major fuel cell stack and ancillary components. This system modelling was completed using AspenPlus, a commercial process simulation computer code produced by Aspen Technology Inc. [59].

6.2 System Model

6.2.1 AspenPlus Code Overview

AspenPlus is an interactive process modelling code widely used in the chemical industry. The code employs an extensive library of physical property and unit operation models allowing the user to build models of varying complexity to simulate a wide range of processes.

This work used version 9.1.3. of AspenPlus with the ModelManager user interface. AspenPlus had previously been used successfully in the exergy analysis of various energy industries and was well recommended to IESVic/Cryofuel Systems at the onset of this thesis work [60].

An AspenPlus process model is produced in three steps, outlined in Figure 6.1. The user produces an input file consisting of the process blocks, components, routing, and thermodynamic property data. The execution of the code calls upon the library data for blocks, components, thermodynamic property models, convergence routines and executes any external FORTRAN code required. The simulation produces an output file containing the block and stream results and any warning/error messages. An AspenPlus run report file of the Steady-State Air Enrichment configuration (Section 6.7.4) is included in Appendix D.

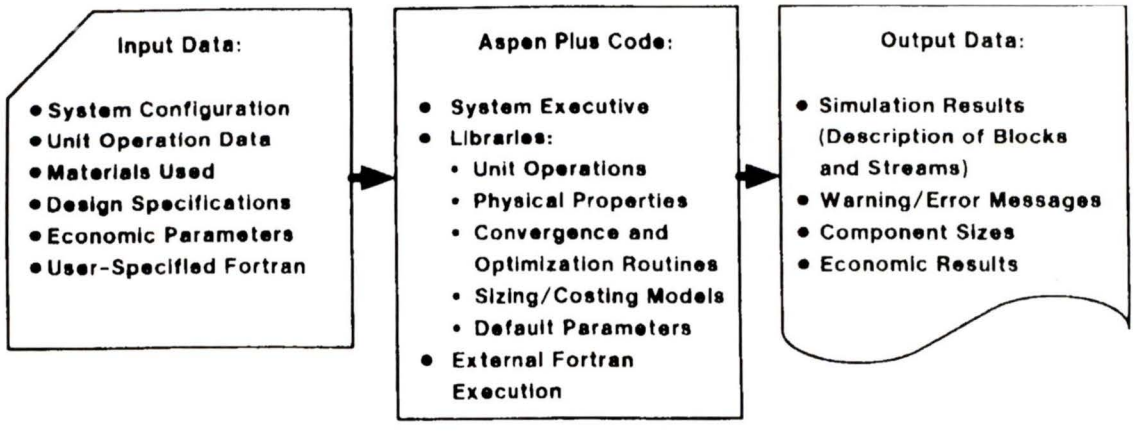

Figure 6.1: AspenPlus code process modelling sequence [60]

The AspenPlus simulation operating platform was a Sun SPARC 10/IPX workstation working with a Sun 4.1.3 operating system.

Although AspenPlus appears to be a powerful tool for modelling of thermodynamic systems, shortcomings were exposed over the course of this work. Thermodynamic data in the cryogenic operating region had to be validated, and is covered in Section 6.3.2. Additionally, AspenPlus version 9.1.3 used for this work appeared quite sensitive to the operating platform and generally was not as robust as was originally expected. Aspen Technology claims to have addressed robustness issues with version 9.2, which has been received at the University of Victoria but at the time of this writing is not yet operational.

6.2.2 Bus Schematic Model

Figure 6.2 illustrates the basic bus model used in the course of this work. This is not intended to be a comprehensive detailed model of the Ballard Phase II Bus system. The purpose of this model was to evaluate the proposed system configurations and their effect on the significant components of the fuel cell stack and ancillaries.

The basic assumptions of this model were as follows;

- Pressure drops across filters and through piping are not significant enough to affect the results of the system enhancements and are omitted.
- The H_2 ejector and recirculation system has been omitted and is represented by a stoichiometric incoming flow of 0.3 MPa H_2.
- The air system compressor and turbocharger are modelled as one compressor and a separate expander. Compressor and expander efficiencies were selected to simulate their respective loads at the design point and are not varied as a function of powertrain output.
- All water produced by the fuel cell reaction is produced at the cathode and carried away in the excess oxidant stream.
- An air flow of twice the stoichiometric ratio is necessary and mandated by fuel cell operating requirements (i.e. water removal).

- LH_2 is the mode of fuel storage as opposed to compressed H_2. In the baseline case an external heater vapourizes the LH_2, with the heat supplied from the cooling water system.
- The cooling water system is represented as a simple external heating load; the water flows, pump work and fan work are not evaluated in detail.
- Some product water is removed in a condenser represented as a dual outlet phase separator. A detailed water balance is not carried out.
- Operating pressure schedule is basically unchanged from the existing bus.

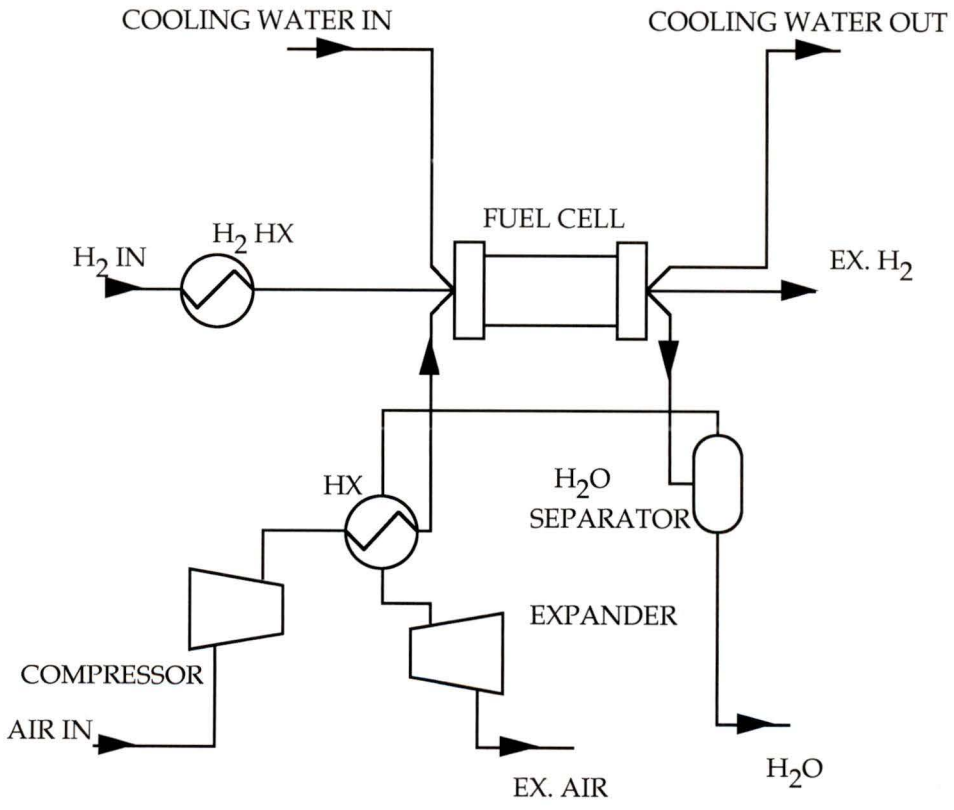

Figure 6.2: Basic bus system

6.3 Thermodynamic Data

6.3.1 Ortho-Para Hydrogen Conversion

H_2 possesses the thermodynamic property of existing in two molecular structures, based on the relative nuclear spins of the molecule. The para-H_2 (p-H_2) state corresponds to the condition of nuclear spins in opposite directions and is a lower quantum energy state. When the proton spins are in the same direction, it is called ortho-H_2 (o-H_2). The equilibrium concentration of ortho- and para-H_2 is temperature dependent and shown in Figure 6.3.

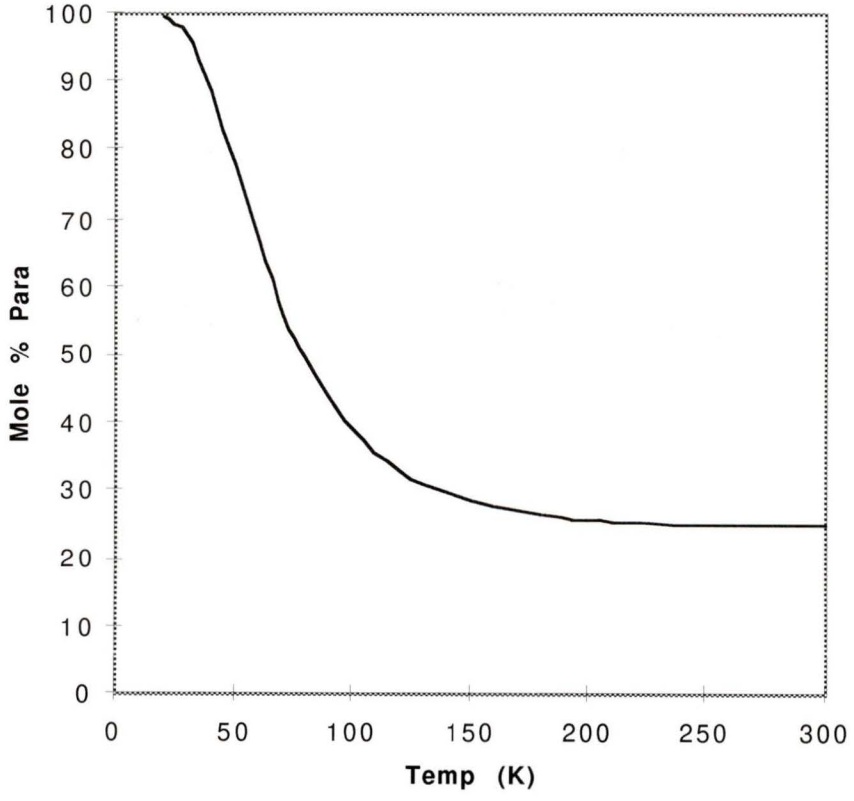

Figure 6.3: Equilibrium para-H_2 concentration as a function of temperature[11]

The equilibrium H_2 (e-H_2) composition is approximately 25% p-H_2 and 75% o-H_2 at 300 K, but is 99.8% p-H_2 at 20 K. The ortho/para equilibrium concentration of 25%/75% is referred to as normal hydrogen (n-H_2) [61]. The conversion from o-H_2 to the lower energy level p-H_2 is exothermic and requires further cooling to remove the heat of conversion. Uncatalyzed, the reversible conversion is quite slow and given by the second order relation:

$$\frac{dx_o}{dt} = -C_2 x_o^2 \tag{6.1}$$

where x_o is the mole fraction of o-H_2 and C_2 is the reaction rate constant, 0.0114 hr^{-1}. The concentration of o-H_2 can be expressed as:

$$x_o = \frac{0.75}{1 + 0.75 C_2 t} \tag{6.2}$$

Thus 48 hours after liquefying a 75/25 o-H_2/p-H_2 mixture, the result will be a 52% p-H_2 mixture. The heat of conversion at the normal boiling point is 703.3 kJ/kg and is greater than the latent heat of vapourization of 443 kJ/kg [11]. A 300 K e-H_2 mixture that is liquefied and stored will result in a large boiloff, so the conversion must be completed at the time of liquefaction. The addition of a catalyst can reduce the reaction to first- or zero-order and speed the conversion time during liquefaction.

The implication for cryogenic exergy recovery from LH_2 is that the fuel stored on-board is actually p-H_2. The thermomechanical exergy is increased by the change in quantum state of the H_2 that has taken place during the liquefaction process.

The thermodynamic modelling of this thesis uses p-H_2 thermodynamic data. The uncatalyzed conversion from p-H_2 to o-H_2 is considerably longer than the H_2 residence time in the cryogenic exergy recovery system. The assumption is made that no conversion takes place in the ECERS system. However, p-H_2 has a higher thermomechanical exergy change from liquid to ambient conditions than o-H_2: this benefit is realized by an ECERS.

6.3.2 AspenPlus Thermodynamic Data

The equation of state data for H_2 available in AspenPlus was verified with known H_2 thermodynamic data. AspenPlus does not differentiate between the two nuclear forms of H_2, but does offer a wide range of thermodynamic data that can be selected to match the requirements of the application.

Several AspenPlus library option sets were evaluated for agreement with known thermodynamic data. Benedict-Webb-Rubin-Lee-Starling, Peng-Robinson, Lee-Kesler-Plocker, and Redlich-Kwong-Soave (RKS) equation of states were all evaluated. The RKS cubic equation of state with Boston-Mathias alpha functions was chosen as best agreeing with known p-H_2 thermodynamic data, verified by GASPAK and PROMIX codes. All of the AspenPlus simulations use the RKS-BM option set. Figure 6.4 indicates enthalpy as a function of temperature at 0.3 MPa pressure, normalized to zero at 300 K, for the AspenPlus RKS-BM, and GASPAK p-H_2 and n-H_2 data. The net change in enthalpy using the AspenPlus data set between 20 and 300 K, which determines the cryogenic heat sink magnitude, was 1.3% less than that derived from GASPAK for p-H_2. This difference was considered acceptable for the purposes of this work.

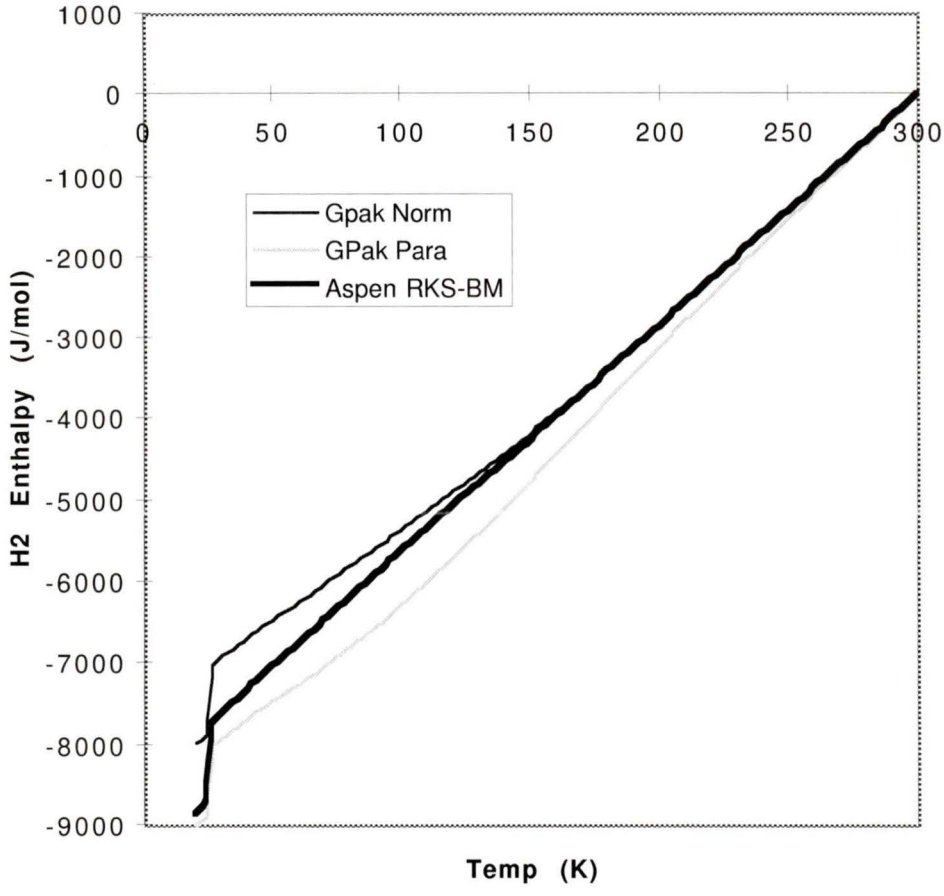

Figure 6.4: H_2 enthalpy vs. temperature data

6.4 Fuel Cell Model

The fuel cell model used in the following system simulations was a FORTRAN programmed block inserted in an AspenPlus process simulation flowsheet. The purpose of the fuel cell block was to evaluate the change in fuel cell performance as a function of the changing reactant stream parameters (composition, flow, pressure). These parameters were altered by an ECERS design. The mathematical model was derived from the RMC model originally developed for the Ballard Mk IV PEM fuel cell and subsequently extended

to the Mk V cell and stack, used in the Phase I bus [62] [63] [64] [65]. This model formed the basis of a system model developed at the University of Victoria in 1995 [66].

The original model of the Mk V cell was calibrated against actual performance data from the larger, more powerful Phase II bus to account for design changes to the 510 cell. The model is used to predict the output voltage of an individual cell as a function of inlet conditions. Appendix A contains a detailed explanation of the voltage model used in this thesis.

In all simulations the fuel cell current density is an independent variable and the voltage is subsequently determined for given fuel cell inlet conditions. The product of the current and voltage determines the stack power output. The model predicted performance increases as O_2 concentration was increased by the ECERS equipment. No attempt was made to evaluate the effect of stoichiometry and air system pressure variations. The effect of air system parameter variations has been well documented for the Mk V cell [67].

6.5 Baseline Bus Model

The baseline bus model is shown in Figure 6.2. In this system the incoming LH_2 is supplied at 20 K, 0.3 MPa and a stoichiometric flow of 4.71 g/s (2.33 mole/s). The incoming air at (stoichiometry of 2) is pressurized in the compression process to 0.3 MPa at the bus design point of 1.076 A/cm^2. The air stream following compression is cooled in counterflow heat exchange with the excess oxidant stream. This heat exchange has the advantages of reducing the fuel cell cooling load and increasing the enthalpy of the excess air stream to obtain a greater work output from the expander. The exiting excess air stream is routed to a water separator specified by a fixed temperature and pressure.

Nominal efficiencies for the compression and expansion processes were set at $\eta_c = 55\%$ and $\eta_e = 50\%$. These were chosen to match the performance of the real components. The efficiencies were not varied as a function of flow. At the standard conditions of 1.076

A/cm^2 (1000 A/ft^2) the model yields the following results, where $\dot{W}_{fc}$ is fuel cell output, $\dot{W}_c$ is compressor input, and $\dot{W}_e$ is expander output:

$$\dot{W}_{fc} = 247.2 \text{ kW}$$

$$\dot{W}_c = 64.4 \text{ kW}$$

$$\dot{W}_e = 18.4 \text{ kW}$$

This gives a net system output of 201.2 kW. This compares to the actual bus gross and net output of 250 and 205 kW respectively [41].

The sensitivity of the results to compressor and expander efficiencies is illustrated in Figure 6.5. Although expander efficiency has a relatively minor influence on the power produced, the compressor input power is strongly dependent on the compressor efficiency.

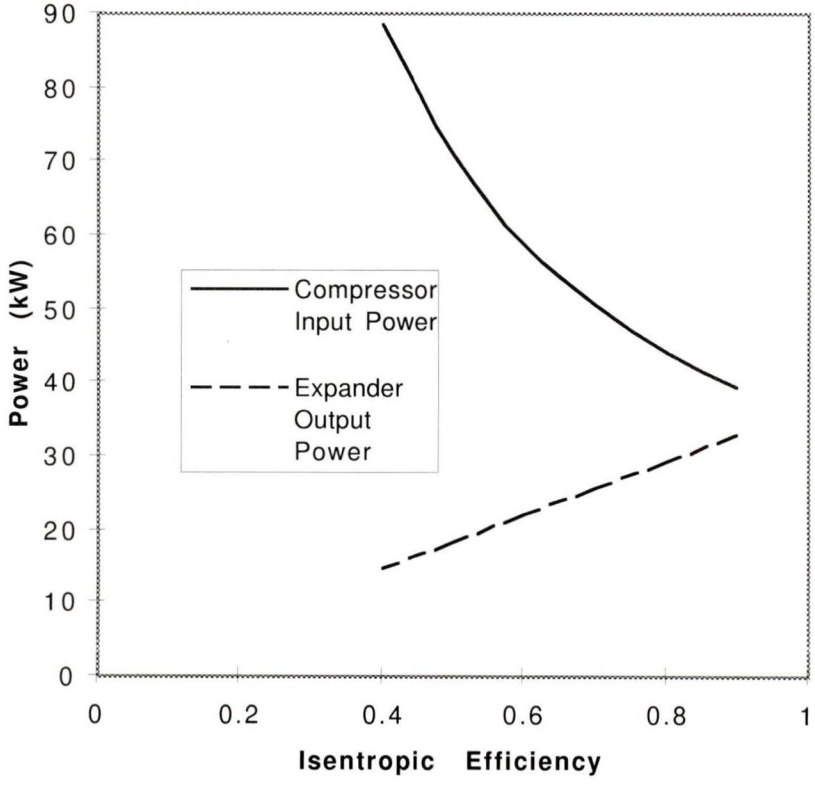

Figure 6.5: Compressor, expander power vs. isentropic efficiency

6.6 Air Precooling

Air precooling reduces the parasitic air compression load by precooling the air stream through heat transfer with the warming cryogenic H_2. The only additional equipment required is an air-to-H_2 heat exchanger and the necessary purification to remove water and CO_2 from the incoming air stream. The latter is necessitated to avoid solids formation in the air system as the air temperature is lowered to the freezing point of CO_2. Figure 6.6 illustrates the air precooling model arrangement.

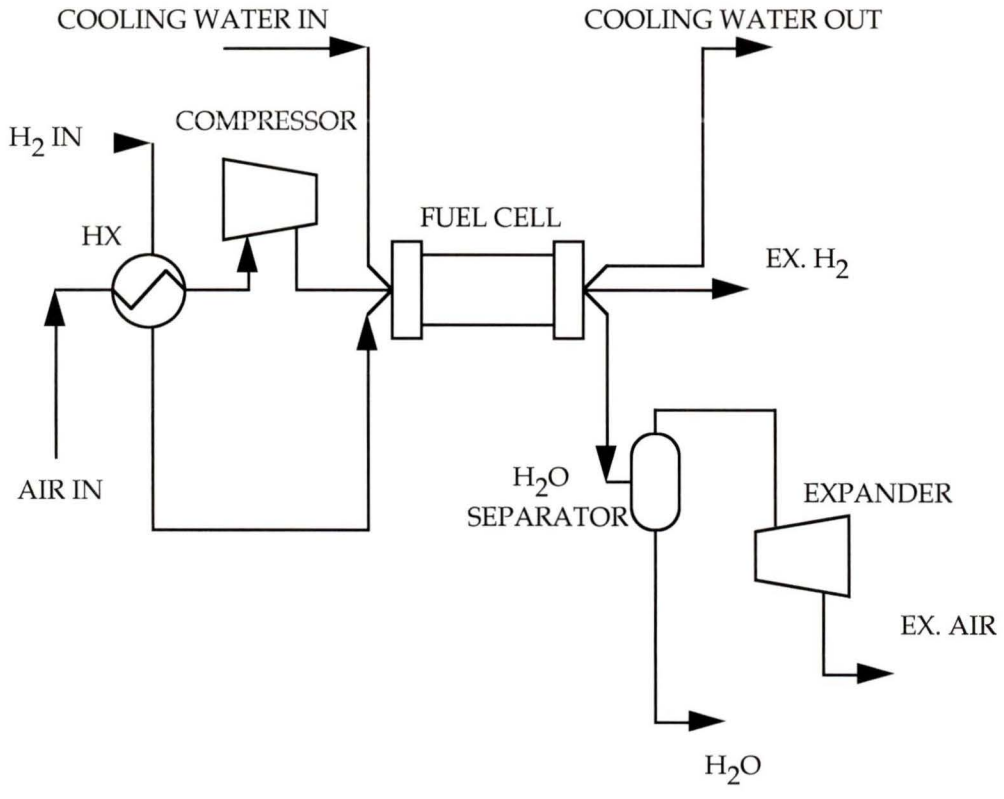

Figure 6.6: Air precooling system model

At the stack design point, air enters the compressor at 235 K, based on a heat exchaterminal temperature differential of 5 K. The nominal results are;

$$\dot{W}_{fc} = 247.2 \text{ kW}$$

$$\dot{W}_{c} = 50.4 \text{ kW}$$

$$\dot{W}_{e} = 13.2 \text{ kW}$$

with a net output of 210 kW. The fuel cell output remains unchanged as expected, while the compressor load is reduced by 14 kW. The expander power output is reduced by 5.2 kW due to the elimination of heat transfer from the compressed air stream to the excess air stream prior to compression. The net power improvement corresponds to an increase of 4.3%.

Figure 6.7 shows the variation of compressor input power as a function of compressor isentropic efficiency. The variation of compressor work as a function of heat exchanger terminal ΔT, defined as air inlet temperature less the H_2 exit temperature, is shown in Figure 6.8. Figure 6.9 illustrates the variation of compressor work and fuel cell output as functions of fuel cell operating pressure. Pressure is not extensively varied in this work. Changing the input parameters and work required for compression with an ECERS system yields an opportunity for pressure optimization.

The sensitivity runs conducted showed the compressor power savings to be insensitive to heat exchanger performance. The power savings are highly dependent on compressor efficiency, with precooling showing large advantages at low compressor efficiencies. For the remainder of the modelling work, compressor efficiency was held constant at 55%.

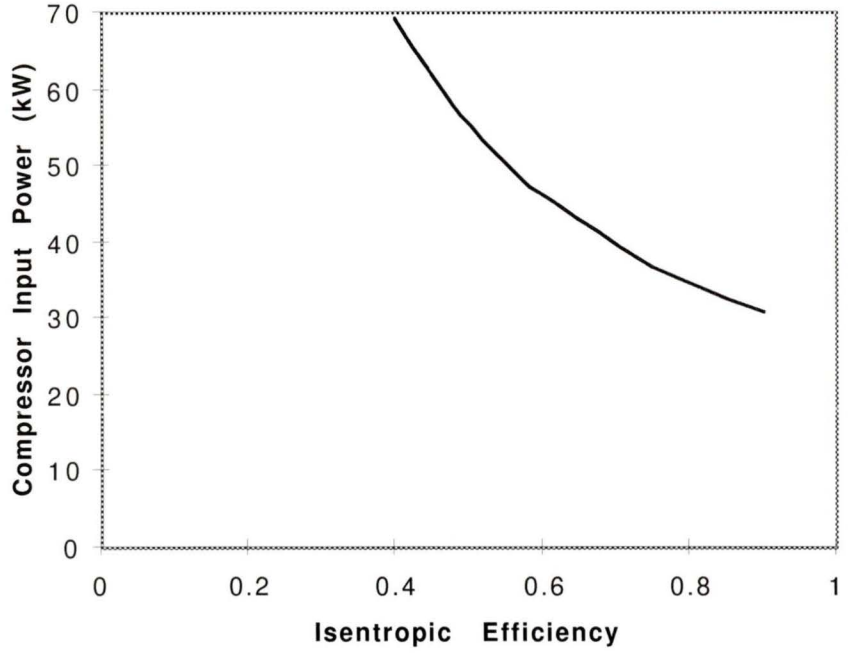

Figure 6.7: Compressor input power vs. efficiency

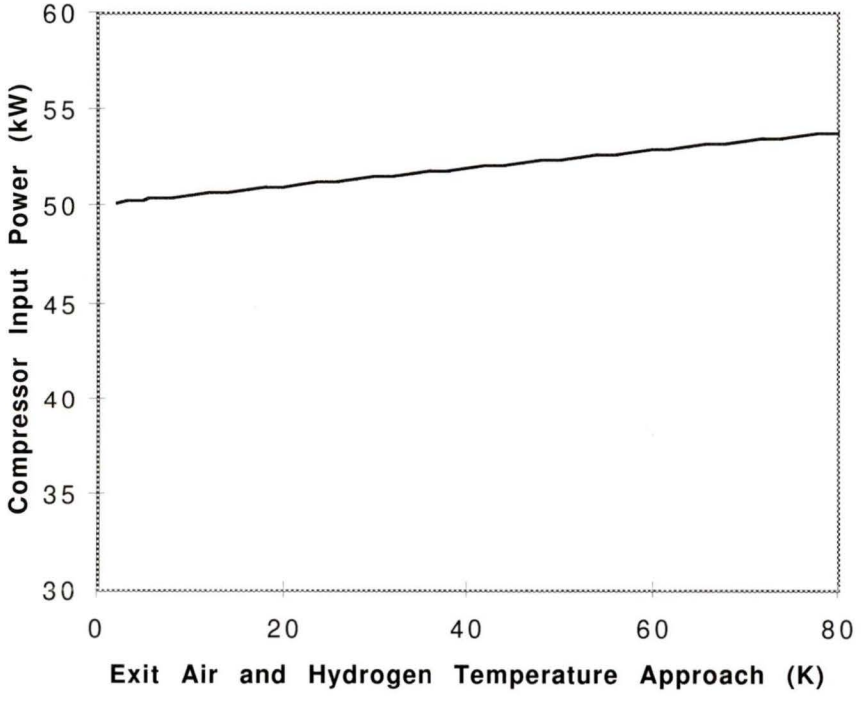

Figure 6.8: Compressor input power vs. heat exchanger ΔT

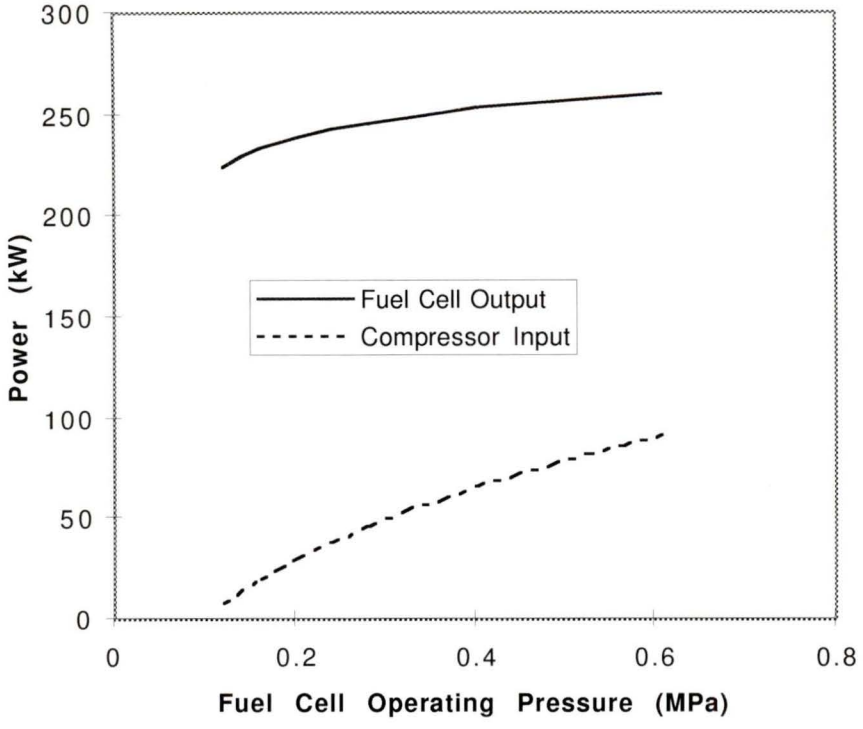

Figure 6.9: Compressor & fuel cell power vs. operating pressure

6.6.1 Direct Expansion/Air Precooling

One of the alternatives investigated is to combine a DE cycle (see Section 4.7) with the air precooling system of Section 6.6. The LH_2 can be pressurized before receiving heat from the air stream. Thus the heat transfer from the air stream to the H_2 stream has two benefits:

- Reduces the work input to the air compression process.
- Provides the heat of vapourization and expansion to the pressurized LH_2, which is recovered as work.

This idea can be applied to any of the above systems but was investigated primarily with the air precooling system to give an appraisal of the work that could be produced and the detrimental effect that H_2 pressurization would have on the subsequent air cooling process. Because LH_2 is a near incompressible fluid, it requires little work input for pressurization and thus has a relatively minor enthalpy increase.

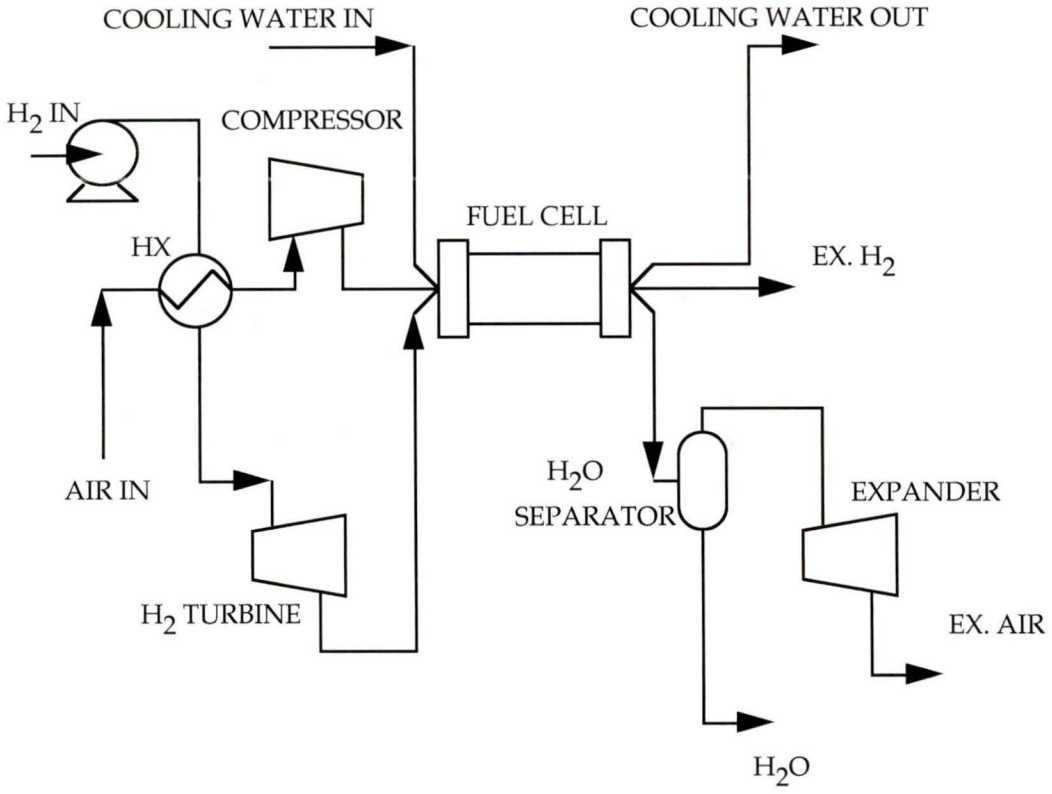

Figure 6.10: DE/air precooling system

Figure 6.11 shows a parametric plot illustrating the effect of maximum DE cycle pressure and varying expander efficiency on compressor and expander power. The minor, but linear dependence of compressor power on pressure and varying expander power are clearly seen. A 60% expander efficiency and 5.0 MPa DE cycle pressure are the basis for comparison with other cycles. The net output of the DE system is 6.3 kW. The parasitic air compression load is reduced 8.3 kW from the baseline case.

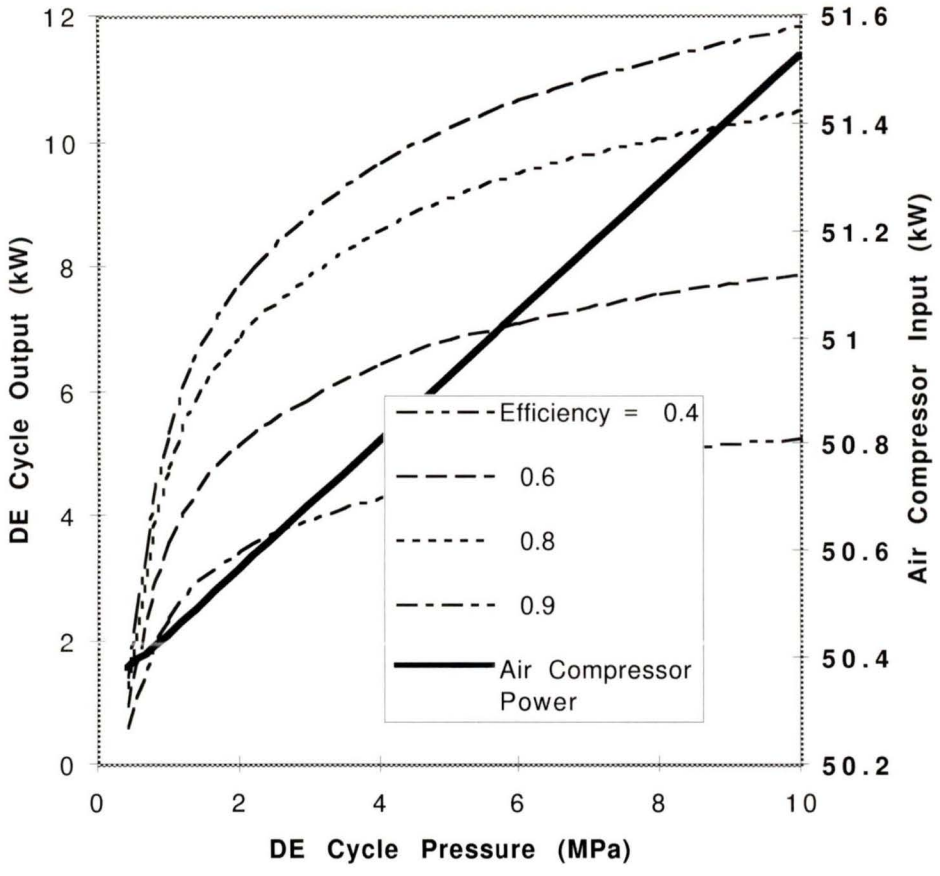

Figure 6.11: DE cycle output at varying expander efficiency and air compressor input vs. H_2 pressure

6.7 Air Enrichment

Section 5.3 covers the principles of cryogenic air separation. Several arrangements are conceivable for air enrichment. Such arrangements include systems that feed the fuel cell powerplant a steady flow of enriched air and systems which could store higher purity enriched air for transient, high load applications. A supply of enriched, compressed air could be generated with very little work input by pressurizing the liquid prior to revapourization. Pump work would displace compressor work. The yield and purity of enriched air can be varied considerably as a function of the complexity of the system. The

purification process is modelled as a single stage phase separator with no heat duty in the separator itself. Further modelling with two separators in series did not indicate a significant improvement in enriched O_2 yield. All cooling is done prior to the air stream being fed to the separator.

6.7.1 Enriched Air Production for Storage

The basic enriched O_2 production scenario is illustrated in Figure 6.12. A twice stoichiometric flow of air is supplied in the stream "AIR IN" to supply the fuel cell's constant O_2 demand. An additional, smaller air stream is fed to a multi-pass heat exchanger (MHX) prior to entering the phase separator. The two air streams are kept separate throughout the system. The three pass heat exchanger cools the "Auxiliary Air" stream to its liquefaction temperature. The two phase mixture consists of a N_2 rich vapour and an O_2 rich liquid. This liquid is referred to as enriched air. The enriched air is pressurized in a cryogenic fluid pump prior to revapourization in the three pass heat exchanger and then is stored as a high pressure gas. The phase separator temperature controls the percentage and composition of the liquid and vapour streams produced.

The higher flow rate N_2 rich vapour is used to precool the main incoming air stream in counterflow heat exchange, and thus a significant cooling effect is still available to the main air stream. The baseline case produces a stream of .405 mole/s O_2 at a concentration of 40%. $\dot{W}_c$ = 51.3 kW while the fuel cell and expander power output remain unchanged for a net powerplant production of 209.2 kW.

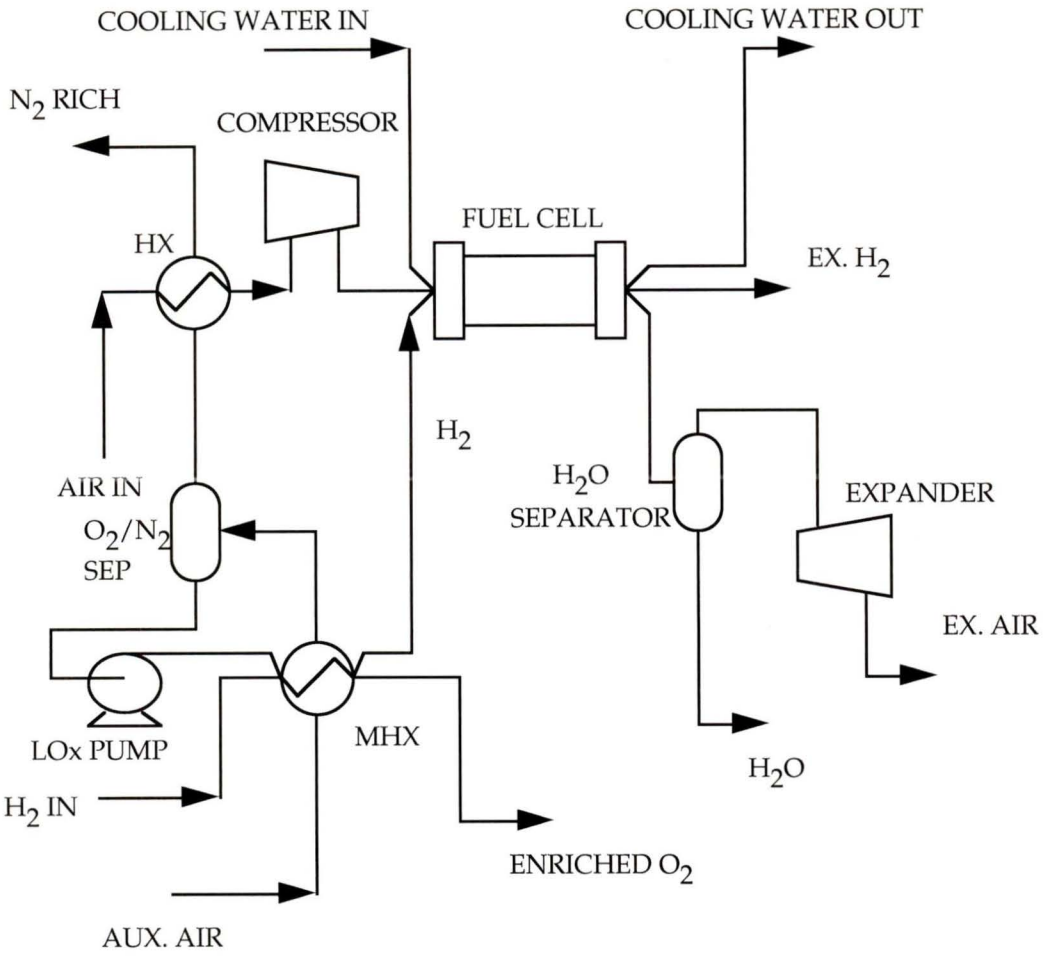

Figure 6.12: Air enrichment schematic

6.7.2 Peak Load Matching

The air enrichment system of section 6.7.1 produces .405 mole/s of O_2 in a 40% O_2/60% N_2 enriched air mixture at the bus design point. This corresponds to approximately 35% of the stoichiometric amount of O_2 required for steady state fuel cell operation, and 17% of the twice stoichiometric amount assumed throughout this modelling.

The vehicle load cycle must be considered to realize the full advantage of this enriched O_2 stream in a transportation application. The enriched O_2 stream can be stored in either

pressurized liquid or gaseous form and used to enhance the performance limiting cathode reaction. Thus a vehicle powertrain system can operate up to its conventional rated output while producing an enriched O_2 stream. This stream can in turn be injected into the fuel cell at peak load requirements.

The benefit from operating on higher concentration O_2 during peak, transient loading is twofold;

1) Increased O_2 concentration speeds the cathode reaction kinetics. A greater power output and H_2 efficiency is realized.

2) Sufficient quantity of pressurized (as a liquid), enriched air can permit the *elimination of compressor load* during peak load operation. A control scheme is possible where the entire oxidant stream requirements are met by the pressurized, enriched air. The net output improvement is the fuel cell performance improvement plus the compression load that is eliminated.

The United States Advanced Battery Consortium Dynamic Stress Test (USABC DST) [66] [72] was used to calculate the net power improvement during peak loading. This system was developed for battery power systems but was selected to be representative of a vehicle duty cycle. The cycle itself is a 360 second interval with operation at various discrete loads, and is included in Appendix C. In operation, the vehicle spends 2.1% of its operating cycle at full load, with the remainder of the cycle made up of various loads between zero and 62.5% of full load.

The thermodynamics of the enriched air production process yield a linear dependence of air production on H_2 flow, and therefore load. A time weighted average of the USABC cycle yields an enriched air production of 0.062 mole/s. If used only for peak loading, the system produces sufficient enriched O_2 for a maximum output at 2.7% of total vehicle operating time. Enriched air produced and stored over the duty cycle can meet the 2.1% peak load duration.

The fuel cell operation is predicted using the same voltage model at higher O_2 concentrations. Figure 6.13 illustrates model results of power output versus current density and O_2 concentration.

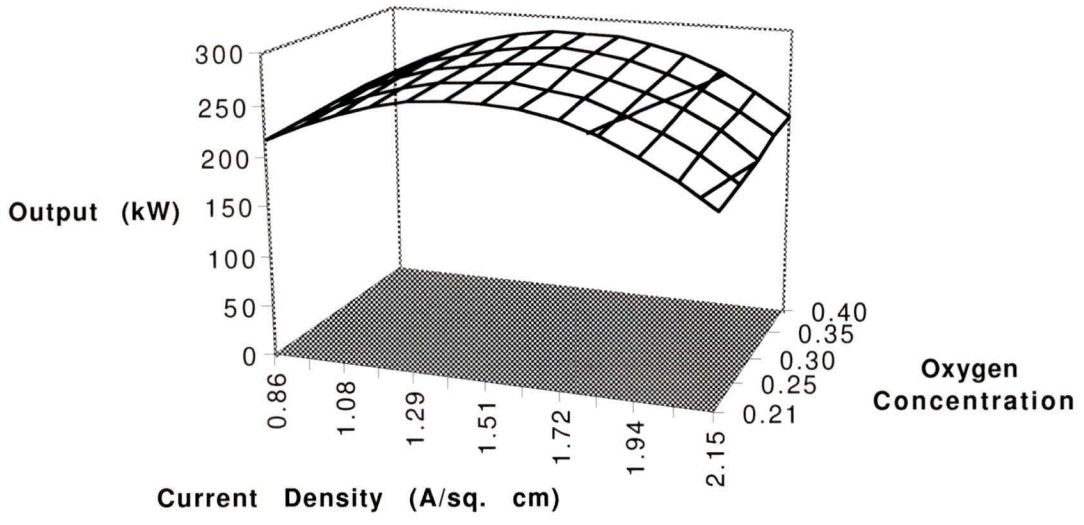

Figure 6.13: Fuel cell output vs. current density, O_2 concentration

The model indicates a slight increase in output and efficiency operating on enriched O_2. At the design point of 1.076 A/cm^2, the fuel cell output is 258.9 kW at 40% O_2 versus the baseline 247.2 kW at 21% O_2. In addition, it is possible to eliminate the net compressor load. A conservative estimate of the power produced would have the compressor and turbocharger bypassed, so no net expander work is recovered. Thus for short timeframes, the powerplant that was rated at 201.2 kW could conceivably produce 258.9 kW, an increase of 29%.

As mentioned previously, the enriched air could be stored as either a cryogenic liquid or compressed gas. For simplicity, to avoid requiring rapid heat transfer to vapourize the liquid, compressed gas storage was considered. A storage capacity for twice the 6 minute USABC cycle duration at 300 K, 20.0 MPa would require 3.75 litres. The only additional required component is a cryogenic pump to pressurize the liquified, enriched air to the high pressure. The power input to this pump, however, is negligible.

6.7.3 Two Pass Heat Exchange

One of the complicating factors in the model of Figure 6.12 is the use of a multi-pass heat exchanger and recirculating heat transfer loop. Multi-pass heat exchangers were incorporated in the systems to take advantage of as many of the warming cryogenic heat sink streams as possible to cool down the inlet air stream prior to condensation. The heat exchangers were limited to a maximum of three fluid streams to avoid excess system complexity. The "waste" N_2 vapour stream could be recirculated through the heat exchanger as a fourth stream, but was routed to precool the main, incoming air stream.

In any multi-pass heat exchanger system, the number of heat transfer streams and the number of recirculating loops will determine the time response of the system. Considering the system of Figure 6.12, it can be seen that as the first air is introduced into the multi-pass heat exchanger, only the warming cryogenic H_2 is available to cool the air to its condensation temperature. Therefore, the inlet flow of air to the process must be initially low before the cooling effect of the returning O_2 rich stream can be utilized. This effect will manifest itself in long response times to varying flow conditions - a major issue in any transportation vehicle powerplant.

To offset the difficulty of designing an ECERS system with respect to transient load response, the system was modelled with a two pass heat exchanger in the air condensation loop replacing the three pass unit. In this configuration the airflow entering the condensation loop will be a function of only the H_2 flow and can be controlled based on that value. The system is shown in Figure 6.14.

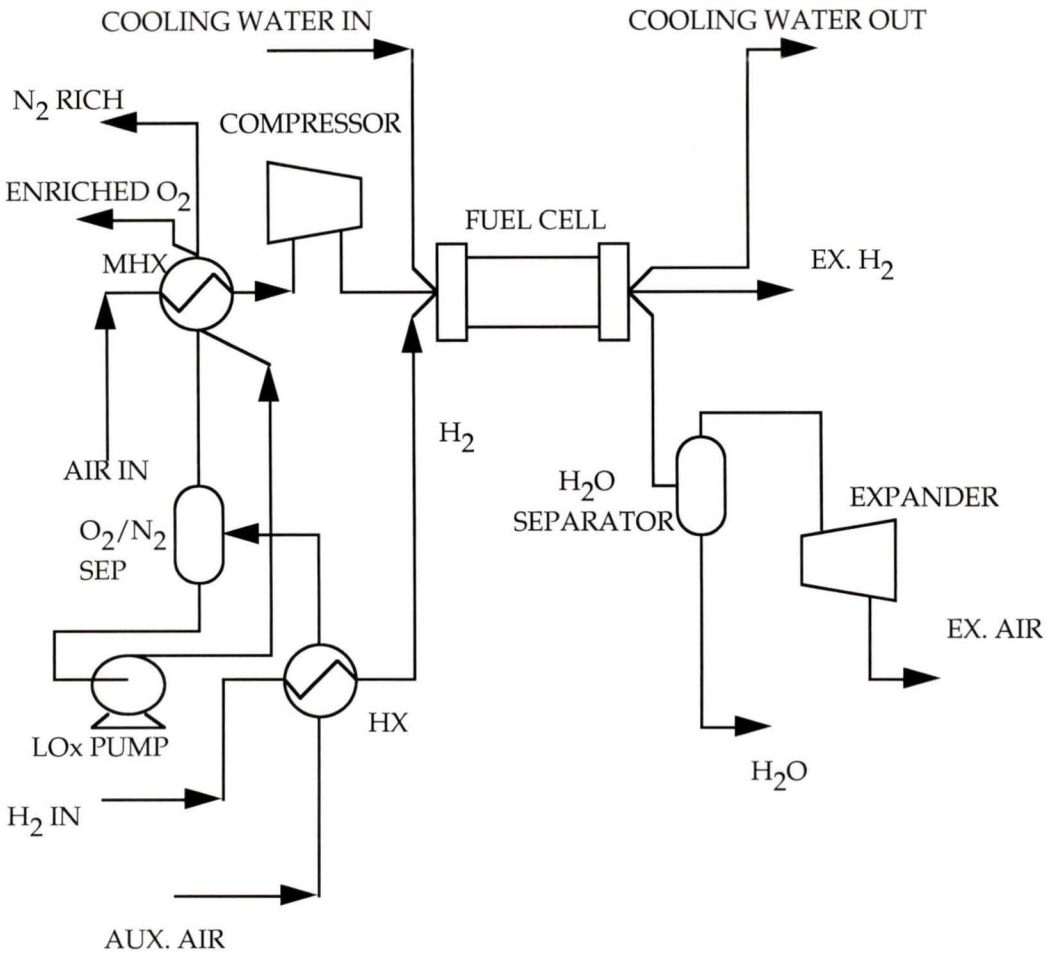

Figure 6.14: Non-recirculating air condensation

The system as shown does incorporate a three pass heat exchanger in the main air precooling loop to take advantage of the warming O_2 and N_2 streams. The major advantage of this arrangement over that of Figure 6.12 is the elimination of the recuperative heat transfer loop containing the separator, multi-pass heat exchanger, and the cryogenic fluid pump.

The simulation at the base design point resulted in a compressor input power requirement of 50.9 kW at an enriched air flow of 0.257 mole/s O_2 and 0.365 mole/s N_2. The delivery pressure of the enriched air was also varied to evaluate the effect on compressor power input. Pressurizing the liquid air prior to vapourization and storage increases the liquid air

stream enthalpy entering the MHX. The compressor power increase is minor, to 51.6 kW at 10.0 MPa delivered excess air pressure and 52.2 kW at 20.0 MPa excess air. The enriched air pressure has no effect on the composition of the stream.

6.7.4 Steady-State Enriched Air Operation

An alternative to producing enriched air for storage is to combine the enriched air with the main compressor outlet stream to obtain a flow of slightly enriched air for continuous operation. This is basically the same system as Figure 6.12 but with the addition of a mixer after the compressor and multi-pass heat exchanger. Figure 6.15 shows the "mixed" schematic. An AspenPlus run report for this model is included in Appendix D.

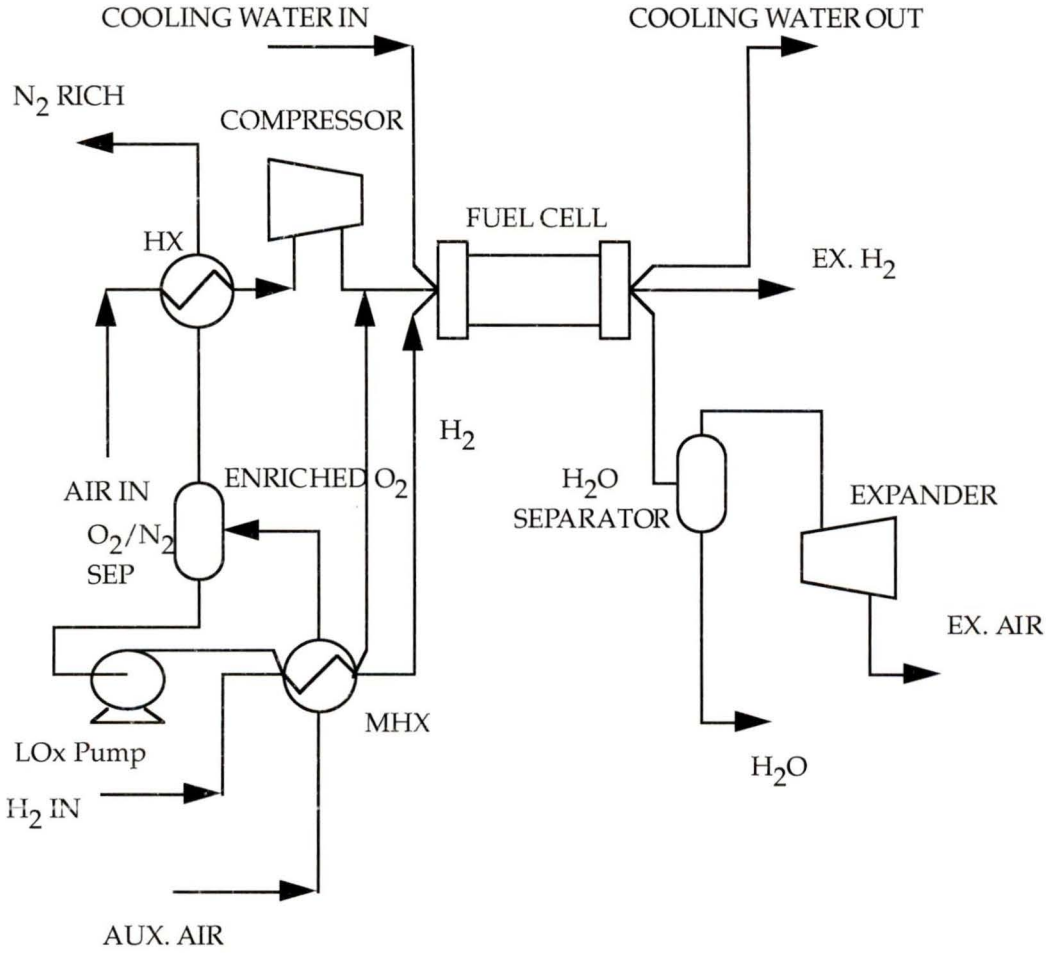

Figure 6.15: Mixed flow air enrichment system

The system as illustrated has two significant advantages over the basic powerplant configuration:

- Improved fuel cell efficiency. Although the O_2 concentration is considerably lower than what could be produced and stored for high load operation, it is still significant enough to improve the fuel cell stack output and efficiency.
- Reduction in compression power. As in the earlier systems the air is precooled prior to compression with the cold, N_2 rich vapour. In addition, the flow through the main air stream is reduced while maintaining the existing stoichiometry of 2. The opportunity also exists to reduce the stoichiometry of air flowing through the stack due to the increased O_2 concentration, but was not explored. O_2 partial pressure and water removal are the main concerns when reducing air flow to the stack.

The design point results are as follows;

$$\dot{W}_{fc} = 248.8 \text{ kW}$$

$$\dot{W}_{c} = 39.5 \text{ kW}$$

$$\dot{W}_{e} = 11.8 \text{ kW}$$

Thus the net power produced is 221.1 kW, a 9.9% increase over the basic bus model. The oxidant feed to the fuel cell stack at steady flow conditions is 24% O_2 by volume.

The separator temperature determines the enriched air flow in the system and the O_2 concentration. At temperatures below 80.5 K, the auxiliary air flow must be reduced to maintain a positive temperature differential in the multi-pass heat exchanger. If the separator temperature is lowered to 79.5 K, suggesting a possible greater flow of enriched O_2, the actual inlet auxiliary air flow is limited to 2.7 mole/s. No improvement was observed at temperatures below 80.5 K. Above this temperature, the O_2 concentration of the enriched air was reduced.

6.8 Cryogenic Exergy Recovery to Increase Cooling

A low temperature heat engine could theoretically increase the amount of cooling available when the cryogenic H_2 is used as a low temperature heat sink for air precooling and purification. A Stirling heat engine can operate between the phase transformation of LH_2 (23 K) and the air stream condensation temperature (~80 K). This heat engine would have the double benefit of producing useful mechanical work while increasing the cooling, and thus yield, of the air enrichment system. The Carnot efficiency operating between these temperatures is 71%. If $\eta_s = 0.5$, with a heat sink of 2.2 kW, the power produced (and thus additional cooling effect) is 1.2 kW. Comparing this value to the 21 kW of heat duty transferred to the H_2 heat sink in the multi-pass heat exchanger of Section 6.7, the additional cooling effect of the cryogenic heat engine is minor.

This system presents an interesting thermodynamic balance in which an increase in heat engine efficiency has the twofold benefit of increasing power output and the magnitude of the desired cooling effect. However, at this point in time it is not foreseen as a practical option. Improvements in Stirling heat engine efficiency would make the concept more practical for this application.

6.9 Cooling Load Reduction

The function of the fuel cell cooling system is to maintain the fuel cell operating temperature at a constant level. To accomplish this, the heat of reaction must be removed from the fuel cell stack. An energy balance in the fuel cell stack obtains the amount of heat that must be removed.

$$0 = \frac{\dot{Q}}{\dot{m}} + h_{R \to P} - \frac{\dot{W}}{\dot{m}} \tag{6.3}$$

where $h_{R->P}$ is the heat of reaction, $\frac{\dot{W}}{\dot{m}}$ is the electrical work produced and $\frac{\dot{Q}}{\dot{m}}$ is the heat rejected through the cooling water system. In the simplified case with the reactants and

products at the same temperature, $h_{R->P}$ is either the higher heating value (HHV) or lower heating value (LHV) of the reaction. Thus the heat that must be removed is the heat of reaction less the amount of work extracted from the system. Figure 6.16 illustrates the heat of reaction and work produced by a fuel cell at one operating point, converted with Faraday's constant [68]. The net area difference between the two curves is the heat that must be removed from the system. The state of the exiting water determines the use of the HHV or LHV. Figure 6.16 uses the LHV to determine the cooling load.

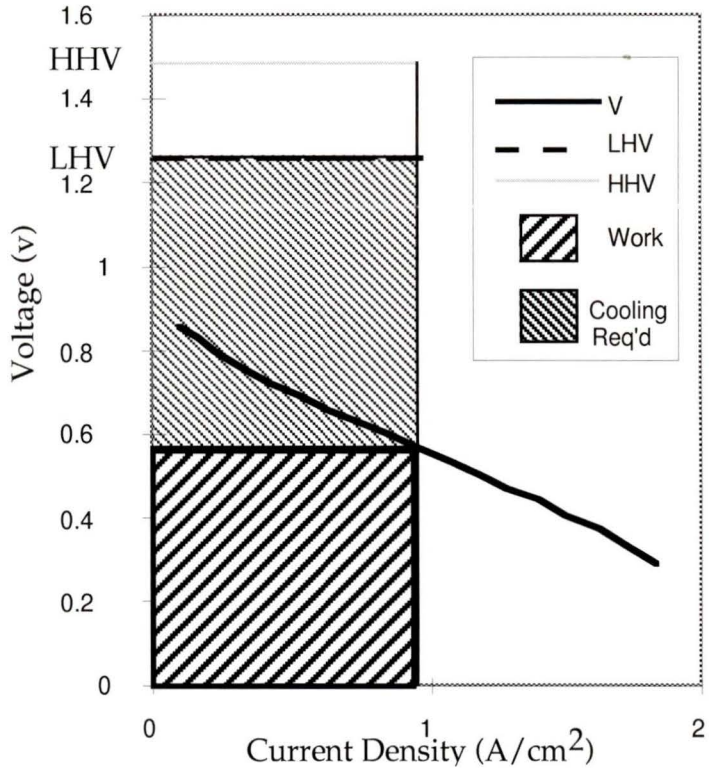

Figure 6.16: Fuel cell output/cooling load

In a real fuel cell system the reactants and products are not typically at the same temperature. Greater energy is carried away with the products, and the exiting water will likely be two phase, resulting in a heat of reaction between the HHV and LHV.

The heat engine cycles of sections 4.6 and 4.7 utilize waste heat from the cooling water system as heat input to the heat engine. The basic LH_2 vapourization system provides the heat of warming from the cooling water system, removing 21.0 kW of heat from the

cooling water. A cryogenic heat engine increases the additional cooling load rejected by an estimated 2-8 kW, but the increase is relatively minor when compared to the 300+ kW cooling load.

6.10 Model Comparisons

The model results of Chapters 4 and 6 are summarized in Table 6.2. Table 6.1 forms a legend of the simulations.

Table 6.1: System descriptions

Designation	System Description
I	Baseline Bus
II	Stirling Heat Engine
III	Direct Expansion Heat Engine
IV	Air Precooling Prior to Compression
V	Air Precooling/Direct Expansion
VI	Enriched Air Production for Storage
VII	Enriched Air Production for Storage (Two Pass Heat Exchange)
VIII	Steady State Air Enrichment

Table 6.2: Steady-state output comparison of exergy recovery systems

System	$\dot{W}_{fc}$	$\dot{W}_{c}$	$\dot{W}_{e}$	$\dot{W}_{gen}$	$\dot{W}_{net}$	% Increase
I	247.2 kW	64.4 kW	18.4 kW	-	201.2 kW	-
II	247.2	64.4	18.4	4.4 kW	205.6	2.2
III	247.2	64.4	18.4	7.6	208.8	3.8
IV	247.2	50.4	13.2	-	210	4.4
V	247.2	50.9	13.2	6.3	215.8	7.3
VI*	247.2	51.3	13.2	-	209.1	3.9
VII*	247.2	50.9	13.2	-	209.5	4.1
VIII	248.8	39.5	11.8	-	221.1	9.9

*Systems VI and VII have an additional peak load capacity of 258.9 kW, not reflected in the above table. Only system VI was able to sustain a high enough production level to meet the USABC DST cycle requirements.

CHAPTER 7 CONCLUSIONS & RECOMMENDATIONS

7.1 Conclusions

Exergy recovery devices show promise in transportation applications using LH_2. This work compared a discrete number of exergy recovery alternatives adapted to the target bus application. The main conclusions of this thesis are as follows:

- Air precooling prior to compression is a simple means of recovering cryogenic thermomechanical exergy. The predicted power improvement at full load is 8.8 kW, a 4.3% improvement. The components required are not as technically challenging as in other exergy recovery systems.

- Enriched O_2 can be produced by relatively simple on-board equipment. The enriched O_2 can be utilized as it is produced, improving the cell cathode reaction and reducing air compression load. The feed O_2 concentration to the fuel cell can be increased to 24% with a simple single stage separator. Such a configuration is well suited for any applications involving near-constant loads.

- Storage of pressurized enriched O_2 can significantly improve transient power output during peak power demand. Based on the duty cycle considered, and utilizing a multi-pass heat exchanger, the powerplant can be rated for transient loads of up to 29% greater than the baseline vehicle. The peak load duration that can be met is 2.7% of the total cycle duration. This compares to 2.1% required for the USABC cycle. The transient load configuration has an 8 kW power savings at the baseline condition, when the fuel cell is not operating on enriched O_2.

The greatest contribution to peak load improvement is the displacement of compressor load. The fuel cell gross output improved 9 kW when operating on a 40% O_2 oxidant.

- Cryogenic heat engine cycles do not show great promise. The limitations of a finite heat sink place excessively tough demands on cycle performance for the engine to be competitive with other exergy recovery options. If heat engines are to be successful in this application, considerable effort must be made to improve cycle efficiency.

  Stirling cryogenic heat engines do not appear to be suitable in the cryogenic heat engine regime, operating with a gasifying cryofuel. Characteristic efficiencies are too low to practically recapture the cryofuel thermomechanical exergy.

  Direct Expansion heat engines appear to offer exergy recovery efficiencies similar to Stirling machines. The expander still poses a significant technical challenge to perform efficiently and manufacture cost effectively.

  The complexity of either heat engine system is significantly greater than the simplest air enhancement system (air precooling) while offering lower power improvement.

- A low temperature heat engine operating between LH_2 and air condensation temperatures does not significantly improve the yield of an air enrichment system. The addition of a heat engine increases system complexity.

- LH_2 fuel does not offer a significant reduction of the vehicle cooling load. If used directly to cool the vehicle cooling water, the cooling load is reduced by 21 kW. The addition of a cryogenic heat engine improves this by an amount equal to the output of the engine, but the cooling load reduction is less than 10% of the total.

7.2 Recommendations for Future Work

This work represents a preliminary thermodynamic analysis of thermomechanical exergy recovery opportunities for the bus system. More detailed design work, including economic analysis, is required before any of the systems could be implemented. In order to determine the overall benefit of incorporating an ECERS into future bus, or any LH_2 powered vehicle, the following work is suggested.

- Detailed design of ECERS precooling and air enrichment systems, with specific attention to the control system required, particularly in respect to transient loads. The air enrichment and distillation processes require detailed optimization and design. Individual components must be specified.

- Manufacturing cost estimation of the various components.

- Design and cost estimation of a LH_2 powered bus. Once a cost can be assigned to a LH_2 vehicle, and the performance improvement with an ECERS quantified, the feasibility of converting to liquid from compressed fuel can be assessed.

REFERENCES

1. Institute Brochure, "Institute for Integrated Energy Systems", University of Victoria, Victoria, 1993.

2. D. S. Scott, "Hydrogen in the Evolving Energy System", *International Journal of Hydrogen Energy.* Vol. 18, No. 3, pp. 197-204, March 1993.

3. T. J. Kotas, *The Exergy Method of Thermal Plant Analysis*, Butterworths, Toronto, 1985.

4. W. C. Reynolds and H. C. Perkins, *Engineering Thermodynamics.*, McGraw-Hill, New York, 1977.

5. P. Crane, *An Exergy Perspective on Selecting Technical Pathways by which Methane can provide Transportation Services.* MASc Thesis, Dept. Of Mechanical Engineering, University of Victoria, Victoria, 1991.

6. C. R. Baker and R. L. Shaner, "A Study of the Efficiency of Hydrogen Liquefaction", *International Journal of Hydrogen Energy*, Vol. 3, pp. 321-334, 1978.

7. D. S. Scott, *Course Notes - Mech 542, Exergy Analysis and Energy Systems*, Dept. Of Mechanical Engineering, University of Victoria, 1994.

8. D. S. Scott, "Energy Currencies", *International Journal of Hydrogen Energy*, Vol. 19, No. 3, March 1994.

9. D. S. Scott, "Liberty", *International Journal of Hydrogen Energy*, Vol. 19, No. 4, April 1994.

10. D. S. Scott, "Hydrogen in the Evolving Energy System", *International Journal of Hydrogen Energy*, Vol. 18, No. 3, pp. 197-204, March 1993.

11. R. F. Barron, *Cryogenic Systems.*, 2nd Edition, Oxford Press, New York, 1985.

12. ASHRAE Handbook,*1981 Fundamentals*, American Society of Heating, Refrigerating and Air-Conditioning Engineers, Inc., Atlanta, 1981.

13. *CRC Handbook of Chemistry and Physics*., 61st Edition, CRC Press Inc., Boca Raton, Fla., 1980.

14. J. M. Bourguet, "Valorisation des frigories contenues dans le G.N.L.", *Techniques de l'Energie*, Vol. 36, pp. 14-18, 1980.

15. H. Shiozawa and M. Hanamure, "The Operation Results of LNG Cold Power Generation in Multicomponent Fluid Rankine Cycle", *Proceeding of the Eighth International Conference on Liquefied Natural Gas*, Los Angeles, June 1986.

16. K. D. Timmerhaus, "Low temperature technology utilization in the solution of energy problems", *International Journal of Refrigeration*, Vol. 6, pp. 274-282, 1983.

17. S. Hirakawa and K. Kosugi, "Utilization of LNG Cold", *International Journal of Refrigeration*, Vol 4, No. 1, pp. 17-21, 1981.

18. M. Ueda, "Manufacture of Liquid Oxygen Using LNG Coldness", *Chemical Economy and Engineering Review*, December 1970.

19. T. Murata and E. Nakanishi, "How Osaka Gas Uses The Cold From LNG", Pipeline and Gas Journal, Vol. 207, No. 3, pp. 23-38, March 1980.

20. N. Yamanouchi and H. Nagasawa, "Using LNG Cold for Air Separation", *Chemical Engineering Progress*, Vol. 75, No. 7, pp. 78-82, July 1979.

21. H. Kataoka, "Use the cold in LNG", *Hydrocarbon Processing*, Vol. 53D, pp. 97-102, November 1974.

22. J. G. Witwer, "Energy Conversion with LNG Cold", *Chemical Engineering Progress*, Vol. 72, No. 1, pp. 50-55, January 1976.

23. M. Arai et al., "Practical Application of an LNG Cold Energy Recovery Power Plant", *Technical Review-Mitsubishi Heavy Industries*, Vol. 21, No. 3, pp. 263-270, October 1994.

24. W. Wong, "LNG Power Recovery", *Journal of Power and Energy*, Vol. 208, 1994.

25. G. Acker Jr. et al., "Experience using LNG as a marine engine fuel", *Marine Technological Society Journal*, Vol 23, pp. 33-39, 1989.

26. D. B. Paul, C. L. Clay, and M. P. Camden, "Hydrogen Active Cooling of Hypersonic Structures", *National Aero-Space Plane and Space Applications, World Hydrogen Conference 8*, pp. 159-170, July 22-27, 1990.

27. N. Karashima and T. Akutsu, "Development of LNG Cryogenic Power Generation Plant', *Proceedings of the 17th Intersociety Energy Conversion Engineering Conference*, pp. 399-404, 1982.

28. K. Horiuchi and S. Tajima, "An LNG Cryogenic Power Generation System", *Energy Developments in Japan*, Vol. 7, pp. 201-215, 1985.

29. M. Ruhemann, "Producing Power from a Cryogenic Liquid", *U.S. Patent # 4,400,947.*

30. G. Bisio, "Combined Plants with High and Cryogenic Temperatures for Power Production and Liquid Hydrogen Vaporization", *Proceedings of the International Symposium on Efficiency, Cost, Optimization and Simulation of Energy Systems,* pp. 413-418, 1992.

31. K. Oshima et al., "The Utilization of LH2 and LNG Cold for Generation of Electric Power by a Cryogenic-Type Stirling Engine", *Proceedings of the Seventh International Cryogenic Engineering Conference*, pp. 310-317, 1978.

32. S. Furuhama, T. Nakajima and T. Honda, "Rankine Cycle Engines for Utilization of LH_2 Car Fuel as a Low-Temperature Source", *International Journal of Hydrogen Energy*, Vol. 18, No. 2, pp. 149-155, 1993.

33. J. Williams, "Nitrogen Powered Automobile", *Alt.energy.renewable, sci.energy Internet Newsgroup*, November 16, 1995.

34. A. Fyke et al., "Recovery of Thermomechanical Exergy from Cryofuels", *Proceedings of the 10th World Hydrogen Energy Conference*, pp. 1007-1016, June 20-24 1994, Cocoa Beach, Fla.

35. A. Fyke, "Enhanced Cryogen Exergy Recovery System: Initial Theory and Design", 2nd Ed. *Work Term Report*, Department of Mechanical Engineering, University of Victoria, 1995.

36. M. A. DeLuchi, "Hydrogen Vehicles: an evaluation of fuel storage, performance, safety, environmental impacts, and cost", *International Journal of Hydrogen Energy*. Vol 14, No. 2, pp. 81-130, 1989.

37. Personal Communication, Dr. Geoffrey Ballard, February 19, 1996.

38. D. E. Daney et al., "A Comparison of Hydrogen Vehicle Storage Options Using the EPA Urban Driving Cycle", *Presented at the ICMC/CEC*, Columbus, July 17-21, 1995.

39. H.-H. Rogner and J. D. Wells, "Fuel Cells for Transportation: A Methodological Market Analysis Approach", *Presented at the Seventh Canadian Hydrogen Workshop*, Quebec City, June 4-6, 1995.

40. Ballard Power Systems, *Fuel Cell Bus Program*, Company literature.

41. Personal Communication, Doug Strasky, SAIC, November 1994-March 1996.

42. H.-R. Zollner, "Liquefaction of Natural Gas with the Aid of Refrigerant Mixtures", *Linde Reports on Science and Technology*, Vol. 32, 1981.

43. M. J. Moran and H. N. Shapiro, *Fundamentals of Engineering Thermodynamics*., 2nd Ed. John Wiley and Sons, New York, 1992.

44. Personal Communication, Engineering work term, Ontario Hydro, Pickering Nuclear Generating Station, Pickering, Ontario, May-August 1987.

45. H. Shiozawa and T. Hiro-oka, "Power Generation Using Cold Potential of LNG in Multicomponent Fluid Rankine Cycle", *Advances in Cryogenic Engineering,* Vol. 27, pp. 971-978, Plenum Press, New York, 1982.

46. H. Kashimura and H. Yoshikawa, "Power Generation Using Cold Potential of LNG in Multicomponent Fluid Rankine Cycle", *Proceedings of the Seventh International Conference on Liquefied Natural Gas*, Jakarta, Indonesia, May 15-19, 1983.

47. W. A. Little and I. Sapozhnikov, "Development of a Low Cost, Cryogenic Refrigeration System for Cooling of Electronics", *Advances in Cryogenic Engineering*, Vol. 39B, pp. 1467-1474. 1994.

48. C. K. Chan, "Closed Cycle Joule Thomson Refrigerator Using Gas Mixtures", *Proceedings of the Fifth International Cryocoolers Conference*, Monterey, CA, 1988.

49. Personal Communication, Dr. Irene Borde, June 19, 1995.

50. G. Walker et al., *The Stirling Alternative*, University of Calgary, 1994.

51. Personal Communication, Dr. Stoian Petrescu, February 9-10, 1996.

52. J. W. L. Kohler, "The Stirling Refrigeration Cycle", *Scientific American*, Vol. 212, No. 4, pp. 119-127, April 1965.

53. W. Martini, *Stirling Engine Design Manual*, NASA Report No. CR-135382.

54. G. Walker and S. Zylstra, "Ross-Stirling Engine: A high Performance Dynamic Space Power System", *Presented at the 22nd Intersociety Energy Conversion Engineering Conference*, Philadelphia, Vol. 1, pp. 138-144, August 1987.

55. K. Oshima et al., "The Utilization of LH2 and LNG cold for Generation of Electric Power by a Cryogenic-Type Stirling Engine", Proceedings of the 7th International Cryogenic Engineering Conference, pp. 310-317, 1978.

56. D. G. Wilson, *The Design of High-Efficiency Turbomachinery and Gas Turbines*, Massachusetts Institute of Technology, 1984.

57. D. S. Scott, "Smelling Land", *International Journal of Hydrogen Energy*, Vol. 19, No. 1, pp. 3-7, January 1994.

58. K. D. Timmerhaus and T. M. Flynn, *Cryogenic Process Engineering*, Plenum Press, New York, 1989.

59. Aspen Technology Inc., Ten Canal Park, Cambridge, MA.

60. M. A. Rosen, *The Development and Applications of a Process Analysis Methodology and Code based on Exergy, Cost, Energy and Mass*, PhD Thesis, Dept. of Mechanical Engineering, University of Toronto, Toronto, 1986.

61. B. I. Verkin, *Handbook of Properties of Condensed Phases of Hydrogen and Oxygen*, Hemisphere Publishing Corporation, 1990.

62. J. C. Amphlett, R. M. Baumert et al., "Performance Modelling of the Ballard Mark IV Solid Polymer Electrolyte Fuel Cell", *J. Electrochem Soc.*, Vol. 142, No. 1, pp. 1-15, January 1995.

63. J. C. Amphlett et al., "The Operation of a Solid Polymer Fuel Cell: A Parametric Model", *Proceedings of the 26th Intersociety Energy Conversion Engineering Conference*, Vol. 3, 1991.

64. J. C. Amphlett, R. M. Baumert et al., "Parametric Modelling of the Performance of a 5-kW Proton-exchange Membrane Fuel Cell Stack", *Journal of Power Sources*, Vol. 49, pp. 349-356, 1994.

65. J. C. Amphlett, R. M. Baumert et al., "A Performance Model for PEM Fuel Cells", *Proceedings of the 28th Intersociety Energy Conversion Engineering Conference*, Vol. 1, pp. 1.1215-1.1220.

66. R. Cownden, "A Performance Model for Hydrogen Fuel Cell Power Systems for Transportation Applications", *Work Term Report*, Department of Mechanical Engineering, University of Victoria, April, 1995.

67. Ballard Power Systems, "Characterization, Modelling, and Improvement of Fuel Cell Performance Using Ambient Air as the Oxidant", *Prepared for NRC Canada*, IRAP-M Project No. 0-8202-M-19.

68. Personal Communication, Mr. Henry Voss, Ballard Power Systems, March 6, 1996.

69. T. E. Springer et al., "Polymer Electrolyte Fuel Cell Model", *J. Electrochem Soc.*, Vol 138, pp. 2334-2342, 1991.

70. J. C. Amphlett, R. F. Mann et al., "An Optimal Experimental Design for Fuel Cell Modelling", *1994 Fuel Cell Seminar; Programs and Abstracts*, pp. 558-561, San Diego, CA, 1994.

71. Personal Communication, Mr. Rob Baumert, Ballard Power Systems, March 8, 1996.

72. D. H. Swan, M. Arikara, B. Dickinson and M. Prabhu, "Cathode Air Control of a PEM Fuel Cell Stack on the USABC Dynamic Stress Test", *Fuel Cell Seminar: Programs and Abstracts*, pp. 217-220, San Diego, CA, 1994.

Appendix A

Fuel Cell Voltage Model

Operating Parameters

Temperature

The fuel cell operating temperature is maintained at 360 K throughout all of the models. The function of the cooling system is to maintain the operating temperature at the desired point and no variation is assumed.

O_2 Partial Pressure

The oxidant stream is assumed to be saturated with water vapour in the humidification section of the cell at the fuel cell operating temperature. The saturation pressure of the water vapour is determined from the parametric relation [69]:

$$P_{H_2O}^{sat} = 10 ** (-2.1794 + 0.02953T - 9.1837e-5T^2 + 1.44e-7T^3) \quad (A.1)$$

where T is given in ° C, P in atm.

The molar vapour fraction of the incoming oxidant stream (assumed dry and consisting of only O_2 and N_2) is:

$$y_{O_2,\,in} = \frac{\dot{n}_{O_2}}{\dot{n}_{O_2} + \dot{n}_{N_2}} \quad (A.2)$$

Thus the inlet O_2 partial pressure in the oxidant stream at P is given by:

$$P_{O_2,\,inlet} = (P - P_{H_2O})y_{O_2} \quad (A.3)$$

The outlet partial pressure is a function of the oxidant stoichiometry as the oxidant stream

becomes depleted in O_2 as it passes through the fuel cell. The outlet partial pressure is given by:

$$P_{O_2,outlet} = P_{O_2,inlet}\left[\frac{1-\frac{1}{\nu_{O_2}}}{1-\frac{y_{O_2,\,in}}{\nu_{O_2}}}\right] \tag{A.4}$$

where ν represents the oxygen stoichiometric ratio. For the purposes of determining the effective O_2 partial pressure at the cathode, constant velocity is assumed through the flow channels due to minor flow variation due to O_2 consumption relative to the total oxidant flow. The effective O_2 partial pressure is determined by a log mean average of the inlet and outlet partial pressures [62]:

$$P^*_{O_2} = \frac{P_{O_2,inlet} - P_{O_2,outlet}}{\ln\left(\frac{P_{O_2,inlet}}{P_{O_2,outlet}}\right)} \tag{A.5}$$

Effective Catalyst O_2 Concentration

The effective oxygen concentration at the catalyst is approximated by the gas/liquid interfacial concentration, determined by a Henry's Law expression [62]. The effective partial pressure of the gas/liquid interface given by:

$$P^{int}_{O_2} = P * \left[1 - y^{sat}_{H_2O} - y_{N_2} * \left(\frac{0.291 * I}{T^{0.832}}\right)\right] \tag{A.6}$$

The effective O_2 concentration at the catalyst is:

$$c^{*}_{O_2} = \frac{P^{int}_{O_2}}{5.08e6 * \exp\left(\frac{-498}{T}\right)} \tag{A.7}$$

H_2 Partial Pressure

Dry, pure H_2 is assumed to be supplied to the anode. The inlet H_2 stream is assumed to be saturated with water vapour at the fuel cell operating temperature. Water transport across the membrane is assumed to 'dry' the H_2 stream across the anode. The effective partial pressure at the anode is found by averaging the assumed saturated inlet and dry outlet:

$$P^{*}_{H_2} = P - (0.5 * P^{sat}_{H_2O}) \tag{A.8}$$

Fuel Cell Voltage Model

The output voltage of the cell is given by:

$$v = E + \eta_{act} + \eta_{ohmic} \tag{A.9}$$

where E is the thermodynamic potential, in volts, of the reaction:

$$H_{2(g)} + \frac{1}{2} O_{2(g)} \rightarrow H_2O_{(l)}$$

given by the Nernst Equation [62]:

$$E = 1.229 - 0.85e-3(T - 298.15) + 4.3085e-5T\left[\ln(P^{*}_{H_2}) + 1/2\ln(P^{*}_{O_2})\right] \tag{A.10}$$

The cathode activation overvoltage is given by the Butler-Volmer Equation [62]:

$$\eta_{act} = \beta_1 + \beta_2 T + \beta_3 T \cdot \ln(c^{*}_{O_2}) + \beta_4 T \cdot \ln(i) \tag{A.11}$$

and represents the losses due to reaction kinetics at the electrodes (dominated by the cathode).

Ohmic overvoltage represents the losses due to the internal electrical resistance of the fuel cell, determined by Ohm's Law. With a parametric expression for the fuel cell internal resistance, the expression becomes [65]:

$$\eta_{ohmic} = -i * (\beta_5 + \beta_6 T + \beta_7 i) \qquad (A.12)$$

The parametric coefficients for equations (A.11) and (A.12) have been determined for the Ballard Mk V cell [70]:

$ß_1$ = -0.944
$ß_2$ = 3.54e-3
$ß_3$ = 7.80e-5
$ß_4$ = -1.96e-4
$ß_5$ = 3.3e-3
$ß_6$ = -7.55e-6
$ß_7$ = 1.1e-6

As a first level approximation, the above equations were modified to accommodate the larger surface area (279 cm^2 versus 232 cm^2) 510 cell by utilizing a 'corrected current' in place of current in equations (A.11) and (A.12) [71]. The corrected current is determined as:

$$i_{corr} = I \times A_{MkV} \qquad (A.13)$$

To align the results of the voltage model, adapted from the earlier cell configuration, with the actual performance of the Phase II bus, a linear correlation was applied to the voltage expression, of the form:

$$v_{corr} = 0.06\ V \times \text{Current Density}/1.076\ A/cm^2 \qquad (A.14)$$

This additional 0.06 V at the design point reflects cell performance improvements since the parametric model for the Mk V cell was developed.

The V-I plot of the modified voltage model vs. experimental data is illustrated in Figure 7.6. For the purposes of evaluating voltage change as a function of air system enhancements it is felt to be adequate and agree well with real data available within the normal bus operating range. Little data is available to correlate performance at higher current densities, which becomes an issue while optimizing performance at higher oxygen concentrations

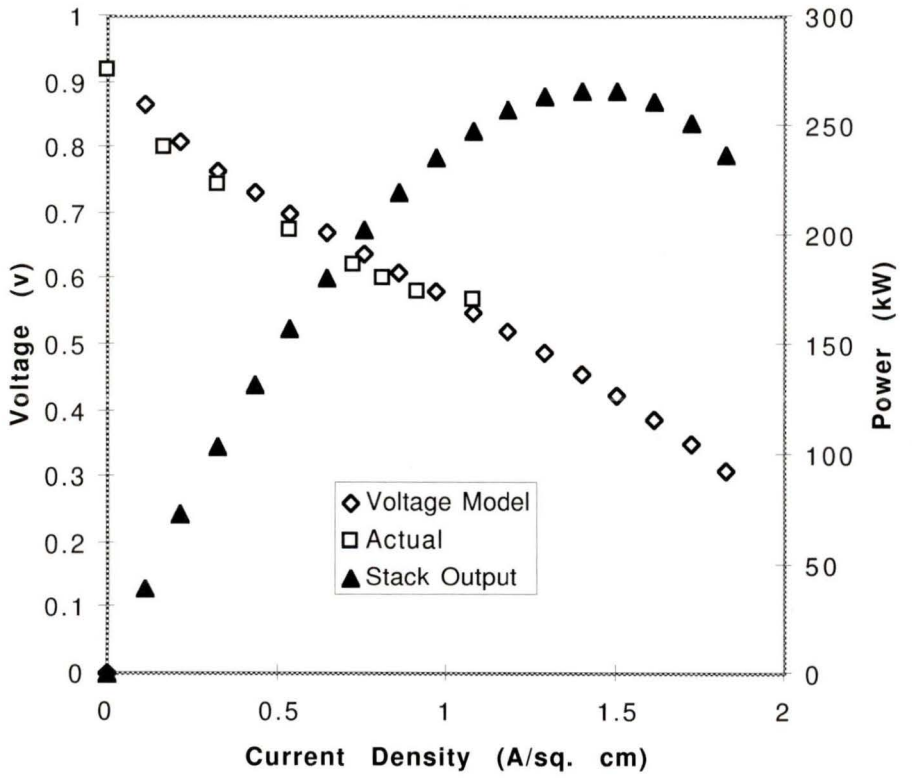

Figure A.1: Voltage model results vs. actual data

H_2 Consumption

The H_2 consumption is determined directly from the current density of the fuel cells. It is assumed that no electrical short circuiting results in 'wasted' current.

The H_2 consumption per cell is determined from Faraday's constant;

$$\frac{H_2 cons}{cell} = \frac{\text{Area} * \text{Current Density}}{[\#\text{Electrons/Mol}][\text{Faraday's Constant}]} \quad \left[\frac{mol}{s}\right] \tag{A.15}$$

Thus the powerplant hydrogen consumption is

$$H_2 cons = \frac{[A/cell][\text{Current Density}][1500\ \text{cells}]}{2 * F} \quad \left[\frac{mol}{s}\right] \tag{A.16}$$

Appendix B

Fuel Cell Types and Applications

Table B.1: Fuel cell types and applications

Type	Electrolyte	Temperature	Issues	Likely Applications
Alkaline (AFC)	Aqueous KOH solution	60-120°C	CO_2 troubles	Electric Vehicles (EVs), space, military
Polymer Electrolyte Membrane (PEMFC)	Polymer Membrane	60-120°C	Humidification of reactant gases	Same as AFC
Phosphoric Acid (PAFC)	Concentrated Phosphoric acid	160-220°C	Electrode CO sensitivity	Cogeneration Systems (<180°C)
Molten Carbonate (MCFC)	Mixture of molten carbonates (Li2CO3 /K2CO3)	600-650°C	CO_2- Recycling necessary	Dispersed and/or Cogeneration Systems (<600°C)
Solid Oxide (SOFC)	Ceramic solid ZrO2 (Y2O3)	900-1000°C	Ceramic cells	Dispersed and/or Cogeneration Systems (<1000°C)

Appendix C

AspenPlus Model of Steady-State Air Enrichment

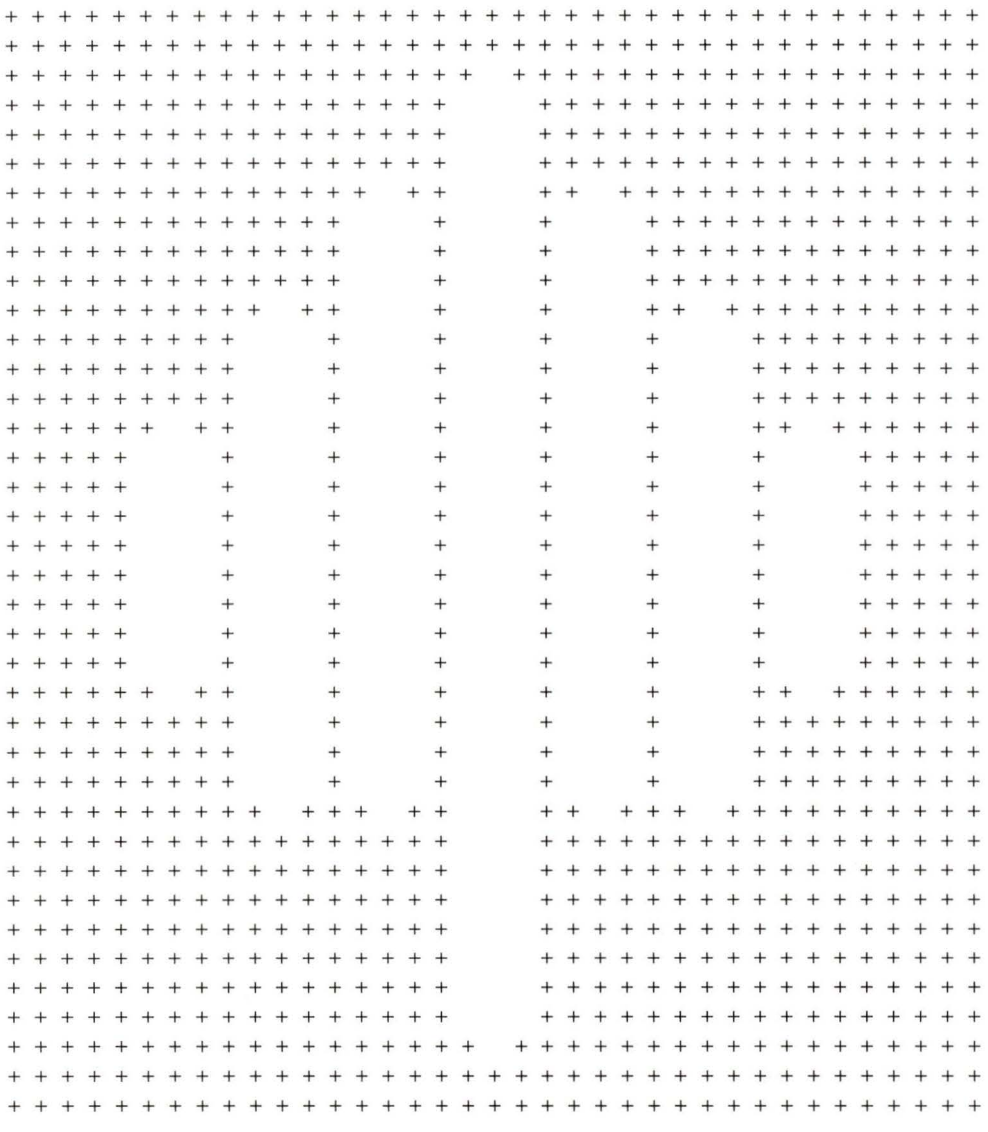

TM

```
AAAAA   SSSSS   PPPPP   EEEEE   NN    N   PPPPP   L       U   U   SSSSS
A   A   S       P   P   E       N N   N   P   P   L       U   U   S
AAAAA   SSSSS   PPPPP   EEEEE   N   N N   PPPPP   L       U   U   SSSSS
A   A       S   P       E       N    NN   P       L       U   U       S
A   A   SSSSS   P       EEEEE   N     N   P       LLLLL   UUUUU   SSSSS
```

ASPEN PLUS IS A TRADEMARK OF
ASPEN TECHNOLOGY, INC.
TEN CANAL PARK
CAMBRIDGE, MASSACHUSETTS 02141
617/577-0100

HOTLINE:
U.S.A. 617/577-0337
EUROPE (32) 2/726-9303

VERSION: SUN-4
RELEASE: 9.1-3
INSTALLATION: UVICTSUN

MARCH 14, 1996
THURSDAY
4:18:59 P.M.

TABLE OF CONTENTS

RUN CONTROL SECTION..... 1
RUN CONTROL INFORMATION..... 1
BLOCK STATUS..... 2

FLOWSHEET SECTION..... 3
FLOWSHEET CONNECTIVITY BY STREAMS..... 3
FLOWSHEET CONNECTIVITY BY BLOCKS..... 3
COMPUTATIONAL SEQUENCE..... 3
OVERALL FLOWSHEET BALANCE..... 3

PHYSICAL PROPERTIES SECTION..... 4
COMPONENTS..... 4

U-O-S BLOCK SECTION..... 5
BLOCK: B10 MODEL: MHEATX..... 5
BLOCK: B11 MODEL: FLASH2..... 7
BLOCK: B12 MODEL: PUMP..... 8
BLOCK: B13 MODEL: MIXER..... 9
BLOCK: B4 MODEL: COMPR..... 10
BLOCK: B6 MODEL: COMPR..... 11
BLOCK: B8 MODEL: HEATX..... 11
BLOCK: B9 MODEL: FLASH2..... 14
BLOCK: FUELCELL MODEL: USER..... 15

STREAM SECTION..... 16
13 16 19 20 22..... 16
23 24 26 27 28..... 17
AIR AIRIN ALTAIR ENRO2 EXAIR..... 18
EXH2 H2 H2IN WATER WATOUT..... 19
5..... 20

RUN CONTROL SECTION

RUN CONTROL INFORMATION

```
THIS COPY OF ASPEN PLUS LICENSED TO UNIV. VICTORIA

TYPE OF RUN:  NEW

INPUT FILE NAME: _unnamed.inm

OUTPUT PROBLEM DATA FILE NAME: _UNNAMED VERSION NO.   1
LOCATED IN:



PDF SIZE USED FOR INPUT TRANSLATION:
  NUMBER OF FILE RECORDS (PSIZE) =     0
  NUMBER OF IN-CORE RECORDS      =   256
PSIZE NEEDED FOR SIMULATION    =   256

CALLING PROGRAM NAME:          apmain
LOCATED IN:                    /package/AspenPlus-9.1.3/ap913/aspenplus


SIMULATION REQUESTED FOR ENTIRE FLOWSHEET
 ASPEN PLUS   VER: SUN-4     REL: 9.1-3     INST: UVICTSUN  03/14/96  PAGE 2

                            RUN CONTROL SECTION

BLOCK STATUS
------------

*****************************************************************************
*                                                                           *
* ALL UNIT OPERATION BLOCKS WERE COMPLETED NORMALLY                         *
*                                                                           *
*****************************************************************************
 ASPEN PLUS   VER: SUN-4     REL: 9.1-3     INST: UVICTSUN  03/14/96  PAGE 3

                             FLOWSHEET SECTION

FLOWSHEET CONNECTIVITY BY STREAMS
---------------------------------

  STREAM     SOURCE     DEST          STREAM     SOURCE     DEST
  WATER      ----       FUELCELL      AIRIN      ----       B8
  ALTAIR     ----       $B10H02       H2IN       ----       $B10H01
  EXAIR      FUELCELL   B9            EXH2       FUELCELL   ----
  WATOUT     FUELCELL   ----          5          FUELCELL   ----
  28         B4         B13           16         B6         ----
  13         B8         B4            27         B8         ----
  20         B9         B6            19         B9         ----
  22         $B10H02    B11           H2         $B10H01    FUELCELL
  ENRO2      $B10HTR    B13           26         B11        B8
  23         B11        B12           24         B12        $B10HTR
  AIR        B13        FUELCELL      $B10Q01    $B10H01    $B10HTR
  $B10Q02    $B10H02    $B10HTR

FLOWSHEET CONNECTIVITY BY BLOCKS
```

```
--------------------------------

  BLOCK        INLETS                        OUTLETS
  FUELCELL     AIR H2 WATER                  EXAIR EXH2 WATOUT 5
  B4           13                            28
  B6           20                            16
  B8           AIRIN 26                      13 27
  B9           EXAIR                         20 19
  B11          22                            26 23
  B12          23                            24
  B13          ENRO2 28                      AIR
  $B10H01      H2IN                          H2 $B10Q01
  $B10H02      ALTAIR                        22 $B10Q02
  $B10HTR      24 $B10Q01 $B10Q02            ENRO2

COMPUTATIONAL SEQUENCE
----------------------

SEQUENCE USED WAS:
   $B10H02 B11 *B12 B8 B4 $B10H01 $B10HTR B13 FUELCELL B9 B6

OVERALL FLOWSHEET BALANCE
-------------------------

                    ***  MASS AND ENERGY BALANCE  ***
                                  IN              OUT        RELATIVE DIFF.
   CONVENTIONAL COMPONENTS (MOL/SEC )
      O2                        2.75100         1.58380        0.424281
      N2                        10.3490         10.3490       -0.163782E-09
      H2                        2.40000        0.656038E-01    0.972665
      H2O                       100.000         102.334       -0.228115E-01
   TOTAL BALANCE
      MOLE(MOL/SEC )            115.500         114.333        0.101056E-01
      MASS(KG/HR   )            7863.50         7863.50       -0.935125E-11
      ENTHALPY(WATT    )      -0.284304E+08   -0.290586E+08    0.216170E-01
 ASPEN PLUS   VER: SUN-4     REL: 9.1-3     INST: UVICTSUN  03/14/96  PAGE 4

                        PHYSICAL PROPERTIES SECTION

COMPONENTS
----------

 ID       TYPE  FORMULA       NAME OR ALIAS                      REPORT NAME
  O2       C     O2            O2                                  O2
  N2       C     N2            N2                                  N2
  H2       C     H2            H2                                  H2
  H2O      C     H2O           H2O                                 H2O
 ASPEN PLUS   VER: SUN-4     REL: 9.1-3     INST: UVICTSUN  03/14/96  PAGE 5

                             U-O-S BLOCK SECTION

BLOCK:  B10      MODEL: MHEATX
------------------------------

  HOT SIDE:     INLET STREAM     OUTLET STREAM
                ------------     -------------
```

```
              ALTAIR          22

 COLD SIDE:   INLET STREAM    OUTLET STREAM
              ------------    -------------
              H2IN            H2
              24              ENRO2

 PROPERTIES FOR STREAM H2IN
 PROPERTY OPTION SET:   RKS-BM    REDLICH-KWONG-SOAVE EQUATION OF STATE

 PROPERTIES FOR STREAM ALTAIR
 PROPERTY OPTION SET:   RKS-BM    REDLICH-KWONG-SOAVE EQUATION OF STATE

 PROPERTIES FOR STREAM 24
 PROPERTY OPTION SET:   RKS-BM    REDLICH-KWONG-SOAVE EQUATION OF STATE

                    ***  MASS AND ENERGY BALANCE  ***
                                 IN              OUT        RELATIVE DIFF.
  TOTAL BALANCE
    MOLE(MOL/SEC )            7.48118         7.48118             0.
    MASS(KG/HR   )            548.016         548.016             0.
    ENTHALPY(WATT    )       -33296.6        -33296.6       -0.218519E-15

                        ***  INPUT DATA  ***


 SPECIFICATIONS FOR STREAM H2IN    :
 TWO    PHASE  TP  FLASH
 SPECIFIED TEMPERATURE          K                      290.000
 PRESSURE DROP                  BAR                      0.0
 MAXIMUM NO. ITERATIONS                                 30
 CONVERGENCE TOLERANCE                                   0.000100000
ASPEN PLUS   VER: SUN-4     REL: 9.1-3     INST: UVICTSUN  03/14/96  PAGE 6

                           U-O-S BLOCK SECTION

BLOCK:  B10      MODEL: MHEATX (CONTINUED)

 SPECIFICATIONS FOR STREAM ALTAIR  :
 TWO    PHASE  TP  FLASH
 SPECIFIED TEMPERATURE          K                      80.5000
 PRESSURE DROP                  BAR                      0.0
 MAXIMUM NO. ITERATIONS                                 30
 CONVERGENCE TOLERANCE                                   0.000100000

 SPECIFICATIONS FOR STREAM 24      :
 TWO    PHASE      FLASH
 PRESSURE DROP                  BAR                      0.0
 MAXIMUM NO. ITERATIONS                                 30
 CONVERGENCE TOLERANCE                                   0.000100000

                        ***  RESULTS  ***

 INLET                  OUTLET       OUTLET       OUTLET
 STREAM    DUTY         TEMPERATURE  PRESSURE     VAPOR FRAC
           WATT         K            BAR
```

H2IN	20599.	290.00	3.0398	1.000
ALTAIR	-32517.	80.50	1.0132	.7607
24	11918.	284.62	4.0000	1.000

ASPEN PLUS VER: SUN-4 REL: 9.1-3 INST: UVICTSUN 03/14/96 PAGE 7

U-O-S BLOCK SECTION

BLOCK: B10 MODEL: MHEATX (CONTINUED)

*** INTERNAL ANALYSIS ***

FLOW IS COUNTERCURRENT.

DUTY	32517.	WATT
UA	1962.8	J/SEC-K
AVERAGE LMTD (DUTY/UA)	16.566	K
MIN TEMP APPROACH	2.8792	K
HOT-SIDE TEMP APPROACH	10.000	K
COLD-SIDE TEMP APPROACH	60.500	K
HOT-SIDE NTU	13.250	
COLD-SIDE NTU	16.298	

DUTY	T HOT	T COLD	DELTA T	LMTD	UA ZONE	Q ZONE	UA	PINCH STREAM IN/OUT/DEW/
POINT BUBBLE POINT WATT	K	K	K	K	J/SEC-K	WATT	J/SEC-K	
0.	80.50	20.00	60.50					
479.8	80.57	24.74	55.83	58.13	8.254	479.8	8.254	LOC BP H2IN
2596.	80.93	24.74	56.19	56.01	37.78	2116.	46.04	DP H2IN
3252.	81.05	33.42	47.64	51.79	12.66	655.7	58.70	
6228.	81.64	76.91	4.74	18.58	160.1	2976.	218.8	DP ALTAIR
6500.	83.85	80.97	2.88	3.73	73.09	272.7	291.9	

IN 24							
6503.	83.87	81.00	2.88	2.88	1.070	3.082	293.0
GBL							
8257.	98.17	95.08	3.10	2.99	587.4	1754.	880.4
BP 24							
9755.	110.47	95.80	14.67	7.44	201.3	1498.	1082.
0.1301E+05	137.35	97.87	39.48	25.06	129.7	3252.	1211.
0.1412E+05	146.61	98.63	47.98	43.59	25.59	1115.	1237.
DP 24							
0.1626E+05	164.37	120.49	43.88	45.90	46.54	2136.	1284.
0.1951E+05	191.45	154.15	37.30	40.50	80.28	3252.	1364.
0.2276E+05	218.57	187.91	30.66	33.87	96.00	3252.	1460.
0.2601E+05	245.71	221.59	24.13	27.26	119.3	3252.	1579.
0.2927E+05	272.86	255.09	17.77	20.79	156.4	3252.	1736.
0.3215E+05	296.91	284.62	12.28	14.86	193.9	2881.	1929.
OUT 24							
0.3252E+05	300.00	290.00	10.00	11.10	33.38	370.7	1963.

GBL = GLOBAL LOC = LOCAL DP = DEW POINT BP = BUBBLE POINT

BLOCK: B11 MODEL: FLASH2

INLET STREAM: 22
OUTLET VAPOR STREAM: 26
OUTLET LIQUID STREAM: 23
PROPERTY OPTION SET: RKS-BM REDLICH-KWONG-SOAVE EQUATION OF STATE

U-O-S BLOCK SECTION

BLOCK: B11 MODEL: FLASH2 (CONTINUED)

*** MASS AND ENERGY BALANCE ***

	IN	OUT	RELATIVE DIFF.
TOTAL BALANCE			
MOLE(MOL/SEC)	4.10000	4.10000	0.
MASS(KG/HR)	425.832	425.832	0.266976E-15
ENTHALPY(WATT)	-32321.9	-32321.9	-0.109261E-06

*** INPUT DATA ***

TWO PHASE PQ FLASH		
SPECIFIED PRESSURE	BAR	1.01325
SPECIFIED HEAT DUTY	WATT	0.0
MAXIMUM NO. ITERATIONS		30
CONVERGENCE TOLERANCE		0.000100000

*** RESULTS ***

OUTLET TEMPERATURE	K	80.500
OUTLET PRESSURE	BAR	1.0132
VAPOR FRACTION		0.76069

V-L PHASE EQUILIBRIUM :

COMP	F(I)	X(I)	Y(I)	K(I)
O2	0.21000	0.41320	0.14607	0.35352
N2	0.79000	0.58680	0.85393	1.4553

BLOCK: B12 MODEL: PUMP

INLET STREAM: 23
OUTLET STREAM: 24
PROPERTY OPTION SET: RKS-BM REDLICH-KWONG-SOAVE EQUATION OF STATE

ASPEN PLUS VER: SUN-4 REL: 9.1-3 INST: UVICTSUN 03/14/96 PAGE 9

U-O-S BLOCK SECTION

BLOCK: B12 MODEL: PUMP (CONTINUED)

****

* *

* NET POSITIVE SUCTION HEAD IS LESS THAN ZERO *

* *

****

*** MASS AND ENERGY BALANCE ***

	IN	OUT	RELATIVE DIFF.
TOTAL BALANCE			
MOLE(MOL/SEC)	0.981175	0.981175	0.
MASS(KG/HR)	104.767	104.767	0.
ENTHALPY(WATT)	-12367.2	-12335.9	-0.253228E-02

*** INPUT DATA ***

OUTLET PRESSURE (BAR)	4.00000
DRIVER EFFICIENCY	1.00000
FLASH SPECIFICATIONS:	
LIQUID PHASE CALCULATION	
NO FLASH PERFORMED	
MAXIMUM NUMBER OF ITERATIONS	30
TOLERANCE	0.000100000

*** RESULTS ***

VOLUMETRIC FLOW RATE (CUM/)	0.310008-04
PRESSURE CHANGE (BAR)	2.98675
NPSH AVAILABLE (METER)	-0.00085316
FLUID POWER (KW)	0.0092592
BRAKE POWER (KW)	0.031317
ELECTRICITY (WATT)	31.3172
PUMP EFFICIENCY USED	0.29566
NET WORK (KW)	-0.031317

BLOCK: B13 MODEL: MIXER

INLET STREAMS: ENRO2 28
OUTLET STREAM: AIR
PROPERTY OPTION SET: RKS-BM REDLICH-KWONG-SOAVE EQUATION OF STATE

```
                    ***  MASS AND ENERGY BALANCE  ***
                                    IN              OUT        RELATIVE DIFF.
 ASPEN PLUS   VER: SUN-4     REL: 9.1-3     INST: UVICTSUN  03/14/96  PAGE 10

                            U-O-S BLOCK SECTION

BLOCK:  B13      MODEL: MIXER (CONTINUED)
   TOTAL BALANCE
      MOLE(MOL/SEC )            9.98118         9.98118             0.
      MASS(KG/HR   )            1039.52         1039.52        0.218730E-15
      ENTHALPY(WATT    )        19900.4         19900.4             0.

                          ***  INPUT DATA  ***
  TWO    PHASE      FLASH
  MAXIMUM NO. ITERATIONS                                    30
  CONVERGENCE TOLERANCE                                      0.000100000
  OUTLET PRESSURE   BAR                                     4.00000

BLOCK:  B4       MODEL: COMPR
------------------------------
  INLET STREAM:          13
  OUTLET STREAM:         28
  PROPERTY OPTION SET:   RKS-BM    REDLICH-KWONG-SOAVE EQUATION OF STATE

                    ***  MASS AND ENERGY BALANCE  ***
                                    IN              OUT        RELATIVE DIFF.
   TOTAL BALANCE
      MOLE(MOL/SEC )            9.00000         9.00000             0.
      MASS(KG/HR   )            934.753         934.753             0.
      ENTHALPY(WATT    )       -19219.9         20318.5        -1.94593

                          ***  INPUT DATA  ***

   GAS PHASE CALCULATION
   NO FLASH PERFORMED
   TYPE : ISENTROPIC CENTRIFUGAL COMPRESSOR
   OUTLET PRESSURE  BAR                                      3.03975
   ISENTROPIC EFFICIENCY                                     0.55000
   MECHANICAL EFFICIENCY                                     1.00000

                          ***  RESULTS  ***

   INDICATED  HORSEPOWER REQUIREMENT  KW                    39.5384
   BRAKE      HORSEPOWER REQUIREMENT  KW                    39.5384
   NET WORK, KW                                            -39.5384
   ISENTROPIC HORSEPOWER REQUIREMENT  KW                    21.7461
   CALCULATED OUTLET TEMP  K                               375.641
   ISENTROPIC TEMPERATURE  K                               308.380
   OUTLET VAPOR FRACTION                                     1.00000
 ASPEN PLUS   VER: SUN-4     REL: 9.1-3     INST: UVICTSUN  03/14/96  PAGE 11

                            U-O-S BLOCK SECTION

BLOCK:  B6       MODEL: COMPR
------------------------------
```

```
  INLET STREAM:          20
  OUTLET STREAM:         16
  PROPERTY OPTION SET:   RKS-BM    REDLICH-KWONG-SOAVE EQUATION OF STATE

                    ***  MASS AND ENERGY BALANCE  ***
                                    IN              OUT        RELATIVE DIFF.
   TOTAL BALANCE
      MOLE(MOL/SEC )            9.93750         9.93750             0.
      MASS(KG/HR   )            977.930         977.930             0.
      ENTHALPY(WATT    )       -258074.        -269863.        0.436876E-01

                           ***  INPUT DATA  ***

   GAS PHASE CALCULATION
   NO FLASH PERFORMED
   TYPE : ISENTROPIC TURBINE
   OUTLET PRESSURE  BAR                                        1.01325
   ISENTROPIC EFFICIENCY                                       0.50000
   MECHANICAL EFFICIENCY                                       1.00000

                           ***  RESULTS  ***

   INDICATED  HORSEPOWER REQUIREMENT  KW                     -11.7897
   BRAKE      HORSEPOWER REQUIREMENT  KW                     -11.7897
   NET WORK, KW                                               11.7897
   ISENTROPIC HORSEPOWER REQUIREMENT  KW                     -23.5794
   CALCULATED OUTLET TEMP  K                                 304.710
   ISENTROPIC TEMPERATURE  K                                 264.813
   OUTLET VAPOR FRACTION                                       1.00000
 ASPEN PLUS   VER: SUN-4     REL: 9.1-3     INST: UVICTSUN  03/14/96  PAGE 12

                              U-O-S BLOCK SECTION

BLOCK:  B8       MODEL: HEATX
------------------------------
  HOT SIDE:
  ---------
  INLET STREAM:          AIRIN
  OUTLET STREAM:         13
  PROPERTY OPTION SET:   RKS-BM    REDLICH-KWONG-SOAVE EQUATION OF STATE
  COLD SIDE:
  ----------
  INLET STREAM:          26
  OUTLET STREAM:         27
  PROPERTY OPTION SET:   RKS-BM    REDLICH-KWONG-SOAVE EQUATION OF STATE

                    ***  MASS AND ENERGY BALANCE  ***
                                    IN              OUT        RELATIVE DIFF.
   TOTAL BALANCE
      MOLE(MOL/SEC )            12.1188         12.1188             0.
      MASS(KG/HR   )            1255.82         1255.82             0.
      ENTHALPY(WATT    )       -19526.9        -19526.9        0.372611E-15

                           ***  INPUT DATA  ***

  FLASH SPECS FOR HOT SIDE:
```

```
  TWO    PHASE      FLASH
  MAXIMUM NO. ITERATIONS                                  30
  CONVERGENCE TOLERANCE                                    0.000100000

  FLASH SPECS FOR COLD SIDE:
  TWO    PHASE      FLASH
  MAXIMUM NO. ITERATIONS                                  30
  CONVERGENCE TOLERANCE                                    0.000100000

  FLOW DIRECTION AND SPECIFICATION:
    COUNTERCURRENT   HEAT EXCHANGER
    SPECIFIED COLD OUTLET TEMP
    SPECIFIED VALUE                K                     295.0000
    LMTD CORRECTION FACTOR                                 1.00000

  PRESSURE SPECIFICATION:
    HOT  SIDE PRESSURE DROP        BAR                     0.0000
    COLD SIDE PRESSURE DROP        BAR                     0.0000
 ASPEN PLUS   VER: SUN-4     REL: 9.1-3     INST: UVICTSUN  03/14/96  PAGE 13

                              U-O-S BLOCK SECTION

BLOCK:  B8       MODEL: HEATX (CONTINUED)

  HEAT TRANSFER COEFFICIENT SPECIFICATION:
    HOT LIQUID    COLD LIQUID      WATT/SQM-K              850.0000
    HOT LIQUID    COLD 2-PHASE     WATT/SQM-K              850.0000
    HOT LIQUID    COLD VAPOR       WATT/SQM-K              850.0000
    HOT 2-PHASE   COLD LIQUID      WATT/SQM-K              850.0000
    HOT 2-PHASE   COLD 2-PHASE     WATT/SQM-K              850.0000
    HOT 2-PHASE   COLD VAPOR       WATT/SQM-K              850.0000
    HOT VAPOR     COLD LIQUID      WATT/SQM-K              850.0000
    HOT VAPOR     COLD 2-PHASE     WATT/SQM-K              850.0000
    HOT VAPOR     COLD VAPOR       WATT/SQM-K              850.0000

                         ***  OVERALL RESULTS  ***

  STREAMS:
                  ---------------------------------------
                  |                                     |
  AIRIN      ----->|               HOT                   |-----> 13
  T=  3.0000D+02  |                                     |       T=  2.2529D+02
  P=  1.0132D+00  |                                     |       P=  1.0132D+00
  V=  1.0000D+00  |                                     |       V=  1.0000D+00
                  |                                     |
  27         <----|               COLD                  |<----- 26
  T=  2.9500D+02  |                                     |       T=  8.0500D+01
  P=  1.0132D+00  |                                     |       P=  1.0132D+00
  V=  1.0000D+00  |                                     |       V=  1.0000D+00
                  ---------------------------------------

  DUTY AND AREA:
    CALCULATED HEAT DUTY           WATT                 19647.6
    CALCULATED (REQUIRED) AREA     SQM                      0.5566

  HEAT TRANSFER COEFFICIENT:
```

```
   AVERAGE COEFFICIENT (DIRTY)     WATT/SQM-K              850.0000

  LOG-MEAN TEMPERATURE DIFFERENCE:
    LMTD CORRECTION FACTOR                                   1.0000
    LMTD (CORRECTED)               K                        41.5311

  PRESSURE DROP:
    SHELLSIDE, TOTAL               BAR                       0.0000
    TUBESIDE,  TOTAL               BAR                       0.0000
 ASPEN PLUS   VER: SUN-4     REL: 9.1-3     INST: UVICTSUN  03/14/96  PAGE 14

                            U-O-S BLOCK SECTION

BLOCK:  B8       MODEL: HEATX (CONTINUED)

                        ***  ZONE RESULTS  ***

  TEMPERATURE LEAVING EACH ZONE:

                                    HOT
        ------------------------------------------------------------
        |                                                          |
AIRIN   |                           VAP                            | 13
------> |                                                          |------>
 300.0  |                                                          |  225.3
        |                                                          |
27      |                           VAP                            | 26
<------ |                                                          |<------
 295.0  |                                                          |   80.5
        |                                                          |
        ------------------------------------------------------------
                                    COLD

  ZONE HEAT TRANSFER AND AREA:

  ZONE       HEAT DUTY          AREA           DTLM         AVERAGE U
             WATT               SQM            K            WATT/SQM-K
    1           19647.630         0.5566       41.5311        850.0000

BLOCK:  B9       MODEL: FLASH2
------------------------------
  INLET STREAM:          EXAIR
  OUTLET VAPOR STREAM:   20
  OUTLET LIQUID STREAM:  19
  PROPERTY OPTION SET:   RKS-BM    REDLICH-KWONG-SOAVE EQUATION OF STATE

                     ***  MASS AND ENERGY BALANCE  ***
                                  IN              OUT        RELATIVE DIFF.
   TOTAL BALANCE
      MOLE(MOL/SEC )           11.1484         11.1484       -0.159338E-15
      MASS(KG/HR   )           1056.46         1056.46       -0.696039E-10
      ENTHALPY(WATT    )      -577865.        -602924.        0.415627E-01

                          ***  INPUT DATA  ***
  TWO    PHASE  TP  FLASH
  SPECIFIED TEMPERATURE K                                  345.000
```

```
  SPECIFIED PRESSURE    BAR                                    2.60000
  MAXIMUM NO. ITERATIONS                                      30
  CONVERGENCE TOLERANCE                                       0.000100000
 ASPEN PLUS   VER: SUN-4     REL: 9.1-3     INST: UVICTSUN  03/14/96  PAGE 15

                              U-O-S BLOCK SECTION

BLOCK:  B9       MODEL: FLASH2 (CONTINUED)

                           ***  RESULTS  ***
  OUTLET TEMPERATURE    K                                     345.00
  OUTLET PRESSURE       BAR                                   2.6000
  HEAT DUTY             WATT                                  -25059.
  VAPOR FRACTION                                              0.89139


  V-L PHASE EQUILIBRIUM :

     COMP            F(I)          X(I)          Y(I)          K(I)
     O2              0.10120       0.10764E-05   0.11353       0.10547E+06
     N2              0.68941       0.48085E-06   0.77341       0.16084E+07
     H2O             0.20939        1.0000       0.11306       0.11306

BLOCK:  FUELCELL MODEL: USER
------------------------------
  INLET STREAMS:         AIR        H2         WATER
  OUTLET STREAMS:        EXAIR      EXH2       WATOUT     5
  PROPERTY OPTION SET:   RKS-BM    REDLICH-KWONG-SOAVE EQUATION OF STATE

                     ***  MASS AND ENERGY BALANCE  ***
                                  IN              OUT        RELATIVE DIFF.
   TOTAL BALANCE
      MOLE(MOL/SEC )            112.381         111.214        0.103861E-01
      MASS(KG/HR   )            7542.44         7542.44              0.
      ENTHALPY(WATT    )     -0.283905E+08   -0.290214E+08    0.217384E-01

                          ***    ARRAYS    ***
    INTEGER VECTOR AS FOLLOWS   1 VALUES

          99999999
     REAL VECTOR AS FOLLOWS   2 VALUES

         1000.0      2.0000
 ASPEN PLUS   VER: SUN-4     REL: 9.1-3     INST: UVICTSUN  03/14/96  PAGE 16

                                STREAM SECTION

13 16 19 20 22
--------------

STREAM ID               13         16         19         20         22
FROM :                  B8         B6         B9         B9         B10
TO   :                  B4         ----       ----       B6         B11

SUBSTREAM: MIXED
```

PHASE:	VAPOR	VAPOR	LIQUID	VAPOR	MIXED
COMPONENTS: MOL/SEC					
O2	1.8900	1.1282	1.3034-06	1.1282	0.8610
N2	7.1100	7.6857	5.8225-07	7.6857	3.2390
H2	0.0	0.0	0.0	0.0	0.0
H2O	0.0	1.1235	1.2108	1.1235	0.0
TOTAL FLOW:					
MOL/SEC	9.0000	9.9375	1.2108	9.9375	4.1000
KG/HR	934.7528	977.9295	78.5312	977.9295	425.8318
CUM/SEC	0.1661	0.2483	2.9943-05	0.1095	1.9888-02
STATE VARIABLES:					
TEMP K	225.2865	304.7101	345.0000	345.0000	80.5004
PRES BAR	1.0132	1.0132	2.6000	2.6000	1.0132
VFRAC	1.0000	1.0000	0.0	1.0000	0.7606
LFRAC	0.0	0.0	1.0000	0.0	0.2393
SFRAC	0.0	0.0	0.0	0.0	0.0
ENTHALPY:					
J/KMOL	-2.1355+06	-2.7156+07	-2.8479+08	-2.5970+07	-7.8834+06
J/KG	-7.4021+04	-9.9343+05	-1.5808+07	-9.5003+05	-2.7325+05
WATT	-1.9220+04	-2.6986+05	-3.4485+05	-2.5807+05	-3.2322+04
ENTROPY:					
J/KMOL-K	-3936.5680	1354.3460	-1.5819+05	-2818.6987	-5.2632+04
J/KG-K	-136.4476	49.5452	-8781.1189	-103.1147	-1824.2976
DENSITY:					
KMOL/CUM	5.4162-02	4.0022-02	40.4393	9.0693-02	0.2061
KG/CUM	1.5625	1.0940	728.5267	2.4791	5.9477
AVG MW	28.8504	27.3355	18.0153	27.3355	28.8504

STREAM SECTION

23 24 26 27 28

STREAM ID	23	24	26	27	28
FROM :	B11	B12	B11	B8	B4
TO :	B12	B10	B8	----	B13
SUBSTREAM: MIXED					
PHASE:	LIQUID	LIQUID	VAPOR	VAPOR	VAPOR
COMPONENTS: MOL/SEC					
O2	0.4054	0.4054	0.4555	0.4555	1.8900
N2	0.5757	0.5757	2.6632	2.6632	7.1100
H2	0.0	0.0	0.0	0.0	0.0
H2O	0.0	0.0	0.0	0.0	0.0
TOTAL FLOW:					
MOL/SEC	0.9811	0.9811	3.1188	3.1188	9.0000
KG/HR	104.7668	104.7668	321.0650	321.0650	934.7528
CUM/SEC	3.1001-05	3.1050-05	1.9857-02	7.5497-02	9.2581-02
STATE VARIABLES:					
TEMP K	80.5002	80.9702	80.5002	295.0000	375.6415
PRES BAR	1.0132	4.0000	1.0132	1.0132	3.0397
VFRAC	0.0	0.0	1.0000	1.0000	1.0000
LFRAC	1.0000	1.0000	0.0	0.0	0.0
SFRAC	0.0	0.0	0.0	0.0	0.0
ENTHALPY:					

J/KMOL	-1.2604+07	-1.2573+07	-6.3981+06	-9.8442+04	2.2576+06
J/KG	-4.2496+05	-4.2389+05	-2.2375+05	-3442.5557	7.8252+04
WATT	-1.2367+04	-1.2336+04	-1.9955+04	-307.0234	2.0319+04
ENTROPY:					
J/KMOL-K	-1.0827+05	-1.0800+05	-3.5126+04	3125.2647	1862.1602
J/KG-K	-3650.4874	-3641.1023	-1228.3780	109.2917	64.5453
DENSITY:					
KMOL/CUM	31.6500	31.5997	0.1570	4.1311-02	9.7212-02
KG/CUM	938.7466	937.2553	4.4913	1.1813	2.8046
AVG MW	29.6602	29.6602	28.5956	28.5956	28.8504

STREAM SECTION

AIR AIRIN ALTAIR ENRO2 EXAIR

STREAM ID	AIR	AIRIN	ALTAIR	ENRO2	EXAIR
FROM :	B13	----	----	B10	FUELCELL
TO :	FUELCELL	B8	B10	B13	B9
SUBSTREAM: MIXED					
PHASE:	VAPOR	VAPOR	VAPOR	VAPOR	MIXED
COMPONENTS: MOL/SEC					
O2	2.2954	1.8900	0.8610	0.4054	1.1282
N2	7.6857	7.1100	3.2390	0.5757	7.6857
H2	0.0	0.0	0.0	0.0	0.0
H2O	0.0	0.0	0.0	0.0	2.3344
TOTAL FLOW:					
MOL/SEC	9.9811	9.0000	4.1000	0.9811	11.1483
KG/HR	1039.5196	934.7528	425.8318	104.7668	1056.4607
CUM/SEC	7.6203-02	0.2215	0.1009	5.7991-03	0.2934
STATE VARIABLES:					
TEMP K	366.7711	300.0000	300.0000	284.6237	360.0000
PRES BAR	4.0000	1.0132	1.0132	4.0000	3.7309
VFRAC	1.0000	1.0000	1.0000	1.0000	0.9306
LFRAC	0.0	0.0	0.0	0.0	6.9313-02
SFRAC	0.0	0.0	0.0	0.0	0.0
ENTHALPY:					
J/KMOL	1.9938+06	4.7524+04	4.7524+04	-4.2617+05	-5.1834+07
J/KG	6.8918+04	1647.2672	1647.2672	-1.4368+04	-1.9691+06
WATT	1.9900+04	427.7188	194.8496	-418.1479	-5.7786+05
ENTROPY:					
J/KMOL-K	-923.4164	4432.0280	4432.0280	-7236.5992	MISSING
J/KG-K	-31.9189	153.6210	153.6210	-243.9832	MISSING
DENSITY:					
KMOL/CUM	0.1309	4.0622-02	4.0622-02	0.1691	MISSING
KG/CUM	3.7892	1.1719	1.1719	5.0183	MISSING
AVG MW	28.9300	28.8504	28.8504	29.6602	26.3232

STREAM SECTION

EXH2 H2 H2IN WATER WATOUT

STREAM ID	EXH2	H2	H2IN	WATER	WATOUT
FROM :	FUELCELL	B10	----	----	FUELCELL
TO :	----	FUELCELL	B10	FUELCELL	----
SUBSTREAM: MIXED					
PHASE:	VAPOR	VAPOR	LIQUID	LIQUID	LIQUID
COMPONENTS: MOL/SEC					
O2	0.0	0.0	0.0	0.0	0.0
N2	0.0	0.0	0.0	0.0	0.0
H2	6.5604-02	2.4000	2.4000	0.0	0.0
H2O	0.0	0.0	0.0	100.0000	100.0000
TOTAL FLOW:					
MOL/SEC	6.5604-02	2.4000	2.4000	100.0000	100.0000
KG/HR	0.4761	17.4172	17.4172	6485.5007	6485.5007
CUM/SEC	7.1119-04	1.9074-02	5.9710-05	2.4901-03	2.4901-03
STATE VARIABLES:					
TEMP K	360.0000	290.0000	20.0000	353.0000	382.1146
PRES BAR	2.7652	3.0397	3.0397	3.0000	3.0000
VFRAC	1.0000	1.0000	0.0	0.0	0.0
LFRAC	0.0	0.0	1.0000	1.0000	1.0000
SFRAC	0.0	0.0	0.0	0.0	0.0
ENTHALPY:					
J/KMOL	1.7935+06	-2.3193+05	-8.8148+06	-2.8410+08	-2.8189+08
J/KG	8.8969+05	-1.1505+05	-4.3727+06	-1.5770+07	-1.5648+07
WATT	117.6607	-556.6301	-2.1156+04	-2.8410+07	-2.8189+07
ENTROPY:					
J/KMOL-K	-2895.5556	-9938.7628	2.6123+05	-1.5620+05	-1.5620+05
J/KG-K	-1436.3730	-4930.2353	1.2959+05	-8670.5400	-8670.5400
DENSITY:					
KMOL/CUM	9.2245-02	0.1258	40.1945	40.1593	40.1593
KG/CUM	0.1859	0.2536	81.0274	723.4821	723.4821
AVG MW	2.0158	2.0158	2.0158	18.0152	18.0152

STREAM SECTION

5
-

STREAM ID	5
FROM :	FUELCELL
TO :	----
CLASS:	WORK
STREAM ATTRIBUTES:	
WORK	
P KW	254.1852

Appendix D

USABC Dynamic Stress Test

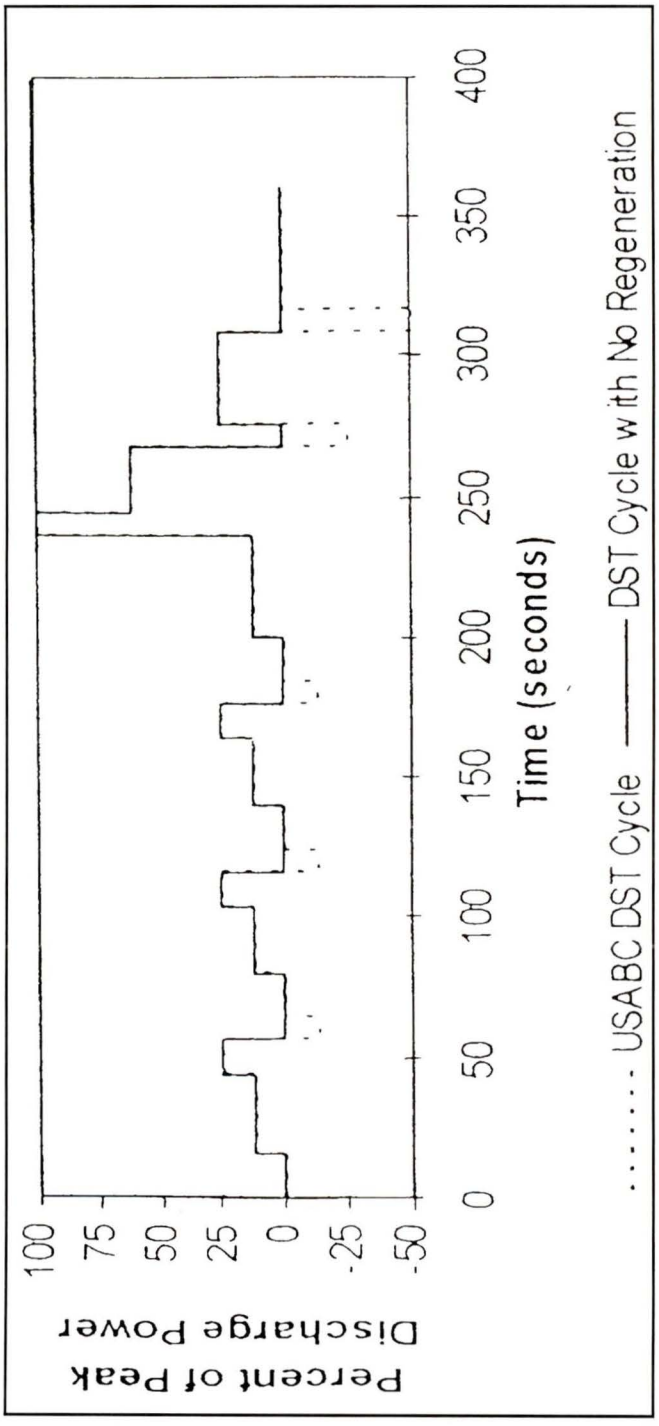

Figure D.1: USABC Dynamic Stress Test [72]

Vita

Surname: Flaherty Given Names: Kenneth Michael

Place of Birth: London, Ontario, Canada

Educational Institutions Attended:

University of Toronto:	1985-1989
University of Victoria:	1994-1996

Degrees Awarded:

B.A.Sc.	University of Toronto	1989

Publications:

D. S. Scott, K. M. Flaherty, P. Crane-Wall, "Harvesting thermomechanical exergy from LH_2: Transportation applications", Hydrogen Energy Progress XI, Proceedings of the 11th World Hydrogen Energy Conference, Stuttgart, Germany, 1996.

PARTIAL COPYRIGHT LICENSE

I hereby grant the right to lend my thesis (or dissertation) to users of the University of Victoria Library, and to make single copies only for such users or in response to a request from the Library of any other university, or similar institution, on its behalf or for one of its users. I further agree that permission for extensive copying of this thesis for scholarly purposes may be granted by me or a member of the University designated by me. It is understood that copying or publication of this thesis for financial gain shall not be allowed without my written permission.

Title of thesis:

Thermomechanical Exergy Recovery From Liquid Hydrogen Cryofuel

Author [redacted]

K. Michael Flaherty

September 24, 1996